School of Civil and Mechanical Engineering

Department of Civil Engineering

Electromechanical Impedance-based Techniques for Structural Health Monitoring

Xingyu Fan

This thesis is presented for the Degree of

Doctor of Philosophy

of

Curtin University

June 2018

DECLARATION

To the best of my knowledge and belief, this thesis contains no material previously published by any other person except where due acknowledgment has been made.

This thesis contains no material that has been accepted for the award of any other degree or diploma at any university.

Signature: 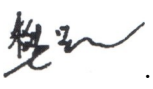 .

Date: 10/04/19

ABSTRACT

In the last several decades, structural health monitoring (SHM) techniques using system identification and damage detection methods to evaluate the safety condition of civil infrastructure have been developed. As one of the widely used smart materials, lead zirconate titanate (PZT), which transforms the energy between mechanical deformation and electricity, has been developed as a transducer patch that can be attached on the structural surface to monitor structural health conditions. The electromechanical impedance (EMI)-based SHM technique has been rapidly developed in recent years. This technique has been successfully applied to monitoring structural systems, i.e., beam and plate-like structures.

On the other hand, there are still many challenges remaining for SHM approaches based on the EMI technique. For conventional EMI-based methods, few efforts have been made to analyse the impedance responses in the time-frequency domain. In addition, when using the model-based EMI methods to quantify structural damage, the accuracy of solutions to the highly underdetermined inverse identification problem still remains as a significant issue.

This thesis attempts to enhance the capacity and performance of the EMI-based SHM approaches by improving the sensitivity of using these approaches in damage detection of complex structures with time-frequency analysis techniques, and by solving the inverse underdetermined identification problem with impedance sensitivity and sparse regularization techniques. A new structural damage detection approach in which the time-domain impedance responses are analysed is proposed. The time-domain responses measured from piezoelectric transducers will be used for analysis. With the use of the time frequency autoregressive moving average (TFARMA) model, a damage index based on singular value decomposition is defined to identify the existence of local structural damage. Experimental studies on a spatial steel truss bridge model in the laboratory are conducted to verify the accuracy and performance of the proposed approach. Four piezoelectric transducers are attached at

different locations and are excited by a sweep-frequency signal. The impedance responses at different locations are analysed with the TFARMA model to investigate the effectiveness and performance of the proposed approach. The results demonstrate that the proposed approach is very sensitive and robust in detecting bolt loosing damage in the gusset plates of steel truss bridges.

To enhance the capacity and performance of using a model-based EMI approach for structural damage quantification, this thesis presents a structural damage identification approach based on model updating with impedance sensitivity and sparse regularization techniques to identify the location and severity of minor damage in structures. The sensitivities of resonance frequency shifts in the impedance responses to the stiffness parameters of the host structure are calculated and used to identify the damage with a small number of resonance frequency shifts. Numerical and experimental studies on beam and plate structures are conducted to validate the performance of the proposed approach. The effects of uncertainties are also discussed. The results demonstrate the effectiveness and accuracy of the proposed approach in structural damage detection and quantification. Minor structural damage can be identified accurately and effectively.

LIST OF PUBLICATIONS

Journal papers:

1. Li, J., Hao, H. & Fan, X. (2015), Structural damage identification with extracted impulse response functions and optimal sensor locations, *Electronic Journal of Structural Engineering*, 14(1): 123-132.
2. Fan, X., Li, J., & Hao, H. (2016). Piezoelectric impedance-based damage detection in truss bridges based on time frequency ARMA model. *Smart Structures and Systems*, 18, 501-523.
3. Fan, X., Li, J., Hao, H., & Chen, Z. (2017). Using multi-type sensor measurements for damage detection of shear connectors in composite bridges under moving loads. *Computers and Concrete*, 20(5), 521-527.
4. Fan, X., Li, J., Hao, H., & Ma, S. (2018). Identification of Minor Structural Damage Based on Electromechanical Impedance Sensitivity and Sparse Regularization. *ASCE Journal of Aerospace Engineering*, 31(5), 04018061.
5. Fan, X., Li, J., & Hao, H. (2019). Impedance sensitivity based structural damage identification with sparse regularization: Experimental studies, *Smart Materials and Structures*, 28(1), 015003.

Conference papers:

6. Fan, X., Li, J., & Hao, H. 2015, Impedance based structural damage detection in a truss structure by time frequency analysis, *Symposium on Reliability of Engineering Systems (SRES2015)*, October, Hangzhou, China.
7. Fan, X., Li, J., & Hao, H. 2017, Using sparse regularization and impedance sensitivity for structural damage detection, *Structural Health Monitoring of Intelligent Infrastructure Conference 2017 (SHMII8)*, Brisbane, Australia.
8. Li, J., Fan, X., & Hao, H. 2018, Experimental study on structural damage quantification based on EMI sensitivity and Sparse Regularization, *The 7th World Conference on Structural Control and Monitoring*, Qingdao, China.

STATEMENT OF CONTRIBUTION OF OTHERS

The analytical and experimental studies presented in this thesis were primarily designed and conducted, and the testing data were analysed and the results were interpreted by the candidate (Xingyu Fan). Significant contributions to the works were also provided by co-authors. Contributions of the co-authors are described below.

Xingyu Fan, Prof. Hong Hao and Dr Jun Li decided the objectives of the proposed research and developed methodologies. Numerical and experimental studies and results analysis in this thesis were carried out by Xingyu Fan. The manuscripts were written by Xingyu Fan with revisions and editions from Prof. Hong Hao and Dr Jun Li. Both of them also provided additional intellectual input in the discussions of analysis and interpretations of results. Dr Shenglan Ma provided assistance for the programming of damage detection method with sparse regularization.

To whom it may concern

I, Xingyu Fan, contributed (carried out numerical simulations, analysed numerical results and wrote the manuscripts which were revised and edited by other co-authors) to the papers contained in this thesis and entitled below.

Fan, X., Li, J., & Hao, H. (2016). Piezoelectric impedance-based damage detection in truss bridges based on time frequency ARMA model. Smart Structures and Systems, 18, 501-523.

Fan, X., Li, J., Hao, H., & Ma, S. (2018). Identification of Minor Structural Damage Based on Electromechanical Impedance Sensitivity and Sparse Regularization. ASCE Journal of Aerospace Engineering, 31(5), 04018061.

Fan, X., Li, J., & Hao, H. (2019). Impedance sensitivity based structural damage identification with sparse regularization: Experimental studies, Smart Materials and Structures, 28(1), 015003.

I, as a co-author, endorse that this level of contribution by the candidate indicated above is appropriate.

(Prof. Hong Hao) (.....)

(Dr. Jun Li) (.....)

(Dr. Shenglan Ma) (.....)

ACKNOWLEDGEMENTS

The completion of this thesis is attributed to the support and encouragement of many people. First and foremost, I want to extend my heartfelt gratitude to my supervisor, John Curtin Distinguished Professor Hong Hao. His conscientious academic spirit and modest, open-minded personality inspire me both in academic study and daily life. In addition, I need to extend my heartfelt appreciation to my co-supervisor, Dr. Jun Li, whose patient guidance, valuable suggestions and constant encouragement allowed me to successfully complete this thesis.

Additionally, I would like to express my sincere gratitude to all the postgraduate students and academics in the School of Civil Engineering who have helped me.

Last but not least, I would like to express my special thanks to my wife and my parents, whose care and support motivate me to move on and make me a better person.

TABLE OF CONTENTS

LIST OF FIGURES

LIST OF TABLES

1 Introduction

1.1 Structural Health Monitoring and Electromechanical Impedance Technique

To satisfy the practical needs for the safety condition management of infrastructure, structural health monitoring (SHM) techniques have been dramatically developed in the last several decades, with improvements in system identification and damage detection. Throughout the years of development and study, SHM systems have been widely applied to infrastructure all over the world. SHM systems can be classified into two categories: global SHM techniques and local damage detection methods.

In general, incipient structural damage can be quickly repaired. Therefore, a critical issue among the studies on SHM is the ability to detect minor structural damage at an early stage to prevent progressive structural degradation and potential failure. In 2007, the bridge carrying Interstate Highway 35W (I-35W, National Bridge Inventory Structure No. 9340) over the Mississippi River in Minneapolis suffered a sudden tragic collapse within a second. According to the post-accident investigation, a total of 111 vehicles were on the collapsed portion. More than 17 vehicles fell into the water. Thirteen people died, and a hundred and forty five people were injured because of the collapse. The investigation led by the National Transportation Safety Board [1] indicated that a damaged gusset plate under a concentrated loading area, as shown in Figure 1.1, was the main reason for this collapse and concluded that the regular loading rating and annual visual inspections may not be able to adequately detect the gusset plate conditions. Early damage is not easily detected since damage at the incipient stage is a minor-scale phenomenon. The mature global SHM techniques based on analysis of mode shapes and the first few natural frequencies of the host structure are insensitive to minor local damage. For most of the global SHM techniques, the indicators only reflect the global defects of the host structure. To further locate and quantify structural damage, prior knowledge of the damage location and severity is necessary. For this reason, many typical local detection

techniques have been developed, such as ultrasonic techniques and impact echo testing. Nevertheless, the obvious drawback of such techniques is that the costly and sophisticated equipment, which becomes a limitation for practical application.

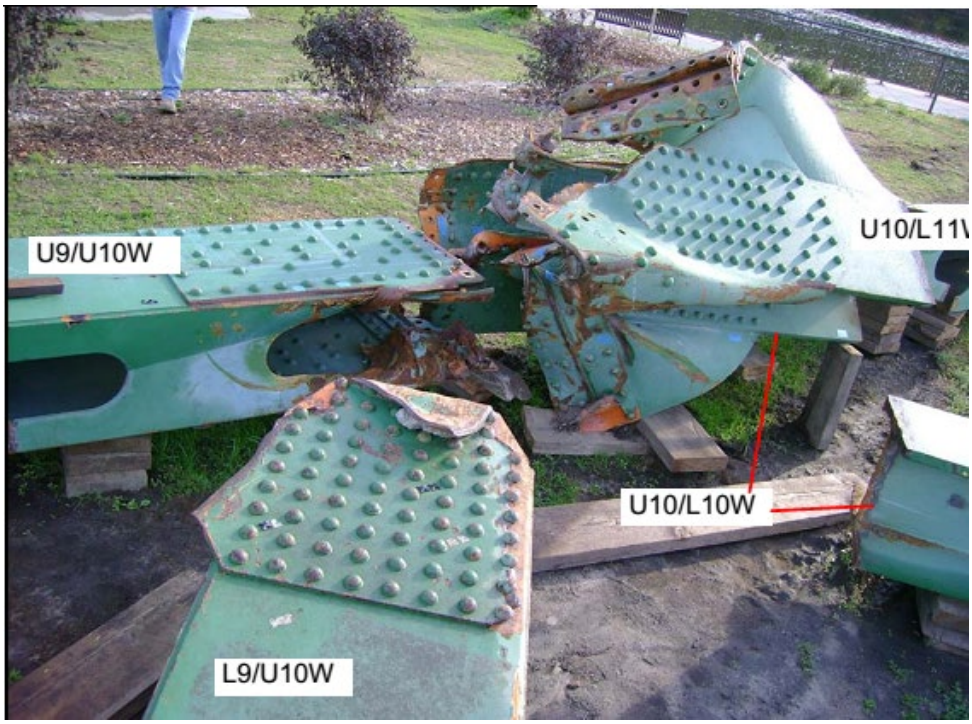

Figure 1.1 Failure node U10 in the I-35W bridge [1]

On the other hand, developments in the application of smart material based SHM systems have attracted the interest of many researchers. The piezoelectric transducer has been widely applied as a transducer patch that can be attached to the structural surface to monitor structural health conditions. Researchers have intensively explored the potential of piezoelectric material in replacing the currently available local damage detection techniques. By making use of the advantages of a piezoelectric transducer, the electromechanical impedance (EMI) technique is carried out based on using piezoelectric transducers as both an actuator and a sensor simultaneously. Lead zirconate titanate (PZT) is a kind of piezoelectric material that is commonly used in

PZT transducers. The PZT transducer is able to generate a voltage output when a compressive force is applied. Conversely, an applied electric field can be transferred to a mechanical strain on a PZT transducer. When using EMI-based techniques for structural health monitoring, PZT patches are bonded onto the surfaces of the monitored structures and are excited directly by an alternating voltage sweep signal using a signal generator or an impedance analyser, as shown in Figure 2. Although the first-hand measurement of the mechanical properties of the host structure is difficult, the electrical impedance of a PZT transducer can directly reflect the changes in the mechanical impedance of the monitored structure. Recent applications of the EMI based SHM methods have shown promising success in detecting the local damage [2, 3].

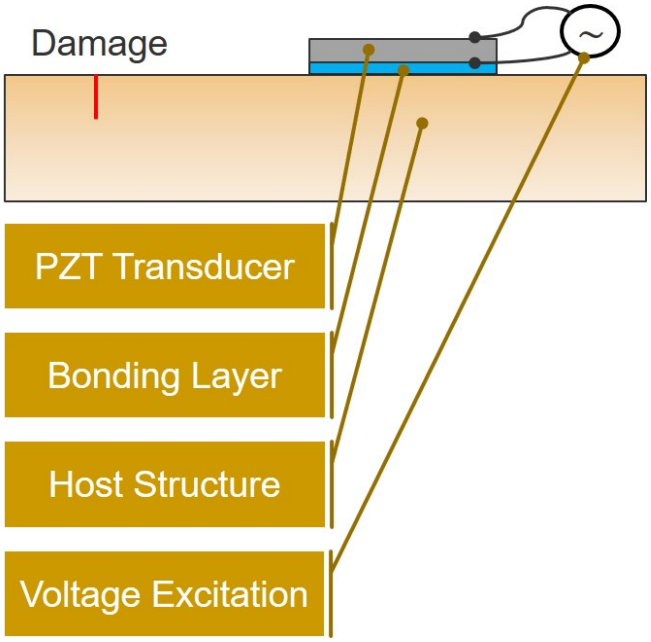

Figure 1.2 Sketch of a PZT patch bonded onto a damaged structure

In the EMI-based SHM methods, the electrical impedance signature in the frequency domain is the main evidence for structural health evaluation. Efforts have been put forth to develop reliable statistical indicators for analysing impedance signatures and

describing the differences between them. Even though a number of applications based on these statistical indicators are reflected in the available literature, various limitations related to the sensitivity of complex structures, such as a gusset plate in steel truss structures as mentioned above, are still waiting to be overcome [4].

Furthermore, the non-model based EMI technique depends on analysing the difference between baseline and current impedance signatures. It is not able to provide detailed information on damage, such as the location and severity, since the cases with minor damage closer to the measured location and severe damage far from the measured location may have the same damage indicator value [5]. This is a significant limitation of most current non-model based EMI methods for structural damage detection.

To precisely locate and quantify structural damage, the model-based EMI technique is developed based on the sensitivity of the impedance signature and model updating. The basic idea of the model-based EMI technique is similar to that of the sensitivity-based global SHM methods using dynamic response sensitivity. The impedance responses and their sensitivities to the physical parameters of the structure are calculated. The identification procedure involves solving the inverse problem to find the changes in structural mechanical properties using the changes in electrical impedance. However, sensitivity based model updating for damage detection using measurements is usually an ill-conditioned problem. Since the number of structural parameters usually far exceeds the number of useful and reliable impedance measurements, the identification problem becomes a highly underdetermined problem. In conventional model updating methods using the modal information and dynamic response sensitivities, the Tikhonov regularization method was employed to solve this ill-conditioned problem. However, the results from Tikhonov regularization lead to the damage being distributed among many elements [6].

1.2 Scope and objective of this dissertation

Most current researches on the development and applications of the EMI based SHM techniques analyse the frequency domain impedance signature estimated by Fourier transform and define some damage indicators. Such damage indices are easy to compute and can be used to indicate the occurrence of structural damage. However, their sensitivity in detecting local minor damage, especially in large-size complex structures, is a significant issue and concern. Thus, the first objective of this PhD research is to develop a new structural damage detection approach based on analysing the time-domain impedance responses from piezoelectric transducers. The measured time-domain responses from the piezoelectric transducers will be directly used for the analysis. With the use of the time-frequency autoregressive moving average (TFARMA) model, a singular value decomposition (SVD)-based damage index is defined to detect the damage. The effectiveness and performance of the proposed approach are investigated by experimental studies on a space steel truss bridge model in the laboratory. Four individual piezoelectric transducers are placed at different locations on the bridge model and excited by a sweep-frequency signal. The time-domain impedance responses are analysed with the TFARMA model to calculate the damage index. The proposed damage index will be compared with two other traditional EMI-based damage indices using the frequency-domain impedance to demonstrate the superiority of the proposed approach.

On the other hand, the non-model based EMI techniques show obvious limitations in locating and further quantifying damage. A new structural damage identification approach based on model updating with impedance sensitivity and the sparse regularization technique is developed in this research to identify the damage location and severity in structures. The sensitivities of resonance frequency shifts in the impedance responses to the stiffness parameters of the host structure are calculated and used to identify the damage. Finite element models are developed, enabling the damage identification to be conducted by model updating. To improve the performance of solving the underdetermined inverse problem, the sparse

regularization method is employed in place of the Tikhonov regularization method. Numerical verifications on beam structures are conducted in this research to validate the accuracy of the proposed approach. Experimental studies on aluminium beam structures and plate structures with single and multiple minor damages are conducted to further demonstrate the effectiveness and performance of the proposed approach for structural damage location and quantification. This research is also conducted to investigate the effects of temperature variation and the bonding layer on the proposed approach. Experimental studies are conducted to verify the performance.

1.3 Organization of this dissertation

Chapter 1: A brief introduction of this research is provided. The aim and objectives are also introduced in detail in this chapter. The background knowledge of SHM and conventional vibration-based methods is presented. Then, the need for investigating the EMI technique is discussed.

Chapter 2: A comprehensive literature review is given in three parts. In the first part, a brief review of the conventional global and local SHM methods and their limitations are given. The second part reviews the basic principle of the EMI technique and the applications of the non-model based and model-based EMI techniques. In the third part, the sensitivity-based method for damage detection is reviewed. The limitations of conventional methods are discussed in this chapter. In addition, the motivation and significance of this research are then presented.

Chapter 3: This section investigates using the TFARMA model-based method for processing the time-domain EMI signatures, in place of the conventional statistics based damage indicators, for structural damage detection. A new damage indicator is obtained based on the evaluation spectrum of the TFARMA model. Experimental studies on a laboratory truss structure are conducted to validate the performance of the proposed approach. In the experimental tests, four PZT transducers are bonded on

the surface of the gusset plate at the joint connection between the main truss beam member and chord members. The identification results obtained using the proposed approach for bolt-loosening damage detection are presented and compared with the traditional damage indicators, i.e. root-mean-square deviation (RMSD) and Cross Correlation (CC), based on the impedance signatures between the baseline and damaged structure in the frequency domain. The noise effect on the detection results is also investigated at the end of this section.

Chapter 4: Numerical studies on aluminium beams are conducted to validate the accuracy and effectiveness of using the proposed model-based EMI technique for structural damage identification based on EMI sensitivity and sparse regularization techniques. The finite element models for a free PZT transducer and PZT-structure interaction are developed in COMSOL Multiphysics software and calibrated based on previous experimental studies Lim and Soh [7]. Then an accurate baseline model is established for an aluminium beam with one surface-bonded PZT patch. The simulated damage is identified by using the frequency shifts of the resonance peaks in the impedance responses and the spares regularization method.

Chapter 5: Experimental studies on beam structures in the laboratory are conducted to verify the performance of the proposed approach. The experimental setup is first introduced in this chapter. The modelling method for impedance response calculations developed in Chapter 4 is used to obtain the analytical impedances of the PZT transducer bonded onto the beam structure. The sparse regularization based sensitivity method is then used to identify the damage location and severity. The results obtained from the proposed approach are compared with those from the traditional Tikhonov regularization based sensitivity method. Finally, numerical studies are carried out to investigate the sensitivity range of the proposed approach for a reliable and accurate structural damage identification.

Chapter 6: Experimental studies on plate structures by using the sparse regularization based model updating method and impedance sensitivity are conducted.

A finite element model of a 300×300 mm square plate is developed based on the modelling techniques in Chapters 4 and 5. Damage is introduced in the plate structure as a drill hole. A two-step identification strategy is developed based on the proposed approach. Prediction of the damage location and severity is then presented. In addition, the temperature variation effect on the accuracy of the proposed approach for damage identified in the plate structures is investigated.

Chapter 7: The conclusions and discussion of this research are presented. Future work based on this study is also suggested.

2 Literature review & theoretical background

2.1 Background of conventional SHM methods and applications

2.1.1 Global vibration based SHM technique

The basic concept of SHM is to implement a damage detection strategy. The process includes the extraction of features from the measurements of a structure observed over a period of time and evaluation of these features to determine the state of the system. For global vibration based SHM methods, the structure is subjected to the externally applied global excitation, and the corresponding responses are used to estimate the condition of the structure. The basic vibration characteristics, including natural frequencies and mode shapes identified from the dynamic vibration measurements, are the most commonly used features for vibration based damage detection. A detailed review of the practical applications can be found in Farrar and Worden [8].

The limitation of these techniques based on the first few modes of natural frequencies and mode shapes in the low frequency range, is that they might not be sensitive to the minor structural damage. Since the wavelength of global vibration is larger than that of incipient damage or small cracks, these techniques are not sensitive enough to detect minor changes in the structural physical properties. Additionally, minor damage introduces only very small changes in the global structural parameters.

2.1.2 Local damage detection technique

The basic idea of local damage detection techniques is similar to that of global SHM methods, i.e., analysing features of structural responses corresponding to the external excitation. Only a local specific portion of the whole structure is estimated in the local damage detection techniques. Most of the local damage detection techniques are based on magnetic flux or acoustic waves. For the detection of minor surface cracks,

the magnetic particle inspection technique has been developed using the difference between the magnetic flux passing through the materials that can be magnetized and the cracks. This technique is especially sensitive to surface cracks on metal structures. However, expert skill is required to operate the equipment to obtain satisfactory results. To quantify the crack depth and the damage beneath the surface of the structure, the eddy current technique uses the ratio of the magnetic flux to the current to detect the distortion of the eddy current passing through the cracks. The main drawback is that the technique cannot distinguish the length and depth of an oblique crack, which could lead to damage overestimation.

The acoustic wave based local damage detection methods normally use the propagation of an ultrasonic wave in the host structure and analyse the reflection or distortion when the wave passes through the damages, as shown in Figure 2.1. Time-of-flight diffraction and the impact echo technique are two of the most commonly used techniques for ultrasonic wave based damage detection. In the time-of-flight diffraction method, several pairs of actuators and receivers are used to measure the diffracted wave generated by the initial ultrasonic wave hitting a crack tip. Through the difference between the reception times of the original wave and the diffracted wave, it is possible to estimate the location and severity of the damage. For the impact echo technique, a reflected wave will be generated when the original wave encounters the damage. The location of the damage can be determined by comparing the features between the original wave and the reflected wave. The major limitation of these techniques is the high cost of the equipment. Moreover, the large size of the wave generator requires a sufficient space to implement the technique, which is unsuitable for small specimens.

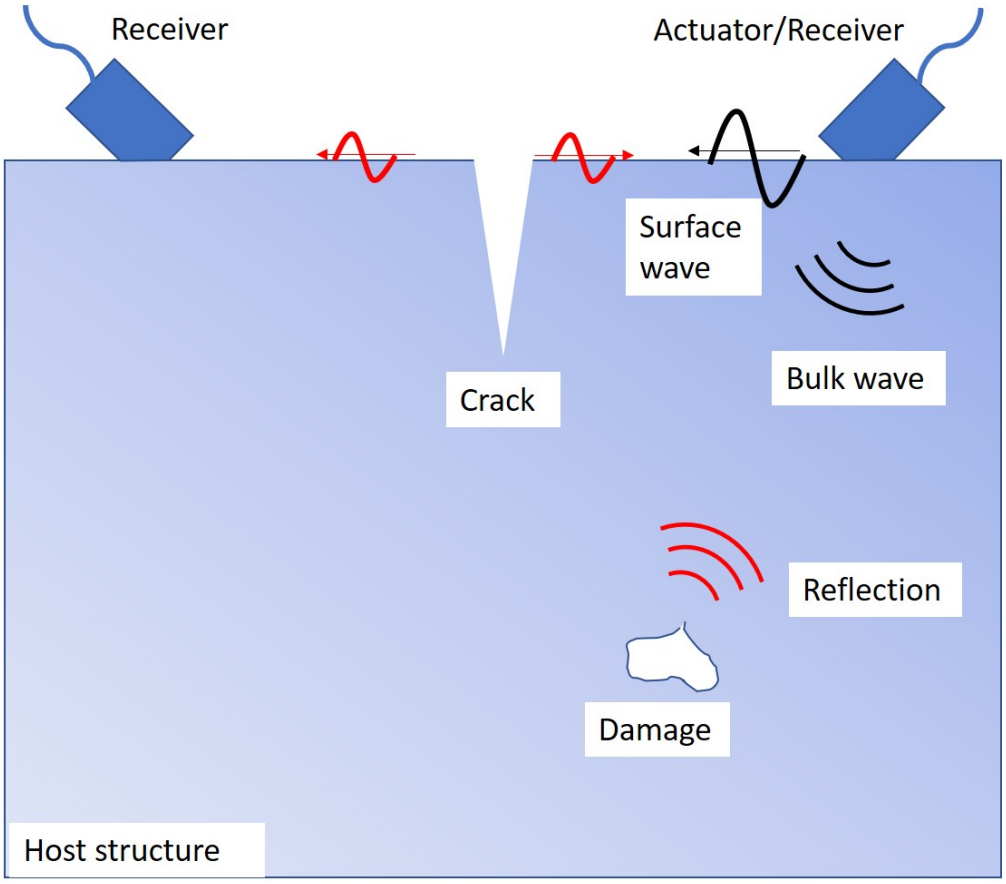

Figure 2.1 Configuration of the acoustic wave based damage detection method

2.2 Electromechanical impedance technique in SHM

2.2.1 Piezoelectricity and Piezoelectric Materials in SHM

Piezoelectricity has been known and demonstrated since 1880 when Pierre and Jacques Curie were studying the effects of pressure on the generation of electrical charge on a group of crystals, such as quartz, tourmaline, and Rochelle salt. They found that these crystals generate an electrical charge when a mechanical strain is applied to them. This effect is the so-called direct piezoelectric effect. The converse

piezoelectric effect was then found in which a mechanical stress is generated when an electrical field is applied. In the 1950s, lead zirconate titanate (PZT) was discovered, which then became the most widely used piezoceramic.

The direct and converse piezoelectric effects can be expressed by the general constitutive equations given by the IEEE Standard [9]:

$$S_k = d_{jk}^c E_j + s_{km}^E T_m \tag{2.1}$$

$$D_i = \varepsilon_{ij}^T E_j + d_{im}^d T_m \tag{2.2}$$

Where s_{km}^E is the mechanical compliance of the material measured at zero electric field and ε_{ij}^T is the dielectric permittivity measured at zero mechanical stress. The variable d_{im}^d is the piezoelectric coupling between the electrical and mechanical variables. $[D]$ is the electric displacement vector, $[S]$ is the second-order strain tensor, $[E]$ is the applied external electrical field vector, and $[T]$ is the stress tensor. Equation (2.2) reflects the direct piezoelectric effect, while Equation (2.1) refers to the converse piezoelectric effect. The constitutive equations can be rewritten into compressed matrix notation:

$$\begin{bmatrix} D \\ S \end{bmatrix} = \begin{bmatrix} \varepsilon^T & d_d \\ d_c & s^E \end{bmatrix} \begin{bmatrix} E \\ T \end{bmatrix} \tag{2.3}$$

Figure 2.2 shows the common configuration of the rectangular piezoelectric plate to introduce the direct effect, where E is the electrical field applied on the PZT transducer. A PZT transducer is normally manufactured into a symmetrical shape. Therefore, the stress tensor can be simplified into a 6×1 vector,

$[T]=[T_{11},T_{22},T_{33},T_{44},T_{55},T_{66}]^T$, as well as the stress tensor $[S]=[S_{11},S_{22},S_{33},S_{44},S_{55},S_{66}]^T$. The piezoelectric strain coefficient matrix is determined by the structure of the crystal. For a PZT transducer, the matrix $[d_c]$ is given by

$$[d_c]=\begin{bmatrix} 0 & 0 & d_{31} \\ 0 & 0 & d_{32} \\ 0 & 0 & d_{33} \\ 0 & d_{24} & 0 \\ d_{15} & 0 & 0 \\ 0 & 0 & 0 \end{bmatrix} \tag{2.4}$$

In Equation (2.4), the coefficients d_{31}, d_{32} and d_{33} denote the resulting strains on planes 1-3, 2-3 and 3-3, respectively, for an externally applied electrical field on axis 3. Coefficient d_{24} is the shear strain in plane 2-3 under the applied electrical field E_2. Coefficient d_{15} relates the shear strain in plane 1-3 to the electrical field E_1. Kumar [10] noted that the sensing capability of a PZT transducer is significantly related to coefficients d_{31} and d_{33}, and their numerical values should be maximized while the mechanical loss factor ε_{33} should be minimized.

The compliance matrix $[S]$ is given as

$$\left[s^E\right]=\begin{bmatrix} s_{11} & s_{12} & s_{13} & 0 & 0 & 0 \\ s_{21} & s_{22} & s_{23} & 0 & 0 & 0 \\ s_{31} & s_{32} & s_{33} & 0 & 0 & 0 \\ 0 & 0 & 0 & s_{44} & 0 & 0 \\ 0 & 0 & 0 & 0 & s_{55} & 0 \\ 0 & 0 & 0 & 0 & 0 & s_{55} \end{bmatrix} \tag{2.5}$$

In general, the PZT patch is polarized in the thickness direction, axis 3. Therefore, the electrical field is applied in this direction, while the mechanical stress and strain act on axis 1 and axis 2. Thus, the electromechanical coupling of 31 and 32 is mainly analysed. The electrical input along the thickness direction E_3 induces the surface strains S_{11} and S_{22}.

For a PZT transducer, the permittivity matrix can be expressed as

$$\left[\varepsilon^T\right]=\begin{bmatrix} \varepsilon_{11}^T & 0 & 0 \\ 0 & \varepsilon_{22}^T & 0 \\ 0 & 0 & \varepsilon_{33}^T \end{bmatrix} \tag{2.6}$$

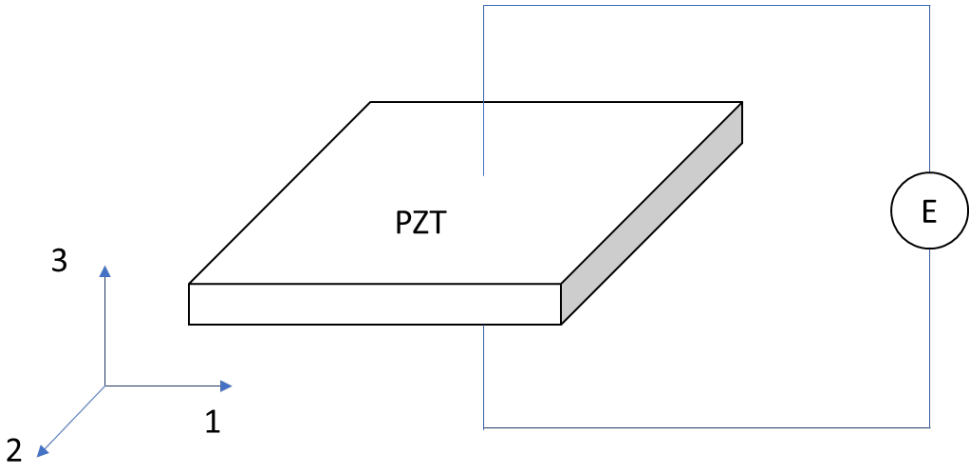

Figure 2.2. Sketch of a piezoelectric element with excitation voltage

In recent decades, piezoelectric materials as active sensors have attracted the interest of many researchers. For non-destructive evaluation, low-cost PZT transducers have been developed as actuators for the generation and sensing of guided waves. PZT transducers have been investigated with a continuous sinusoidal or pulsed excitation using the wave propagation technique [11, 12].

Since the EMI technique was presented a decade ago, efforts have been made toward its improvement and application. In the EMI technique, the PZT transducer actuates the host structure and senses the response simultaneously. The electrical signature directly reflects the changes in the mechanical properties of the host structure. The advantages of the EMI technique include the following [13]: 1) the technique uses light, non-intrusive small-size transducers that can monitor inaccessible locations; 2) the piezoelectric transducers have a large range of linearity, a fast response, a high conversion efficiency and long-term sensitivity; and 3) due to the high working frequency, the technique is sensitive to detect the minor damage.

2.2.2 Principle of the EMI technique

The basic principle of the EMI technique is similar as that of the vibration based SHM method. However, the PZT transducer plays the role of both actuator and sensor simultaneously. Furthermore, the working frequency is generally higher than 10 kHz, which is much higher than the conventional vibration based methods [14]. In such a high frequency range, the wavelength is small enough to make the EMI technique sensitive to minor changes in structural properties. On the other hand, the localized detection area causes the electromechanical impedance to be less dependent on the boundary conditions. Park et al. [15] noted that multiple frequency ranges containing 20 to 30 peaks are normally selected for damage evaluation due to the fact that a higher density of modes implies a larger dynamic interaction.

In the EMI-based SHM method, the PZT transducer surface is bonded onto or embedded into the host structure. An impedance analyser will drive the transducer by a sinusoidal alternating voltage. Due to the piezoelectric effect, the force generated by the PZT patch will excite the host structure to vibrate, and the electrical response of the PZT transducer is directly related to the mechanical impedance of the host structure. Thus, the changes in the electrical impedance of the PZT patch can be utilized to detect changes in the mechanical properties of the host structure. The circuit for the PZT-based electromechanical impedance measurement is shown in Figure 2.3. The electrical impedance can be calculated by dividing the driving voltage of the PZT transducer by the current passing through the transducer. An approximation of the impedance is estimated by taking the ratio of the fast Fourier transform analysis of the supply voltage V_i to the voltage V_o across the sensing resistor R_s, I is the current through the sensing resistor [2].

$$Z = \frac{V_i}{I} = \frac{V_i}{V_o / R_s} \tag{2.7}$$

PZT is a capacitive element in the circuit. Thus, the current passing through it increases with frequency. To solve this, the inverting amplification circuit can be used to provide a larger output voltage [15].

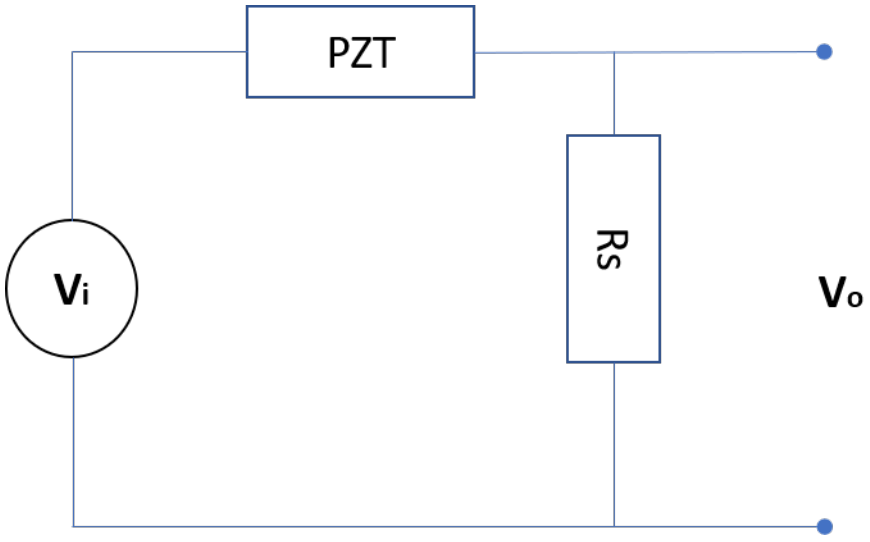

Figure 2.3 Circuit for measuring electrical impedance

2.2.3 Signal processing and evaluation of the non-model-based EMI technique and its applications

Generally, analytical modelling of the response of a PZT transducer is not required for the traditional EMI-based damage detection methods since they are based only on correlating the measured impedance signals before and after damage. The impedance response in the frequency domain is most commonly used for damage detection. To detect the existence of structural damage, the impedance signature for the undamaged structure is compared with that measured from the damaged structure. The statistical damage index, i.e., the-root-mean-square deviation (RMSD), was proposed by Sun et al. [16] to detect the occurrence of damage in a typical aluminium-frame structure by

defining a threshold. The difference between impedance signatures can be quantified by using the RMSD as

$$RMSD(\%) = \sqrt{\frac{\sum_{j=1}^{N}\left(G_j^1 - G_j^0\right)^2}{\sum_{j=1}^{N}\left(G_j^0\right)^2}} \tag{2.8}$$

where G_j^1 is the measured impedance signature from the current state and G_j^0 is the impedance response from the structure under the healthy state.

The correlation coefficient (CC) has also been obtained to quantify the changes in the impedance signatures. CC is given as:

$$CC = \frac{\frac{1}{N}\sum_{i=1}^{N}\left(x_i - \overline{x}\right)\left(y_i - \overline{y}\right)}{\sigma_X \sigma_Y} \tag{2.9}$$

where $\overline{x}$ and $\overline{y}$ denote the average of the pristine impedance x and measured impedance y, respectively. σ_x and σ_y are the standard deviations of two impedance signatures, N denotes the number of impedance data. For two same impedance signatures, their correlation coefficient is equal to 1. Other damage indicators, such as the correlation coefficient deviation (CCD) and the mean absolute percentage deviation (MAPD), have also been developed for the same purpose. The comparison between these indicators shows that RMSD is the most sensitive one for the detection of new occurrence of damage, while CC and CCD are more suitable for the detection of the extent of increasing damage ([17, 18]).

Based on the development of the statistical damage indicators, the EMI technique has been widely applied for the health monitoring of several structures in different areas.

In the study by Raju et al. (1998), PZT patches were attached to a composite reinforced concrete wall to detect structural failure under loading. In 2014, an experimental study on the monitoring of concrete strength based on embedded PZT transducers was carried out by Wang et al. (2014). Sohn et al. (2003) investigated the EMI technique on a simulated three-story moment-resisting frame structure and monitored the bolt loosening on the brackets. Park et al. (2008) implemented the k-mean clustering–based unsupervised pattern recognition with the electromechanical impedance-based wireless SHM system to detect bolt loosening in a bolt-jointed aluminium structure. Pavelko et al. (2014) applied the EMI technique on a Mi-8 helicopter tail beam to monitor the condition of its bolt joints. Wang et al. (2007) used the impedance characteristics to detect a crack in a Timoshenko beam structure. Park et al. (2005) presented the results of a feasibility study on an impedance-based damage detection technique using the thickness modes of PZT patches for steel structural members. The frequency-domain impedance responses were compared between undamaged and damaged structures to detect the existence of damage. Sun et al. [19] presented a debonding identification method for RC beams strengthened with FRP based on PZT impedance transducers.

It can be noted that the above-mentioned studies based on the difference between baseline and current impedance signatures are not able to provide detailed information on damage, such as the location and severity, since scenarios with minor damage closer to the measured location and severe damage far from the measured location may have the same indicator value [5]. This is a significant limitation of most current non-model based EMI methods for damage detection.

On the other hand, most of the conventional EMI techniques use the frequency domain impedance signature, which is processed by fast Fourier transformation (FFT). Such damage indices are easy to compute and can be used to indicate the occurrence of structural damage. However, their sensitivity in detecting local minor damage, especially in large-size complex structures, is a significant issue and concern. Only a few studies about processing the time domain impedance signature with other

signal processing approaches have been developed in this field. Vieira Filho et al. [20] carried out time domain analysis of the electromechanical impedance signature using multilevel wavelet decomposition instead of FFT. The new method is significantly more sensitive to detect the damage than the frequency domain based EMI technique. Thus, research on the new processing method of the impedance response is necessary to improve the performance of the EMI technique.

Due to computational efficiency and performance, such non-parametric damage indicators have been widely used. However, they may not be used for damage quantification [21]. Efforts have been made to enhance the performance of approaches based on statistical indicators. Taking advantage of the machine learning approaches for pattern recognition, such as artificial neural networks (ANNs) and clustering analysis, EMI-based methods have been combined with different machine-learning algorithms and used for extending the capacity of the conventional methods.

In 2000, Lopes et al. [22] presented a non-model based EMI technique for damage location and characterisation by combining the EMI approach with an ANN. In their research, the area, root-mean-square value and correlation coefficient of damaged and undamaged impedance signatures are utilized to train the network. Experimental studies on a $1/4$ scale bridge section and a spare truss structure were used to verify the performance of the proposed method. The results showed that this technique can be applied to a complex structure for which no prior model is available. In 2012, a similar technique was applied to a real scale bridge to detect multiple damages by Min et al. [23]. Impedance signatures were split into multiple sub frequency ranges. The correlation coefficient of each range of the impedance signature was utilized for the training of the neural network. In this test, bolt loosening and notches were implemented on the structure at the same time. The proposed method correctly classified these two kinds of damage. In 2005, Giurgiutiu and Zagrai [24] studied damage detection using EMI technique combined with a probability neural network. The analytical two-dimensional model for a thin-wall structure was included in this

study to predict the electromechanical impedance for implementation of a probability neural network. The CCD metric was applied to estimate impedance responses, showing the change between the pristine and damaged situations. Since the severity of damage and the distance between the PZT transducer and damage both influence the value of the statistical indicators, estimating the exact location becomes extremely difficult with the conventional EMI technique. Na and Lee [25] investigated the improved EMI technique with the neural network approach to predict the damaged area of a composite structure. The 20 cm square composite plate was divided into 6 parts, and the location of the drilled hole was successfully identified by 3 PZT transducers. In 2013, Selva et al. [26] presented a damage localization method using EMI combined with an ANN as well. The experimental study in a carbon fibre-reinforced plate with fixed boundaries showed the correct identification in 6 pre-set areas using the impedance signatures of three PZT transducers.

The above-mentioned methods were demonstrated to effectively identify multi-type damages, quantify the severity of damage and locate damage under defined levels based on recognised patterns from a large numbers of data samples. Nevertheless, the methods only classify phenomenological characterizations of the changes in impedance curves under specific patterns as well as in the statistical indicators, and they still cannot accurately relate the changes of impedance responses to changes in the structural physical properties, such as stiffness, mass or damping [27]. To quantify in detail the structural damage by the EMI technique, an accurate model is necessary to provide the prediction of impedance signatures.

2.2.4 Modelling of EMI and the model-based EMI technique

Analytical models

Liang et al. [28] first presented that the one-dimensional interaction of a PZT transducer and the host structure is governed by the following equation

$$Y(\omega) = \frac{I}{V} = i\omega a(\bar{\varepsilon}_{33}^{T} - \frac{Z(\omega)}{Z(\omega) + Z_a(\omega)} d_{3x}^2 \hat{Y}_{xx}^{E}) \tag{2.10}$$

where Y denotes the electrical admittance (the inverse of impedance) of the PZT transducer, the two-dimensional wave number $\kappa = \omega\sqrt{\rho\left(1-\upsilon^2\right)/E_p}$, and Z and Z_a denote the mechanical impedance of the PZT transducer and the host structure, respectively. Y_{xx}^{E} is the complex Young's modulus. $\bar{\varepsilon}_{33}^{T}$ denotes the complex electric permittivity. d_{3x} is the piezoelectric strain coefficient between directions X and 3. ω is the he angular frequency of the driving voltage and a is a geometric constant of the PZT. In this equation, only parameter Z_a is determined by the properties of the host structure, which can be derived as:

$$Z_a = \frac{\kappa\omega_a h_a Y_{11}^{E}}{(i\omega)\tan(\kappa l_a)} \tag{2.11}$$

The first term in the bracket of Equation (2.10) is the capacitive admittance of a free PZT transducer. The second term in the bracket of this model includes the mechanical impedance of PZT itself and the host structure's mechanical impedance. For a bonded PZT transducer, it can be assumed that its own impedance is constant. Any variation in electrical admittance would be attributed to a change in structural parameters. Consequently, the electrical impedance measurement of a PZT transducer is directly related to the mechanical properties of the host structure.

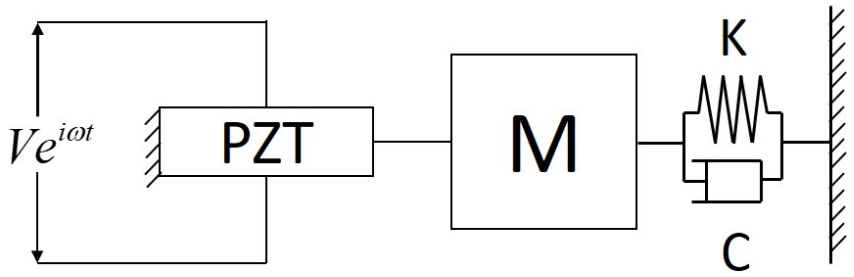

Figure 2.4 One-dimensional model for the electrotechnical impedance of a PZT patch

Since Liang et al. [28] first proposed an analytical model of EMI, efforts have been made to enhance the performance of the model for the PZT-structure interaction. A two-dimensional electromechanical impedance model was then developed by Zhou et al. [29]. In their research, the one-dimensional impedance model is extended to a two-dimensional model. The direct mechanical impedance and cross-impedance between the x and y directions are involved in this model, as shown in Figure 2.4. Based on this definition, the output impedance of a PZT transducer can be governed by the equation

$$Y = i\omega \frac{w_p l_p}{h_p}\left[\bar{\varepsilon}_{33}^{T} - \frac{2d_{33}^2 E_p}{(1-\upsilon)} + \frac{d_{33}^2 E_p}{(1-\upsilon)}\left\{\frac{\sin\kappa l_p}{l_p}\frac{\sin\kappa w_p}{w_p}\right\} N^{-1}\begin{Bmatrix}1\\1\end{Bmatrix}\right] \tag{2.12}$$

where υ denotes Poisson's ratio, w_p, h_p and l_p are respectively the width, thickness and length of the PZT patch, and the matrix N can be calculated as

$$N=\begin{bmatrix} \kappa\cos(\kappa l_p)\left\{1-\upsilon_a\frac{w_p}{l_p}\frac{Z_{xy}}{Z_{axx}}+\frac{Z_{xx}}{Z_{axx}}\right\} & \kappa\cos(\kappa w_p)\left\{\frac{l_p}{w_p}\frac{Z_{yx}}{Z_{ayy}}-\nu_a\frac{Z_{yy}}{Z_{ayy}}\right\} \\ \kappa\cos(\kappa l_p)\left\{\frac{w_p}{l_p}\frac{Z_{xy}}{Z_{axx}}-\nu_a\frac{Z_{xx}}{Z_{axx}}\right\} & \kappa\cos(\kappa w_p)\left\{1-\upsilon_a\frac{l_p}{w_p}\frac{Z_{yx}}{Z_{ayy}}+\frac{Z_{yy}}{Z_{ayy}}\right\} \end{bmatrix} \quad (2.13)$$

where Z_{axx} and Z_{ayy} denote the mechanical impedance of the PZT transducer in the x and y directions, respectively. Z_{xy} and Z_{yx} are the cross-impedances of the host structure. In the study by Rogers [13], the two-dimensional impedance model is enhanced and then applied to plate, shell and beam structures. They verified the performance of the generic impedance model and noted that the stiffening effect of the piezoelectric transducer significantly influences the dynamic performance of the host structure. Even though the two-dimensional model can provide an accurate prediction of the impedance signature, the number of unknowns is larger than the number of equations. Thus, this highly indeterminate model is limited in its direct application for the extraction of the mechanical impedance of the host structure.

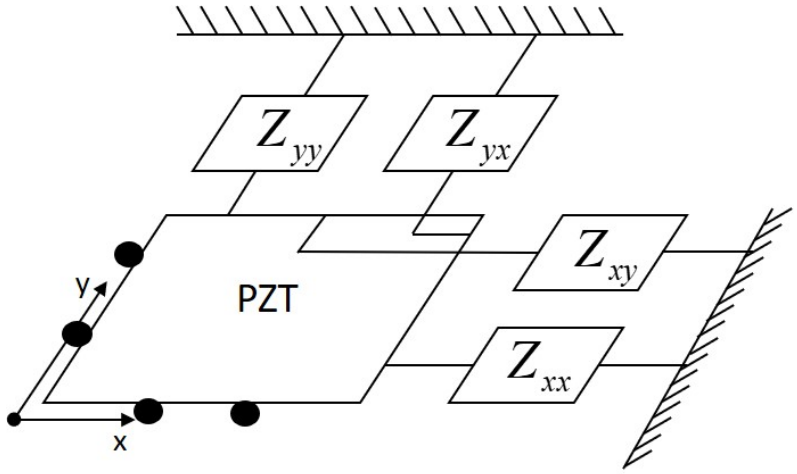

Fig 2.5 Sketch of a two-dimensional model for the electromechanical impedance of the PZT-structure interaction

To overcome the drawbacks of the existing two-dimensional models for impedance calculations, Bhalla and Soh [30] used an effective impedance instead of the mechanical impedance, which was directly restricted at the end points of the PZT patch. They noted that the actual interaction between the transducer and the host structure is on the whole edge of PZT patch. An effective velocity was adopted in their study to ensure that the force transmission between the PZT transducer and the host structure occurs along the entire boundary of the transducer. The effective displacement of the PZT transducer $u_{eff} = \delta A / p_0$, where δA denotes the change in the surface area of the PZT transducer and p_0 denotes the perimeter in its undeformed condition. Thus, the effective mechanical impedance of the PZT patch is defined as

$$Z_{p,eff} = \frac{\iint_S f \cdot \hat{n} ds}{\dot{u}_{eff}} \tag{2.14}$$

where $\hat{n}$ is the unit vector normal to the boundary. Based on the definitions, the output electrical impedance can be calculated by the following equation

$$\overline{Y} = 4\omega j \frac{l_p^2}{h_p}\left[\varepsilon_{33}^T - \frac{2d_{31}^2 \overline{Y}^E}{(1-\upsilon_p)} + \frac{2d_{31}^2 \overline{Y}^E}{(1-\upsilon_p)}\left(\frac{Z_{p,eff}}{Z_{s,eff}+Z_{p,eff}}\right)\left(\frac{\tan \kappa l_p}{\kappa l_p}\right)\right] \tag{2.15}$$

where $Z_{s.eff}$ is the effective impedance of the host structure. The performance of this new model is further verified by Bhalla and Soh [31]. Experimental studies of surface-bonded PZT patches on concrete structures show that the new methodology provides more accurate predictions than the conventional model. In 2005, Yang et al. [32] developed a two-dimensional impedance model for a plate structure based on the Rayleigh-Ritz method. The force impedance at the boundary of the PZT transducer was used to present the effect of the host structure in EMI signature. The study was

based on the assumption that the dimensions of the structure are much larger than those of the PZT transducer and that the transducer is not close to the boundary of the host structure. The results of experimental studies have shown that the model can acceptably predict the electromechanical impedance of the PZT-structure interaction system.

Three-dimensional models for impedance prediction were first presented by Annamdas and Soh [33]. In their study, the three-dimensional interaction between the PZT patch and the structure considered both extensional and longitudinal actuations of the transducer. The model was experimentally verified using a PZT transducer embedded in the epoxy bonding layer of a sandwiched aluminium plate and a PZT transducer surface bonded to an aluminium plate.

Based on these modelling approaches, the analytical expressions of the EMI for some simple structures have been obtained [17, 34-37]. In 2014, Park [38] investigated the EMI of a PZT transducer from the perspective of wave propagation using an analytical model. In this study, a two-dimensional model of a PZT patch surface bonded to an aluminium beam was developed, and the first flexural wave group induced by the PZT transducer was compared with the finite element analysis. It is found that the sensing region of the PZT transducer depends on the material damping, which significantly influences the travel distance of the flexural waves induced by the PZT transducer. In 2014, Sepehry et al. [39] developed a PZT-plate interaction model considering the temperature effect using the Rayleigh-Ritz method.

Although these simplified analytical models provide a physical understanding of the interaction between the PZT transducer patch and the host structure, the accuracy of the impedance calculation results will be significantly affected by the complicated boundary conditions and complexity of geometrical configurations. The key problem for an analytical model of EMI simulations is the analytical expression of the structural mechanical impedance Z_s. Since the structural damage may possibly change the structural properties inhomogeneously, it is very difficult to derive an analytical

model. Thus, obtaining insight into the relationship between the EMI signature and changes in structural mechanical properties using only analytical expressions for EMI is not easy. To achieve more accurate impedance signature predictions, numerical models are developed to obtain a closer approximation.

Numerical models

To improve the accuracy of the EMI model, the finite element method is used to express the PZT-structure interaction. In 1990, Lerch [40] applied the finite element method to perform the vibration analysis of piezoelectric sensors and actuators with arbitrary structures. The objective was to use the simulation results to optimize the device with piezoelectric transducers. This research revealed deeper insights into the physical mechanisms of the acoustic property of piezoelectric media. Fairweather and Craig [41] first developed a semi-analytical model to predict the impedance output of a PZT transducer. The model embedded the finite element method to express the physical properties of the host structure and to simplify the PZT patch as a force or moment. The model used the advantage of finite element analysis in the modelling of anisotropic material and non-uniform boundary conditions.

Since commercially available finite element modelling software packages have become convenient tools for researchers, a number of studies have been carried out based on the commercial packages, i.e., ANSYS, ABAQUS and COMSOL Multiphysics. In 2007, Annamdas and Soh [42] developed a three-dimensional finite element model in ANSYS for calculating the EMI responses. The model only considered one quadrant of the specimen due to symmetry in the X and Y directions. The host structure, PZT patch and bonding layer were all involved in their study. A three-dimensional brick element was used to mesh the model.

In 2008, Yang et al. [43] presented a numerical simulation of a free PZT patch and a PZT-structure interaction. Various finite element simulations were investigated in

their study considering the effects of the bonding layer and variation in temperature. The commercial finite element analysis software ANSYS version 8.1 was used to accurately simulate the electrical impedance for a freely suspended PZT transducer, an aluminium beam and an L-shaped aluminium beam with surface-bonded PZT transducers. Zhang et al. [44] presented a quantitative simulation of the impedance response of a Timoshenko beam with a crack. The shear lag model was adopted to express the load transfer between the PZT transducer and the host structure. Based on an accurate numerical simulation using ANSYS software, a parametric study of the effect of the crack and the inertial force on impedance was carried out. The results showed that the accuracy of damage identification is influenced by the frequency range of the impedance signature. In 2014, a damping model for EMI simulation was discussed by Lim and Soh [7]. It is noted that using a hysteretic damping model in place of the conventional Rayleigh damping model can significantly improve the accuracy of predictions. Compared with Rayleigh damping, the hysteretic damping model is more suitable for the analysis of a large frequency range. The advantages of the finite element modelling method include the achievement of a more accurate result for a structure with complex geometry and material, the involvement of the entire PZT transducer in the simulation instead of simplifying the patch as a force or moment acting on points or boundaries and the ability to physically simulate the bonding layer.

Based on the development of finite element models for the EMI technique, efforts have been made to investigate structural damage using finite element method. Annamdas [3] successfully predicted the impedance response using a finite element model of a damaged beam before the propagation of a crack was obtained. Using the analytical approach, it is hard to achieve an accurate simulation of impedance for complex geometries, such as hollow structures or those containing a slot. Hamzeloo et al. [45] developed a finite element model for a hollow structure using ABAQUS software. In their research, crack damages were implemented on the host structure,

and the simulation result showed a promisingly high accuracy compared with the experimental study.

It is well known that the finite element model requires a fine mesh size which is smaller than the wavelength involved. Due to the high frequency range of the EMI technique to achieve the precise prediction of a dynamic response, the finite element model needs a large number of elements, requiring high computation costs for the simulation of an accurate impedance response. To improve the computational efficiency, an investigation of modelling EMI by making use of the spectral element method (SEM) was carried out. Since Doyle [46] presented an analysis of the wave propagation problem using the SEM with an infinite number of wave trains at different frequencies, studies solving the high frequency impedance problem by the SEM have attracted the interest of many researcher. Esteban [47] developed the spectral element model incorporated with the one-dimensional analytical model (Liang et al. [28]) to evaluate the sensing region of the EMI of a PZT transducer. Ritdumrongkul et al. [48] simulated bolt joint connections using a modified SEM model based on the study of Lee and Kim [49] about the active constrained layer SEM model. Compared with the finite element model, although the SEM model can be more efficient in predicting the high frequency impedance response, the method cannot be applied to a structure with complex geometry and boundary conditions.

By combining the advantage of a numerical model of EMI with the sensitivity-based model updating method, the model-based impedance method was developed for damage detection. Wang and Tang [21] applied the spectral element model for a beam structure with a surface-bonded PZT transducer and employed inverse sensitivity analyses to detect structural damages. The location and severity of damage, which are simulated as a stiffness reduction, were identified. In 2014, Kim and Wang [27] developed the adaptive piezoelectric circuitry based on the research of Wang and Tang [21] to improve the accuracy of damage identification by enriching the measured data. Nevertheless, as mentioned above, these studies only developed the

one-dimensional beam model for the host structure, under stationary conditions, because of the limitation of SEM in modelling structures with complex geometry.

In conventional model-based EMI damage detection methods, the impedance amplitudes of frequency points around each resonance frequency peak are employed for damage detection to enrich the measurements. However, structural property changes cause not only variations in the impedance amplitudes but also frequency shifts of the resonances of the impedance curves [50]. This frequency shift is more sensitive to structural damage than the change in amplitude. Furthermore, the model-based damage detection method requires a highly accurate simulation result. Ensuring that the simulation result of every frequency point is a good match to the test result is quite difficult. Minor errors in the baseline model could cause large false predictions in the identification result. In addition, it is difficult to select frequency points in impedance curves to ensure the full rank of the sensitivity matrix. Therefore, the resonance frequency shifts in impedance curves are adopted for updating the EMI model and identifying structural damage in this study.

2.3 Sensitivity-based model updating method in SHM

2.3.1 Sensitivity-based model updating and Tikhonov regularization

The sensitivity-based model updating method is one of the most popular and practical methods for finite element model updating. The basic idea of this method is minimizing the discrepancy between analytical prediction and experimental result to estimate changes in structural properties. First, the method seeks the relationship between small changes in the measurements and small changes in the parameters that need to be identified. The relationship can be expressed as:

$$\Delta\lambda = S\Delta\theta \tag{2.16}$$

where $\Delta\theta$ represents the changes in the structural parameters, $[S]$ is the sensitivity matrix, and $\Delta\lambda$ represents the changes in the measurement due to structural damage.

For damage identification using the sensitivity-based model updating method, Equation (2.16) can be rewritten as

$$[S]\{\Delta p\} = \{\Delta\lambda\} \tag{2.17}$$

In Equation (2.17), $\{\Delta p\}$ $(0 \le \Delta p \le 1)$ denotes the damage factor. The damage factor can be calculated using $\Delta p = p_i - p_{i-1}/p_i$, where p_{i-1} and p_i denote the structure parameters in the $i-1$-th and i-th iterations, respectively. Therefore, $\Delta p = 0$ denotes that the host structure is intact, while $p = 1$ means that the host structure is completely damaged. In this study, damage is simulated as a reduction in the width of the cross section of a specific individual segment. $[S]$ is the sensitivity matrix of the changes in measurements with respect to the measurement of structural damages on the host structure. In identifying the location and severity of structural damage based on an accurate numerical model, one difficulty is solving a large number of unknown parameters of the host structure with a limited amount of measured data. To stabilize this inverse problem, one extensively used method for solving such a problem is to use Tikhonov regularization. According to the definition of the Tikhonov regularization method, a least-squares solution $\{\Delta\tilde{p}\}$ by solving the following optimization problem can be obtained

$$\text{Minimize } \left\|[S]\{\Delta p\} - \{\Delta\lambda\}\right\|_2 + \lambda\left\|\{\Delta p\}\right\|_2 \tag{2.18}$$

where $\| \ \|_2$ denotes the l_2 norm.

2.3.2 Sparse regularization for the underdetermined optimization problem

The major limitation of the Tikhonov regularization method is that its solution for the ill-conditioned problem tends to be overly smooth, which means that the predicted damages are usually distributed on many structural segments. This behaviour is not corresponding to the practical structural damage pattern, which only occurs at a few locations. The damage vector of a real damaged structure is usually sparse. Recently, there has been a stream of research efforts on damage identification strategies based on the sparse recovery theory. Wang and Hao [51] discussed the potential application of the compressed sensing (CS) technique in structural damage detection. Hernandez [6] illustrated a damage identification method by using l_1 regularization in place of Tikhonov regularization. Zhou et al. [52] accurately identified structural damages via a l_1 regularization based method using only data of the first few frequencies. Due to the advantage of solving the underdetermined problem with only a few measurements, l_1 regularization is used to replace Tikhonov regularization in this study.

According to the definition, the optimization objective function can be written in the following form with the sparsity restriction [6]

$$\text{Minimize } \left\| [S]\{\Delta p\} - \{\delta_f\} \right\|_2 + \lambda \left\| \{\Delta p\} \right\|_1 \tag{2.19}$$

where $\| \ \|_1$ denotes the l_1 norm. This equation is the Lagrangian form of a *least absolute shrinkage and selection operator* (LASSO) problem, which can be rewritten as

$$\text{Minimize } \left\| [S]\{\Delta p\} - \{\delta_f\} \right\|_2 \text{ subject to } \left\| \{\Delta p\} \right\|_1 \le t \tag{2.20}$$

Both Tikhonov regularization and l_1 regularization can be interpreted as minimizing the same objective function $\left\|[S]\{\Delta p\}-\{\delta_f\}\right\|_2$, but with respect to different constraints, i.e., $\left\|\{\Delta p\}\right\|_1 \le t$ for l_1 regularization and $\left\|\{\Delta p\}\right\|_2 \le t$ for Tikhonov regularization. As seen in Figure 2.6, the constraint region defined by the l_1 norm is a rotated square, while the region defined by the l_2 norm is a circle. The possible solution that lies tangent to the boundary, such as the red line shown in Figure 2.6, is likely to encounter a corner of the l_1 norm constraint on the coordinate axes. This solution possesses a sparse property. For Tikhonov regularization, the point on a boundary possessing a sparse property is not distinguished from other points. Therefore, the solution is more likely to have nonzero coordinates of w_1 and w_2, and is not sparse.

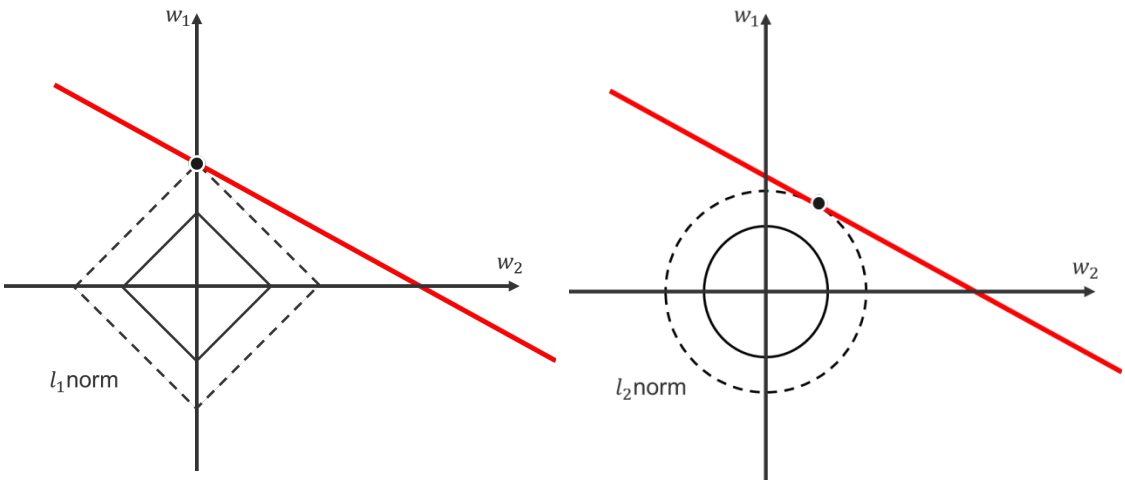

Figure 2.6. Approximate solution of the underdetermined equation using the l_2 and l_1 norms

To solve the l_1 minimization equation, studies have been conducted for numerical methods. Tropp [53] presented a greedy algorithm, orthogonal matching pursuit (OMP), to solve the sparse approximation problem. In 2001, Chen et al. [54] replaced the combinatorial l_0 problem with a convex l_1 problem and solved the convex optimization problem with exploit algorithms. In this study, a spectral projected gradient method is employed to solve the LASSO problem. The complete procedure for this approach was expressed in detail by Van den Berg and Friedlander [55].

2.4 Summary and research gaps

According to the detailed literature review, the EMI technique using self-sensing interrogation has been successfully applied to different structures for monitoring the occurrence of various failure modes. The non-model based approaches utilize statistical damage indicators to estimate the difference between impedance responses to analyse the fault type, location and severity. However, there are two noteworthy limitations of such techniques. First, the sensitivity of the conventional analysis of the impedance response based on the frequency domain for complex structures is a significant issue and concern [5]. Second, the evaluation of changes in the impedance response using statistical indicators is not capable of obtaining detailed information about the damage, such as location and precise severity. This is because such estimation only provides phenomenological characterizations of the impedance changes that do not clearly relate the fault indices to the changes in structural properties. Meanwhile, analytical and numerical models have been obtained to reveal insight into the physical relationship between the impedance response and structural properties. Therefore, the model-based damage identification approach using the EMI technique is developed as an alternative. Nevertheless, there are remarkable challenges in the sensitivity-based damage identification algorithms adopted to solve the model-based EMI approaches. The main difficulty is that attempting to identify a large number of unknown structural properties with a limited number of

measurements leads to the inverse problem becoming highly underdetermined. This could cause large errors and false predictions during identification.

This research investigates the applications of the EMI-based method using a new time frequency analysis method instead of frequency domain methods. The proposed method is applied on a laboratory-scale truss structure to detect bolt-loosening damage. Furthermore, a new model-based EMI technique is developed in this research using finite element analysis to simulate the interaction between a piezoelectric transducer and the host structure. A new sparse regularization based algorithm is applied to solve the underdetermined inverse identification problem with a limited number of available measurement information. Experimental studies are conducted to validate the performance of the proposed approach, including damage detection on a plate structure.

3 Piezoelectric impedance based damage detection with TFARMA

As mentioned in Chapter 2, to quantify the difference between impedance signatures, FFT is one of the most commonly used processing methods in the conventional EMI technique. Time-frequency analysis methods, such as wavelet analysis and Hilbert-Huang transform (HHT), are popular and well adopted in SHM applications [56-61]. The merits of time-frequency analysis methods lie in their ability to reflect both time- and frequency-domain information [62]. An impedance-based SHM technique with a time-frequency analysis method is investigated in this study as one of the potential approaches that can be applied to damage detection for the gusset plates of steel truss bridges. Thus far, few investigations have used other processing methods for impedance signatures for complex structures [20, 63, 64].

The performance of the EMI technique using a new time-frequency signal processing method is validated by detecting bolt-loosening damage in a complex steel structure. In the conventional EMI-based methods, the acquired impedance response is first transferred into the frequency domain using FFT. In this study, the TFARMA model is applied to process the impedance response. Figure 3.1 shows the procedure of the proposed method. The analysis of the impedance response by using the proposed method is carried out based on the time-frequency spectrum of the TFARMA model. A new damage indicator is developed to improve the sensitivity of the EMI-based method.

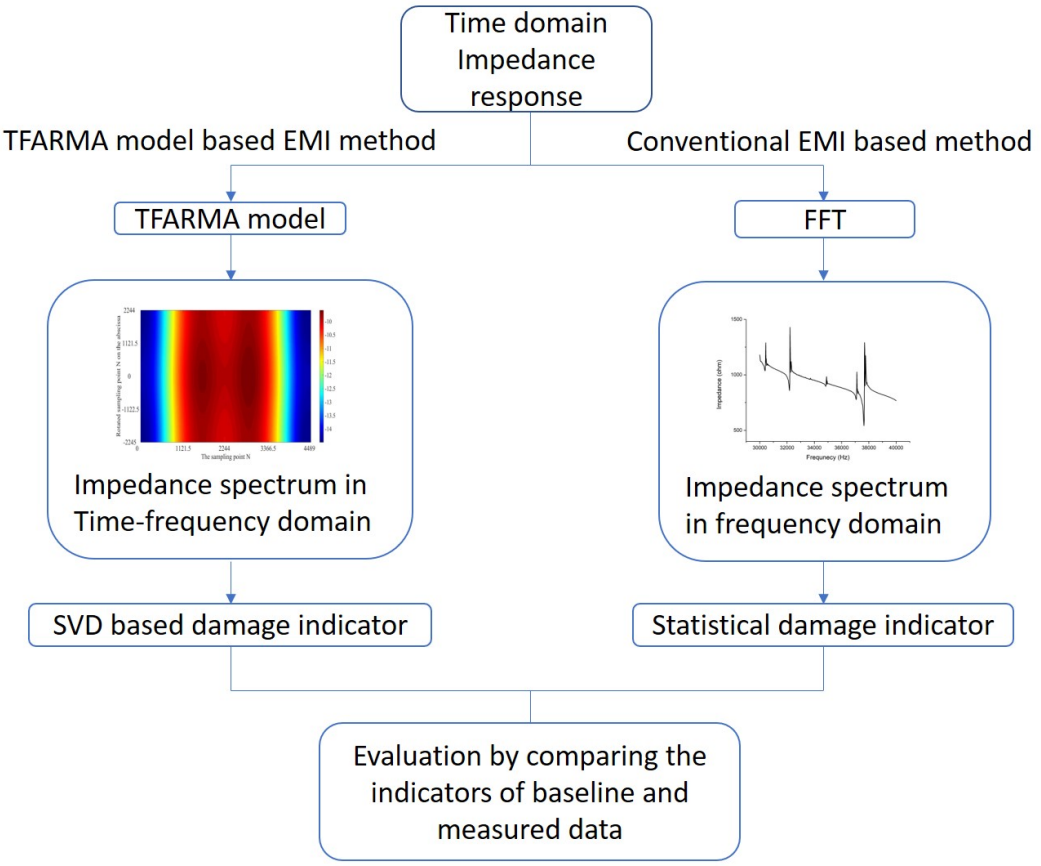

Figure 3.1 Comparison of the conventional EMI-based methods and the proposed TFARMA model-based method

3.1 Time frequency auto-regressive moving average model

The theoretical background of the TFARMA model is briefly presented here. A structural damage detection approach based on TFARMA is proposed with an SVD-based damage index. The main difference between the traditional damage indices, i.e., RMSD and CC presented in Chapter 2, and the proposed damage index is that the present study analyses and represents the impedance data through the TFARMA model in a multi-dimensional space. By analysing the measured time-domain

impedance signals with TFARMA, the feasibility, sensitivity and performance of the proposed approach will be investigated.

The impedance signal from a PZT transducer is a non-stationary random process. The parametric models for random processes, such as auto-regressive (AR), moving average (MA), and auto-regressive moving average (ARMA), are well known and have been applied to signal analysis and system identification. Jachan et al. [65] presented the TFARMA model for non-stationary random processes. Both time delays and Doppler frequency shifts are added to the time invariant ARMA models. The TFARMA model that reveals the non-stationary and spectral correlation is given as [66]

$$x(n) = -\sum_{m=1}^{M}\sum_{l=-L_A}^{L} a_{m,l}\exp(j\frac{2\pi}{N}nl)x(n-m) + \sum_{m=1}^{M_B}\sum_{l=-L_B}^{L_B} b_{m,l}\exp(j\frac{2\pi}{N}nl)e(n-m) \tag{3.1}$$

where *e(n)* is the white noise with variance equal to 1. The time-varying AR parameters a_m and time-varying MA parameters b_m are expressed as

$$a_m(n) = \sum_{l=-L_A}^{L_A} a_{m,l}\exp(j\frac{2\pi}{N}nl) \tag{3.2}$$

$$b_m(n) = \sum_{l=-L_B}^{L_B} b_{m,l}\exp(j\frac{2\pi}{N}nl) \tag{3.3}$$

In above equations, M_A, M_B, L_A and L_B denote the model orders. In this TFARMA model, the under-spread process is applied to obtain the results of non-stationary

processes with small high-lag temporal and spectral correlations. The substance of this process is to assume the lags of the time–frequency shifts to be small values. As a result, the proposed TFARMA model is effective for detecting the slowly varying components of signals.

Parameters $b_{m,l}$ can be estimated by a recursive algorithm based on a complex time-frequency spectrum expressed as

$$b_{m,l} \approx \frac{1}{N} \sum_{m'=0}^{m-1} \sum_{l'=-L_B}^{L_B} \frac{m-m'}{m} b_{m',l'} C(m-m', l-l') \tag{3.4}$$

initialized by

$$b_{0,l} \approx \frac{1}{N} F_{n \to l} \exp\left[\frac{1}{2} F_{l' \to n}^{-1} C(0, l') \right] \tag{3.5}$$

where $F_{\to}(\square)$ and $F_{\to}^{-1}(\square)$ denote Fourier transform and inverse Fourier transform, respectively. The complex time-frequency cepstrum is given by

$$C(m,l) = F_{k \to m}^{-1} F_{n \to l} \log\left[F_{m' \to k} F_{l' \to n}^{-1} A(m', l') \right] \tag{3.6}$$

The ambiguity function is given by

$$A_x(m,l) = F_{n \to l} x(n) x^*(n-m) \tag{3.7}$$

Under the underspread condition, parameters $a_{m,l}$ can be estimated based on the underspread time–frequency Yule–Walker equation [67], which is given as

$$\sum_{m'=1}^{M_A}\sum_{l'=-L_A}^{L_A} a_{m',l'}A(m-m',l-l') = -A(m,l) \tag{3.8}$$

where $m = 1,\ldots,M_A$, $l = -L,\ldots L_A$.

The TFARMA model parameters can be estimated by combining the above estimations of parameters a_m and b_m. Under the underspread condition, the TFAR parameters $a_{m,l}$ can be calculated by the Wax–Kailath algorithm [68], which is given as

$$\sum_{m'=1}^{M}\sum_{l'=-L_A}^{L} a_{m',l'}A_x(m-m',l-l') = -A_x(m,l) \tag{3.9}$$

where $m = 1+M_B,\ldots,M_A+M_B$, $l = -L_A,\ldots L_A$.

For the TFAM part, parameters $b_{m,l}$ can be obtained by the following recursive algorithm:

$$\begin{aligned} b_{m,l} = \frac{1}{N}\sum_{m'=0}^{m-1}\sum_{l'=-L_A}^{L_A}\frac{m-m'}{m}b_{m',l'}A_x(m-m',l-l')\sum_{m''=0}^{m-1}\sum_{l''=-L_A}^{L_A}\frac{m-m'}{m}a_{m'',l''}b_{m'-m'',l'-l''} \\ +\sum_{m'=1}^{m-1}\sum_{l'=-L}^{L}\frac{m-m'}{m}(a_{m-m',l-l'}b_{m',l'}-a_{m',l'}b_{m-'m',l-l'})\sum_{l''=-L_A}^{L_A}a_{m,l}b_{0,l-l'} \end{aligned} \tag{3.10}$$

where $m = 1,\ldots,M$, $l = -L_B,\ldots L_B$ and $L = \max(L_A, L_B)$

After the TFARMA parameters are estimated, the order of the TFARMA model can be calculated according to an information criterion by minimizing the following AIC function

$$AIC(M_A L_A M_B L_B) = \log\left[\frac{1}{N}\sum_{n=0}^{N-1}\left|\hat{e}(n)\right|^2 + \frac{2}{N}\left[M_A(2L_A+1)+(M_B+1)(2L_B+1)-1\right]\right] \quad (3.11)$$

To visualize the TFARMA model parameters and provide a better demonstration for damage detection, the evolutionary spectrum is calculated from the estimated TFARMA model parameters. The evolutionary spectrum of the TFARMA process is defined by [69]

$$P[n,k] \equiv \frac{|B[n,k]|}{|A[n,k]|} \quad (3.12)$$

where

$$A[n,k] = \sum_{(m,l)\in \mathrm{A}} a_{m,l}\, e^{j\frac{2\pi}{N}(nl-km)} \quad (3.13)$$

$$B[n,k] = \sum_{(m,l)\in \mathrm{B}} b_{m,l}\, e^{j\frac{2\pi}{N}(nl-km)} \quad (3.14)$$

In equations (3.13) and (3.14), A and B denote the delay-Doppler support regions given by $\mathrm{A} = \{1,...,M_A\}\times\{-L_A,...,L_A\}$ and $\mathrm{B} = \{0,...,M_B\}\times\{-L_B,...,L_B\}$. M_A and M_B denote the TFAR and TFMA delay order, and L_A and L_B denote the TFAR and TFMA Doppler order, respectively.

3.2 Calculation of TFMA and TFAR parameters

A damage index is defined based on analysing the characteristics of the evolutionary spectra resulting from the TFARMA model. To compare the evolutionary spectra of the healthy and damaged responses from PZT transducers, SVD is applied to identify the pattern of the evolutionary spectrum. It can be expressed as

$$SVD(spectrum^T) = U_{i*j} S_{j*j} V_{j*j} \tag{3.15}$$

where the singular values are given by the diagonal elements of the matrix *S*. The largest singular value corresponding to the first column vector in the matrix *U* reflects the most important principal component of the spectrum; that is, the largest singular value and its associated vector can be used to reveal the characteristics of the evolutionary spectrum.

Base on the SVD results, the damage index from TFARMA model analysis is defined as

$$Damage \quad index = \frac{\|D - H\|}{\|H\|} \tag{3.16}$$

where *H* and *D* denote the first column vectors in matrix *U* from the SVD of the evolutionary spectrum under healthy and damaged conditions, respectively. This damage index quantifies the correlation between the evolutionary spectra from the healthy and damaged structures. All the damage indices, as shown in Equations (2.8), (2.9) and (3.16), have a value from zero to unity, where zero means that the measured responses have a very close correlation and the structure is in a healthy condition, whereas unity means that the measured responses have a very bad correlation and the structure is in a severely damaged condition. These three damage indices are used to

identify the structural conditions. The effectiveness of the proposed approach will be demonstrated in the following experimental studies. The performance of the TFARMA damage index will be compared with that of traditional EMI damage detection techniques based on RMSD and CC damage indices to demonstrate the superiority of the proposed approach.

3.3 Impedance measurements in the time domain

The frequency-domain impedance from PZT transducers is measured by different electrical circuits, as presented by Yang et al. [32]. The normal impedance analysers may not provide the time-domain impedance measurement [70], so a new experimental measurement system is developed in this study based on the circuit proposed by Baptista and Vieira Filho [71] to excite the transducer and obtain the corresponding time-domain impedance response.

The experimental measurement system design used in this study is shown in Figure 3.2. This is a new system proposed to measure the time-domain impedance signal of PZT. The excitation signal is expressed as *x(t)*, and the time-domain response from PZT is denoted as *y(t)*. The output *y(t)* will vary with the impedance of the PZT transducer. The resistance *Rs* is chosen by taking into account both the PZT material specification and the amplitude of the excitation signal *x(t)*. LabVIEW based impedance analysis software is used to control the impedance analyser to generate the excitation signal *x(t)* and record the response signal *y(t)*. The excitation signal *x(t)* is a sweep frequency signal, generated by the impedance analyser. The impedance converter network analyser EVAL-AD5933EB from Analog Devices is used in the experimental tests. This impedance analyser can measure the electrical impedance in the range of 10 to 100 kHz using a USB connection with the software. Based on experiences with the sensitive frequency range of PZT impedance methods [72], the frequency range of the excitation signal *x(t)* is defined from 40 kHz to 60 kHz. The magnitude and phase of impedance from the PZT transducer are collected by the

board. The time-domain impedance response *y(t)* is recorded by a National Instruments data acquisition device (NI 9215). The communication between the DAQ device and computer also occurs through the USB port. In this paper, the measured time-domain impedances will be analysed with the TFARMA model and used for calculating the damage index as shown in Equation (3.16).

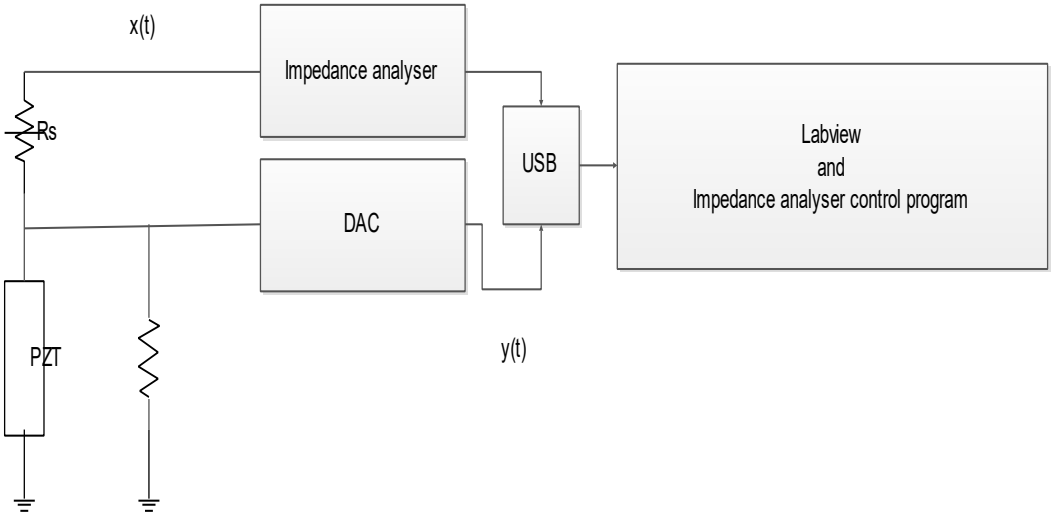

Figure 3.2 Experimental measurement system design used in this study

3.4 Experimental validation

3.4.1 Experimental setup

The impedance-based SHM methods are widely and successfully applied in the monitoring of civil structures, such as beam and plate-like structures. The truss bridge represents a main bridge type on highways and roads, and gusset plates in such bridges play a significant role in ensuring the rigidity and load-carrying capacity of the bridges. The gusset plate in steel truss bridges is the target area for damage detection and condition monitoring in this study.

A simplified truss bridge model was fabricated in the laboratory, as shown in Figure 3.3, for the experimental tests to validate the effectiveness and performance of the proposed damage detection approach. The truss bridge model consists of four equal angles to serve as beams, a number of steel-plate bar members as chords and some gusset plates at joint locations as connections. M6 bolts are used to connect all the chord members and gusset plates at equal angles. More than 300 bolts are used in the whole bridge model. The length, width and height of the bridge model are 2 m, 0.5 m and 0.5 m, respectively. The gusset plate in the central bottom of the model is selected as the target area to place PZT transducers and perform condition monitoring. Measured impedance responses from these PZT transducers are used for the damage detection of the loosened bolts in the gusset plate, which is the main focus of this study.

Figure 3.3 Test configuration of the truss bridge model

Four PZT transducer patches of PSI-5H4E (20×20×0.75) were bonded onto the testing gusset, and the numbering of the placed sensors is shown in Figure 3.4. They are denoted as PZT 1, PZT 2, PZT 3 and PZT 4. During testing, the impedance analyser will excite these PZT transducers to generate a small deformation of the truss bridge model. The vibration of the local area on the truss model bridge will be transferred back to the PZT transducer and produce a variation in the electrical impedance response. The local damage is simulated by removing specific bolts in the target gusset plate. In this study, two bolts, marked in Figure 3.4 with two circles, connecting the vertical chord member and the target gusset plate were removed to simulate local damage to the gusset plate. PZT 1 was located 10 mm from the location of the introduced damage. PZT 2 and PZT 3 were placed 80 mm from the damage and on the left and right sides of the damage locations, respectively. It is noted that PZT 1, PZT 2 and PZT 3 were all bonded to the surface of the gusset plate. However, PZT 4 was bonded to the vertical chord member and 100 mm from the location of the local damage.

The time-frequency domain damage indictor value will increase with the severity of bolt loosening, which can be used to identify the change in bolt connection conditions, i.e., partial or complete bolt loosening. However, the traditional statistical damage indicator calculated from impedance responses, e.g. RMSD, can only distinguish damages with different severities on a certain location [2]. The scenario with a bolt loosening close to the PZT transducer may have a similar damage indicator value as that with a bolt loosening damage far from the transducer but with a more severe damage, making it difficult to quantify the bolt loosening condition based on such damage indictors. For the proposed TFARMA-based damage indicator, the value will also be affected by both damage severity and distance between sensor and structural damage. Therefore, for the complicated structure which has multiple potential damage locations, such as the gusset plate in this study with a number of bolts, it is difficult to identify whether it is a partially loosened bolt or a completely loosened bolt that is farther from the sensor. The method can only identify the existence of

damage in the vicinity. For this reason, in this study, only the damage scenarios with the completely loosened bolts are investigated in the tests.

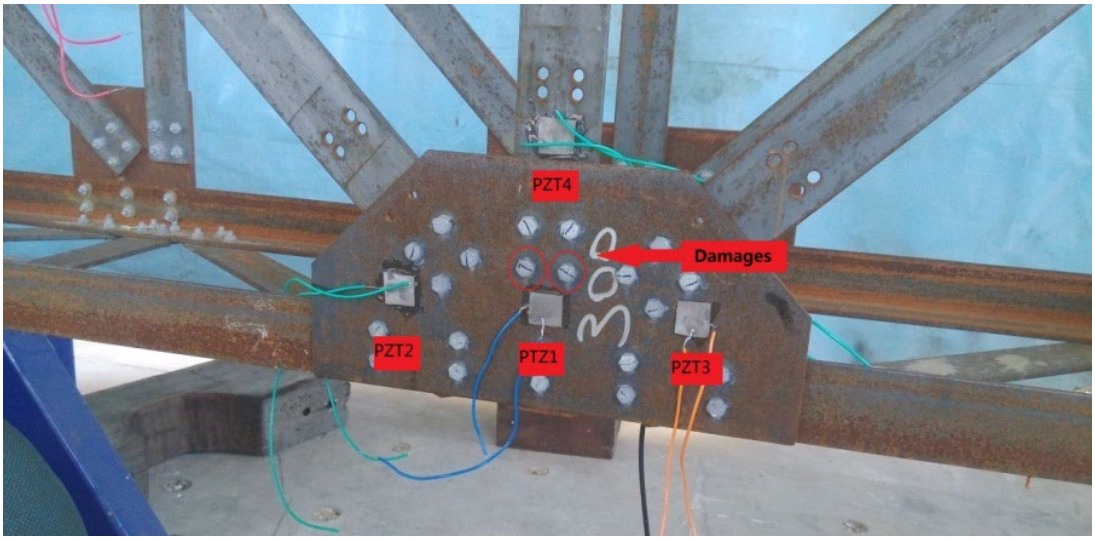

Figure 3.4 Placement of the PZT sensors

A 500 ohm resistor was used to form the electric measurement circuit shown in Figure 3.2 to measure the time-domain impedance. The PZT transducers were excited by the AD5933 impedance analyser, and both the frequency and time-domain impedance signals were collected by using the impedance analyser and the NI data acquisition device, respectively.

3.4.2 Damage detection with traditional damage indices

The impedance signals in the frequency domain measured from healthy and damaged bridge models at each PZT transducer are shown in Figure 3.5. A high frequency band from 40 kHz to 60 kHz is selected as mentioned above. It can be seen that some

differences are observed, especially at the peak impedance responses when the local damage is introduced. Qualitative damage diagnosis with the traditional EMI-based methods is conventionally implemented by computing a scalar damage index. RMSD and CC damage indices, calculated with Equations (2.8) and (2.9), are two such scalar damage indicators, and the damage index values at the four PZT patches are computed with the frequency impedances measured from the undamaged and damaged structures.

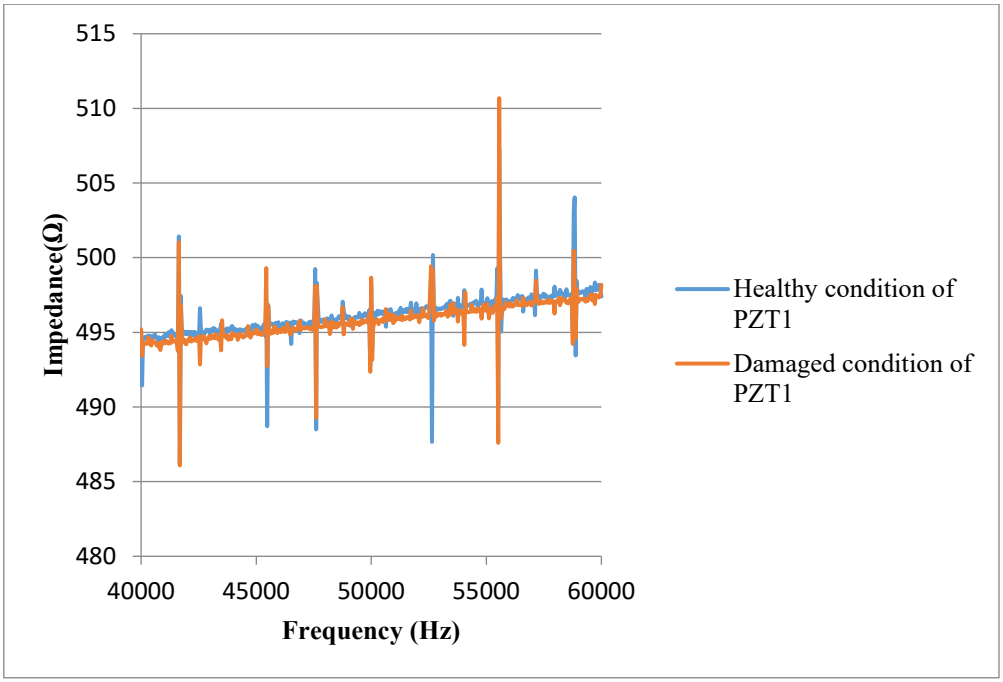

(a)

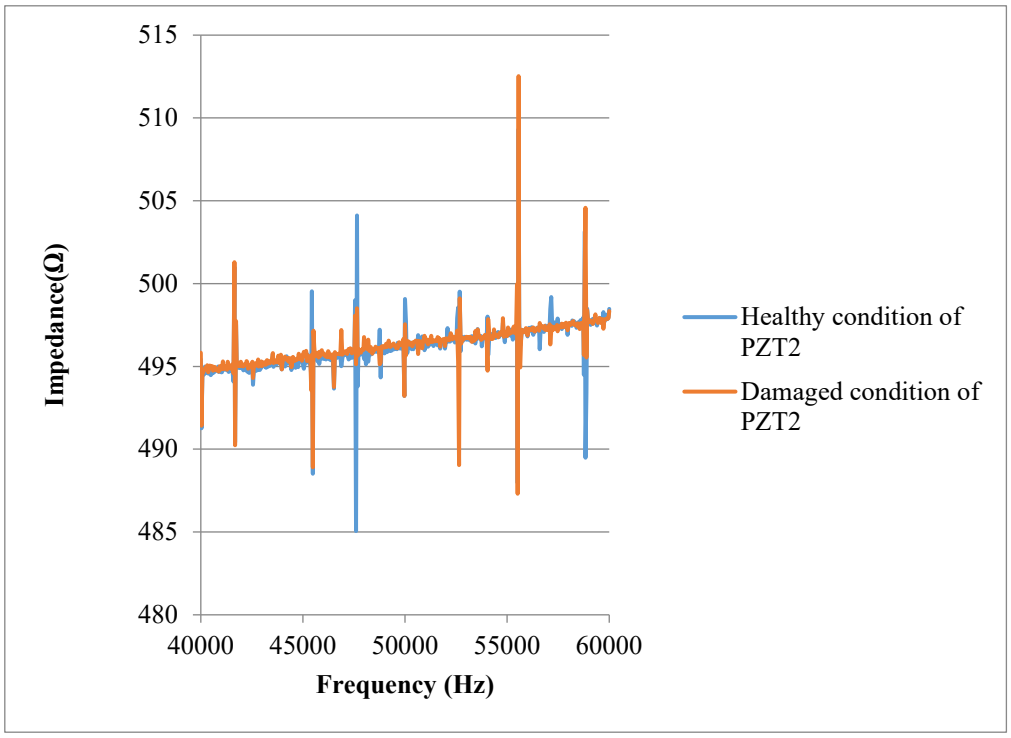
515
510
505
500
495
490
485
480
Impedance(Ω)
40000
45000
50000
55000
60000
Frequency (Hz)
Healthy condition of PZT2
Damaged condition of PZT2

(b)

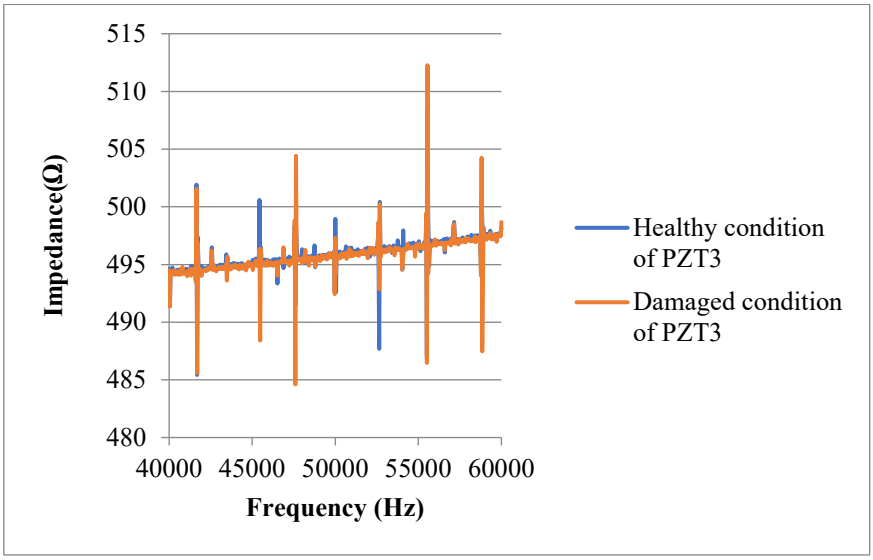
515
510
505
500
495
490
485
480
Impedance(Ω)
40000
45000
50000
55000
60000
Frequency (Hz)
Healthy condition of PZT3
Damaged condition of PZT3

(c)

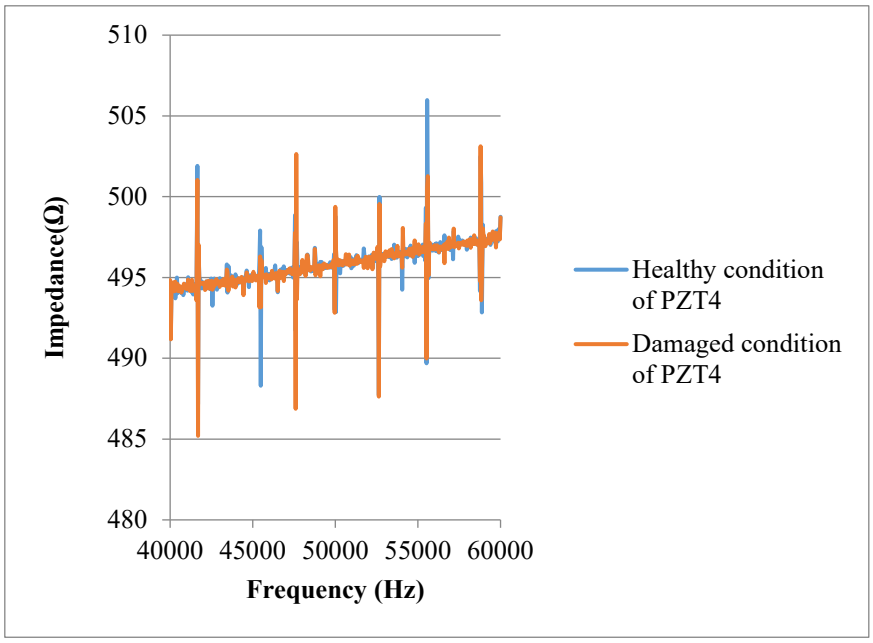

(d)

Figure 3.5 Comparison of impedance signals from healthy and damaged bridge models: (a) PZT 1; (b) PZT 2; (c) PZT 3; (d) PZT 4

3.4.3 Damage detection based on the TFARMA model

The proposed damage detection method based on the TFARMA model includes a two-dimensional analysis of the measured time-domain impedance response, which could give a different perspective on the detection of damage in gusset plates of truss bridges. The TFARMA model could indicate the features and patterns of the varying process of impedance signals in the time–frequency space. The measured time-domain impedance signal with the system design shown in Figure 3.6 consists of the response signals under sweeping excitations and the standby noise signals before and after the sweeping process. One typical measured time-domain impedance from PZT1 under the healthy state is shown in Figure 3.6. Only the signals in the red window denote the measured time response under the sweeping excitations. The signals on

both sides of the red window are the output from the impedance analyser in the standby mode. The TFARMA model will only be built for the selected period under the sweeping excitations.

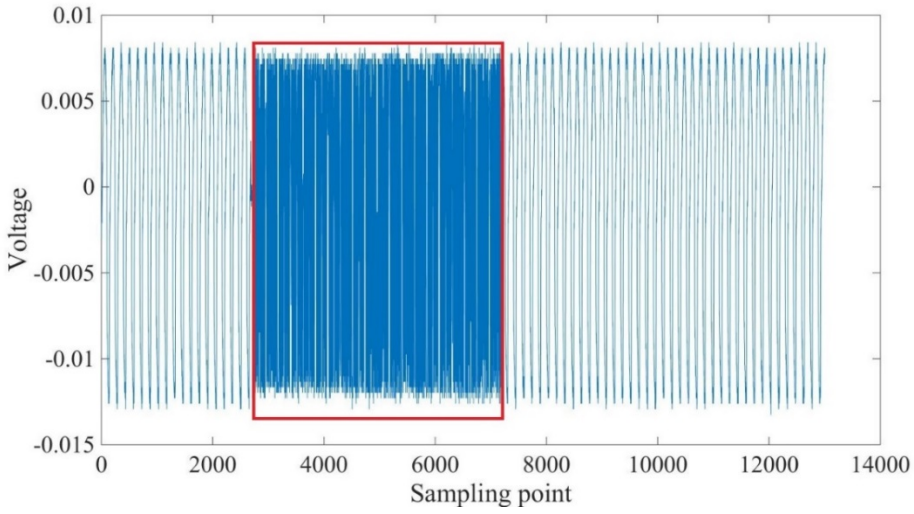

Figure 3.6 Time-domain impedance measured from PZT1 under the healthy condition

The TFARMA model parameters of the time-domain impedance signals are estimated from the procedures and algorithms presented in Chapter 3.2. The evolutionary spectra for all four PZT patches are calculated with Equation (3.12) and are shown in Figure 3.7 to Figure 3.10. It is observed that the calculated spectra of the signals at PZT 1, PZT 2 and PZT 3 for the damaged structure, as shown in Figures 3.7(b), 3.8(b) and 3.9(b), consist of more than two red bands in a wide area, which is a different pattern signature compared to the healthy structure, as shown in Figures 3.7(a), 3.8(a) and 3.9(a). The most obvious distinction is observed at PZT 4 between the healthy spectrum and the damaged spectrum, as shown in Figures 3.10(a) and 13.10(b), respectively. Visible and clear differences are observed in the evolutionary spectra of

the signals obtained from the damaged and undamaged structures, indicating that the existence of the introduced damage may be straightforwardly detected by comparing the evolutionary spectra between the healthy and damaged states.

Based on the truss bridge design and experimental setup, the gusset plate being monitored was fixed to all chord members by twenty-two bolts. However, the vertical chord member was bonded by only four bolts at each end. With the bolt-loosening damage, as shown in Figure 3.4, there are still twenty bolts on the gusset plate to keep it stable. However, the same damage causes a significant reduction in the holding force of the vertical chord member. The introduced damage causes a greater influence on the vertical chord member where PZT 4 is placed. This is why PZT 4 has the most distinct evolutionary spectrum due to the introduced damage among all the transducers, and the identification based on the TFARMA model is expected to reflect this point.

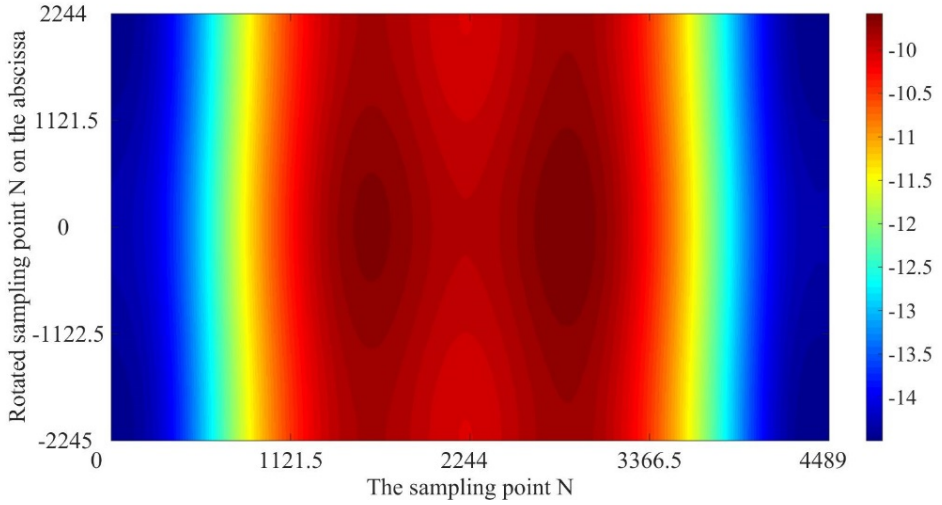

(a)

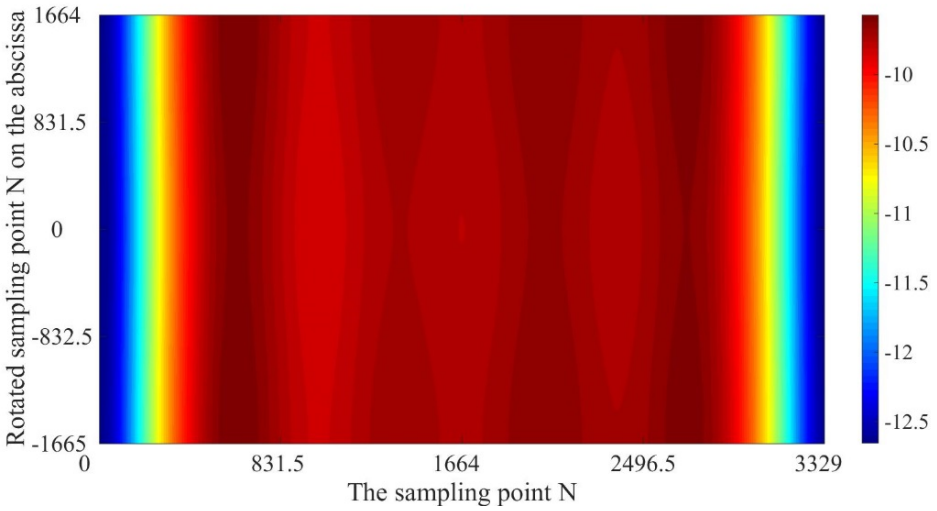

(b)

Figure 3.7 Evolutionary spectra of the time-domain impedance signal from PZT1: (a) healthy structure, (b) damaged structure

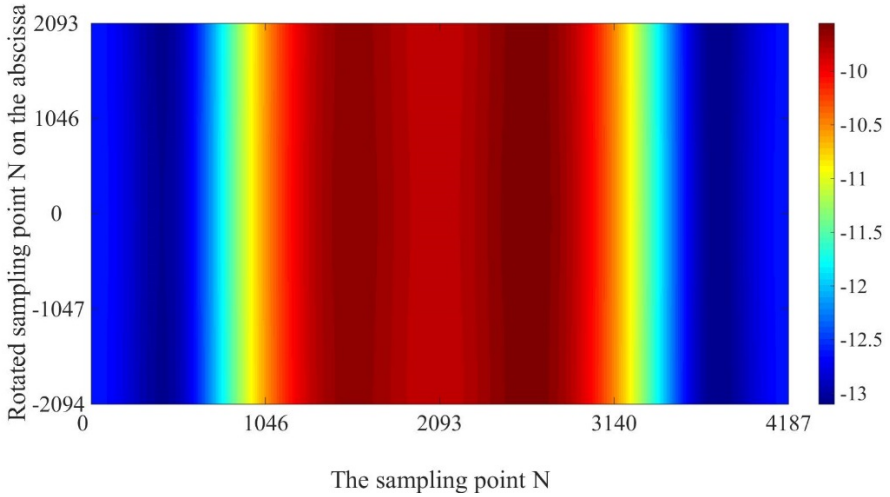

(a)

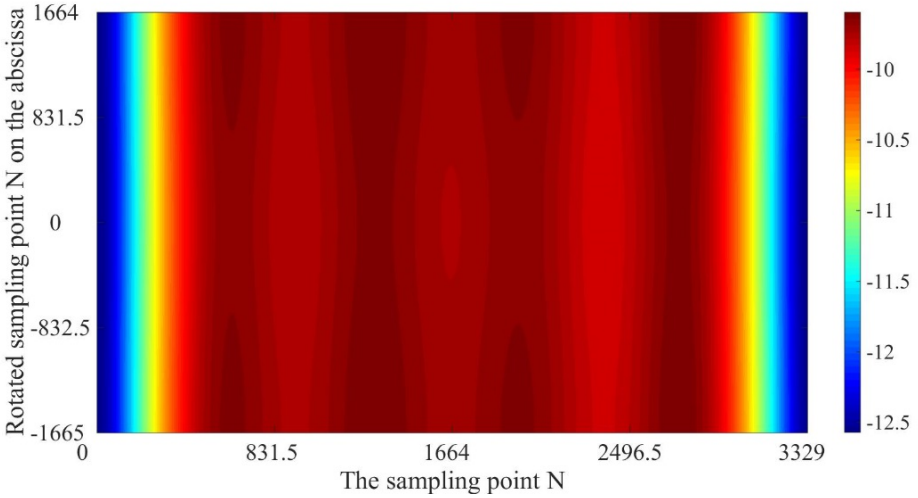

(b)

Figure 3.8 Evolutionary spectra of the time-domain impedance signal from PZT 2: (a) healthy structure, (b) damaged structure

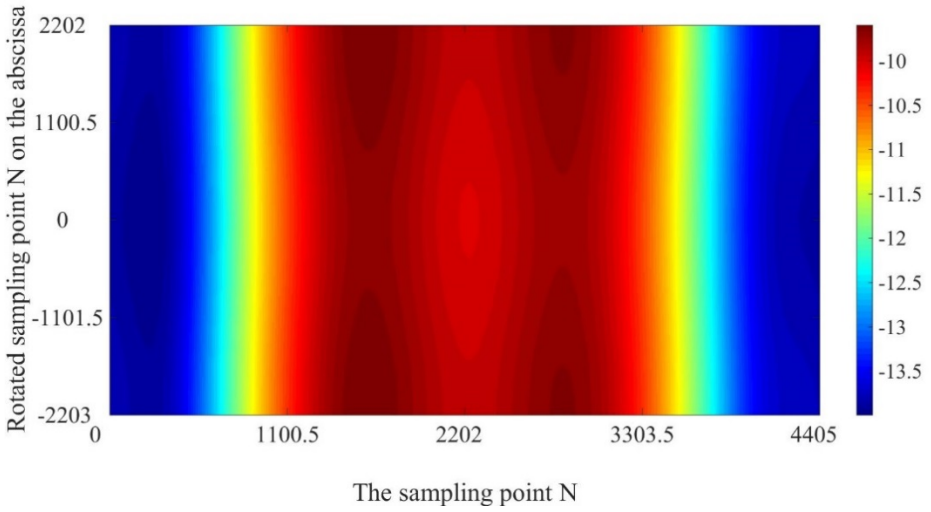

(a)

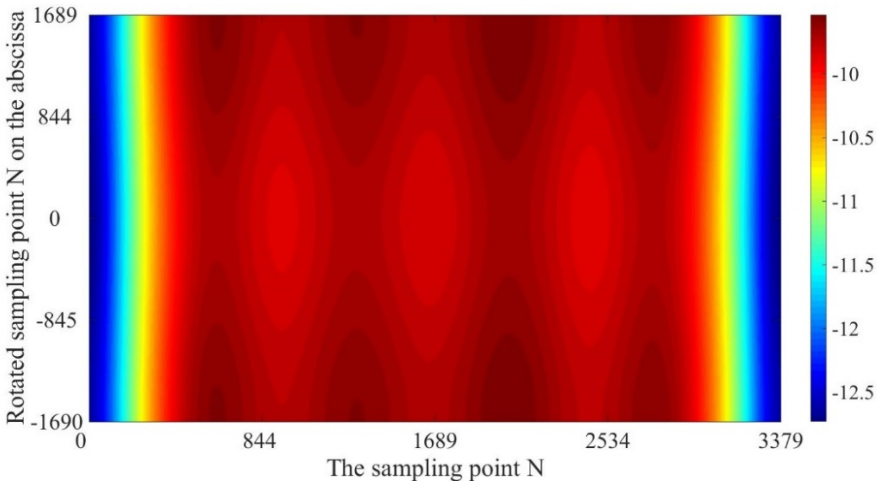

(b)

Figure 3.9 Evolutionary spectra of the time-domain impedance signal from PZT 3: (a) healthy structure, (b) damaged structure

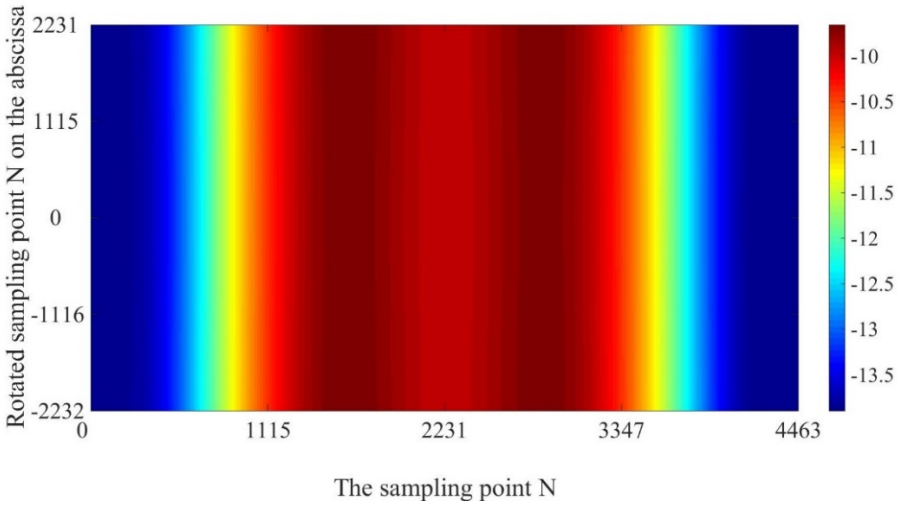

(a)

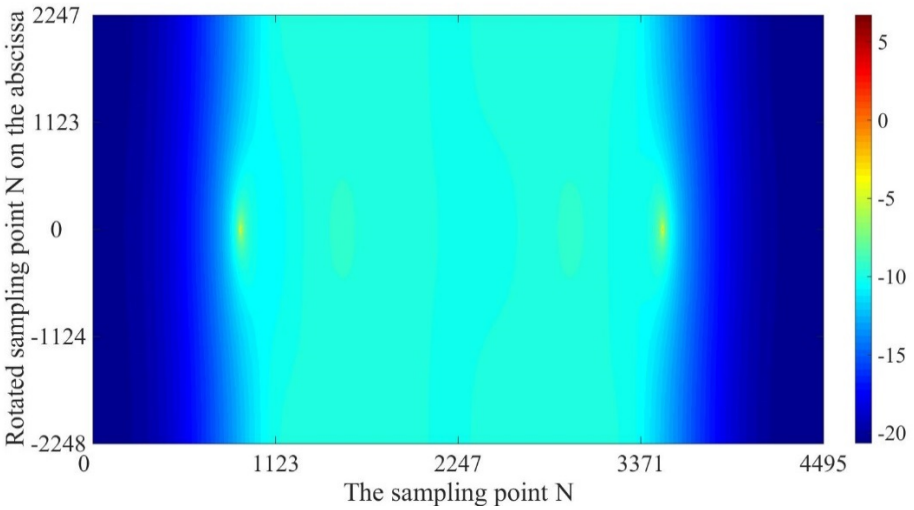

(b)

Figure 3.10 Evolutionary spectra of the time-domain impedance signal from PZT 4: (a) healthy structure, (b) damaged structure

3.4.4 Comparison among RMSD, CC and TFARMA damage indices

The TFARMA damage index is calculated based on the evolutionary spectra obtained under the healthy and damaged states and is used to indicate whether the proposed approach is able to identify the existence of the damage, allowing investigation of the performance and effectiveness of the proposed approach. For example, SVD is performed with the calculated evolutionary spectrum of PZT 2 under the damaged state, and the singular values are shown in Figure 3.11. Only the first ten singular values are shown. Most singular values are close to zero except the first one, indicating that the first column vector in matrix U in Equation (3.15) is dominant in representing the characteristics of the spectrum. Therefore, a comparison between the two evolutionary spectra from the healthy and damaged structures can be made by using the associated first principle column vectors to calculate the TFARMA damage index in Equation (3.16). The first column vectors used to represent the characteristics of the TFARMA evolutionary spectra of PZT 2 in the undamaged and damaged states are shown in Figure 3.12. A very different pattern is observed in the time domain, indicating that the proposed TFARMA could be more sensitive than the traditional one-dimensional data analysis methods to detect structural damage.

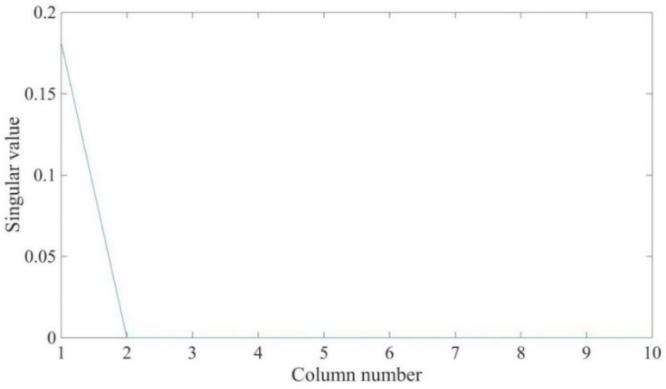

Figure 3.11 Singular values of the TFARMA spectrum from PZT 2 in the damaged state

The TFARMA damage index values at all four PZT transducer locations are calculated and compared with the conventional frequency impedance-based damage indices, such as RMSD and CC. Figure 3.13 shows the damage index values obtained from the proposed approach based on the TFARMA model analysis and the conventional approaches based on frequency-domain impedance analysis. The baseline values for the three damage indices are set at the same value of 0.1, and the damage index values at all four sensor locations are normalized with the baseline value for comparison. The damage indices calculated with two measurements from the healthy state are provided as the baseline values.

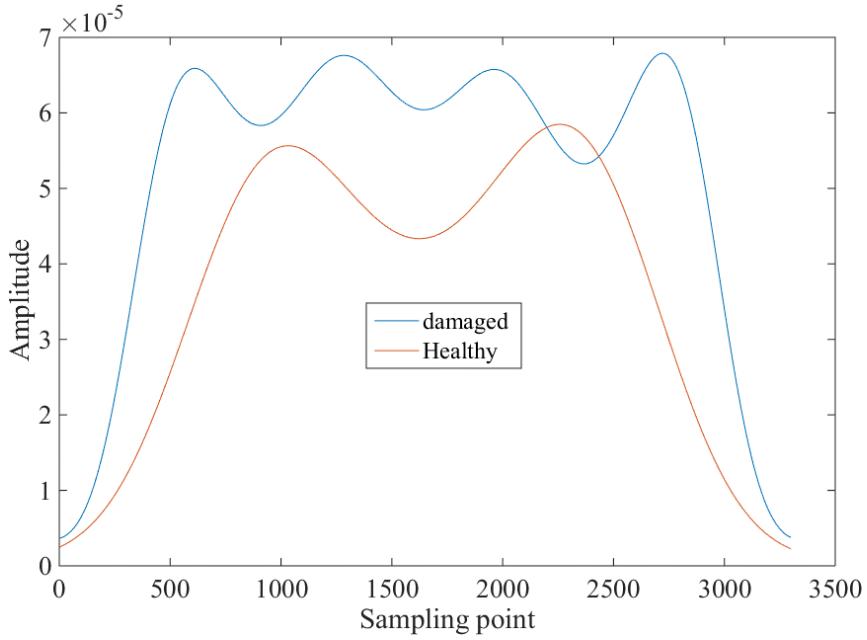

Figure 3.12 First principle column vectors of TFARMA spectra from PZT2 in the healthy and damaged states

It is observed from Figure 3.13 that the RMSD at all four PZT locations is able to identify the bolt-loosening damage in the gusset plate of the truss bridge model. PZT 1 is the closest sensor to the damage location and therefore has the largest RMSD

damage index value and the most sensitive performance. The RMSD damage index values of PZT 2 and PZT 3 are similar because the locations of these two transducers are symmetrical. The damage index value from PZT 4 is the smallest, as it is the farthest sensor from the damage location among all four sensors. The damage detection results obtained with the CC damage index are different from those obtained with RMSD. The CC values from PZT 1, PZT 2 and PZT 3 are slightly higher than the baseline value. However, the CC value from the PZT 4 transducer is very close to the baseline value, indicating that the CC index is not capable of detecting the damage by using the frequency impedance data measured from PZT 4. In general, RMSD is observed to have a better performance than CC. Using these damage indices with a pre-defined damage threshold value for the baseline structure, the monitoring system could signal whether any change has occurred in the monitored local area. It is interesting to note that although PZT 4 is placed on the truss bar member, not on the gusset plate, it still identifies the change in the impedance and detects the damage through the RMSD damage index. Note that the RMSD damage index value from PZT 4 is smaller than those from the other three transducers, as PZT 4 was placed 100 mm from the damage location and is furthest among all the PZT patches. The existence of damage can be detected by using the RMSD damage index; however, the sensitivity of such a damage index depends only on the distance between the sensor and the damage.

It can be seen from Figure 3.13 that the TFARMA damage indices at all four PZT transducer locations are significantly higher than the baseline value or the RMSD/CC damage index values. Similar to the detection with RMSD, the TFARMA damage index of PZT 1 has a higher value than those of PZT 2 and PZT 3 since it is closer to the damage locations. However, it is interesting to note that there is quite a large increase in the TFARMA damage index of PZT 4 compared with its RMSD damage index. The evolutionary spectra from PZT 4, as observed in Figure 3.10, have the most significant and distinct difference between the undamaged and damaged states. Thus, the TFARMA damage index of PZT 4 has the largest value. It is demonstrated

that PZT 4 shows a higher sensitivity than the other three PZT transducers when using the proposed damage detection approach based on TFARMA model analysis. The explanation for this has been given in Section 3.1, i.e., because PZT 4 is placed on the vertical chord member and the other three are placed on the gusset plate. The bolt loosening damage has a significant influence on the holding force of the chord member. However, the conventional impedance-based damage detection with frequency-domain information only, i.e., with RMSD and CC damage indices, is not able to recognize this physical effect on the structures for damage identification. The sensitivity of the RMSD and CC damage indices in the frequency domain depends only on the distance between the PZT patch and the damage location because such damage indices depend only on the change in the frequency-response signal amplitudes. The sensitivity depends mainly on the distance, whereas the evolutionary spectra indicate variations not only in the signal amplitudes of frequency responses but also in the time-domain response pattern. The introduced damage significantly reduces the rigidity of the truss joint; therefore, the signal characteristics and frequencies measured by the PZT transducer on the truss member (PZT 4) will be greatly affected. These observations demonstrate the superiority of using evolutionary spectra to detect the conditions of gusset plates compared with the RMSD and CC damage indices. The sensitivity of using impedance responses for identifying the damage at joint locations could be increased by examining the responses from the connected chord member with the proposed approach. However, it should be noted that the exact sensitivity radius of the proposed approach may depend on the complexity of the structural model and the testing conditions.

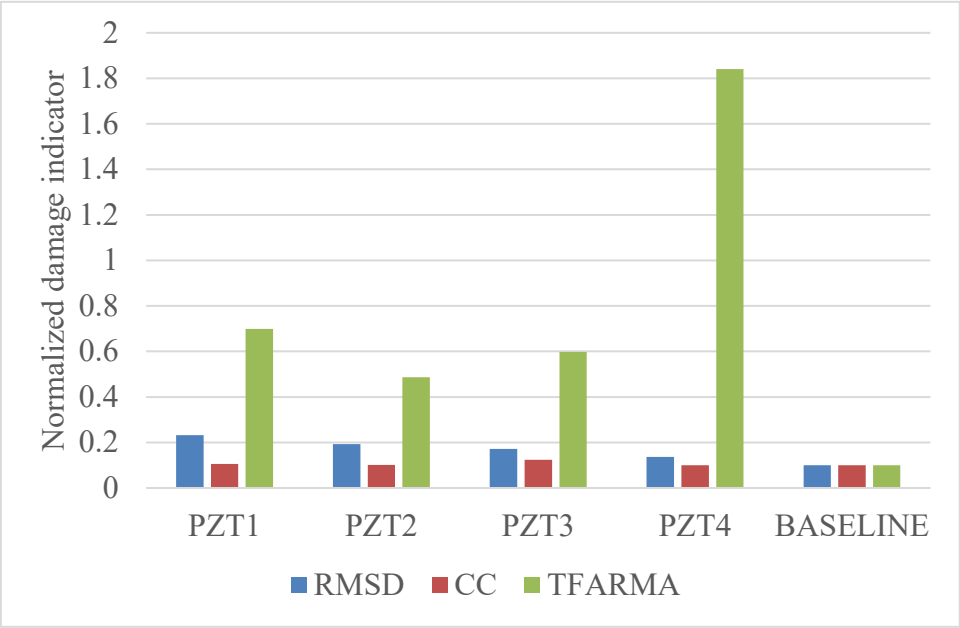

Figure 3.13 - Comparison of RMSD, CC and the proposed TFARMA damage index

3.5 Numerical verification considering a significant noise effect

Even though the measured responses in the above experimental tests already include the noise effect from the environmental vibrations in the laboratory, a numerical simulation considering an extra significant noise effect is conducted to further validate the effectiveness of the proposed approach and compare the performance of the TFARMA damage index with that of the other two damage indices, i.e., RMSD and CC. A white noise is generated using Matlab and is added to the original time-domain impedance response. The signal-to-noise ratio is 11 dB, which means that the power of the added noise effect is approximately 10% of the original signals. The noise is transformed into the frequency domain and added to the frequency-domain impedance signal. Figures 3.14 (a) and (b) show the time-domain and frequency-

domain impedance signals, respectively, from PZT 1 with the noise effect under the damaged state.

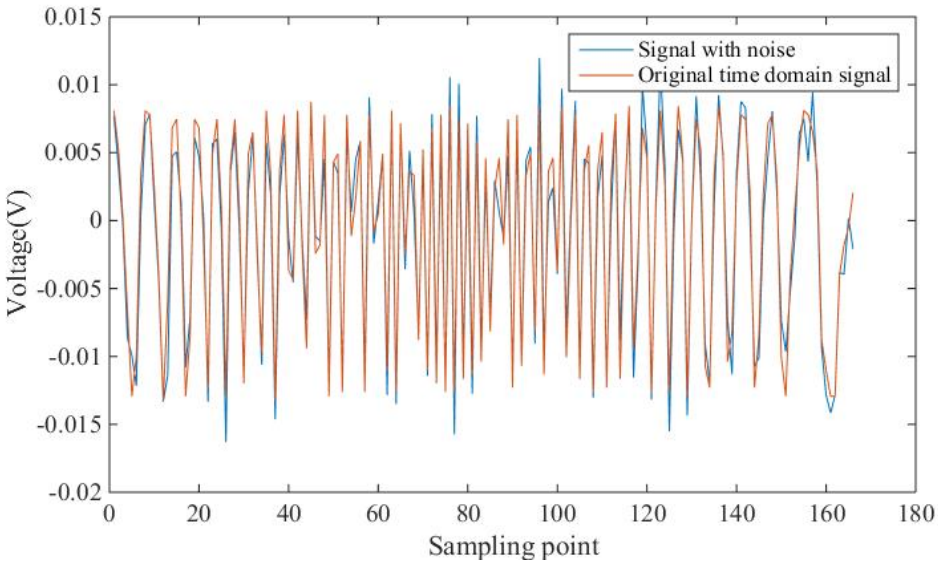

(a)

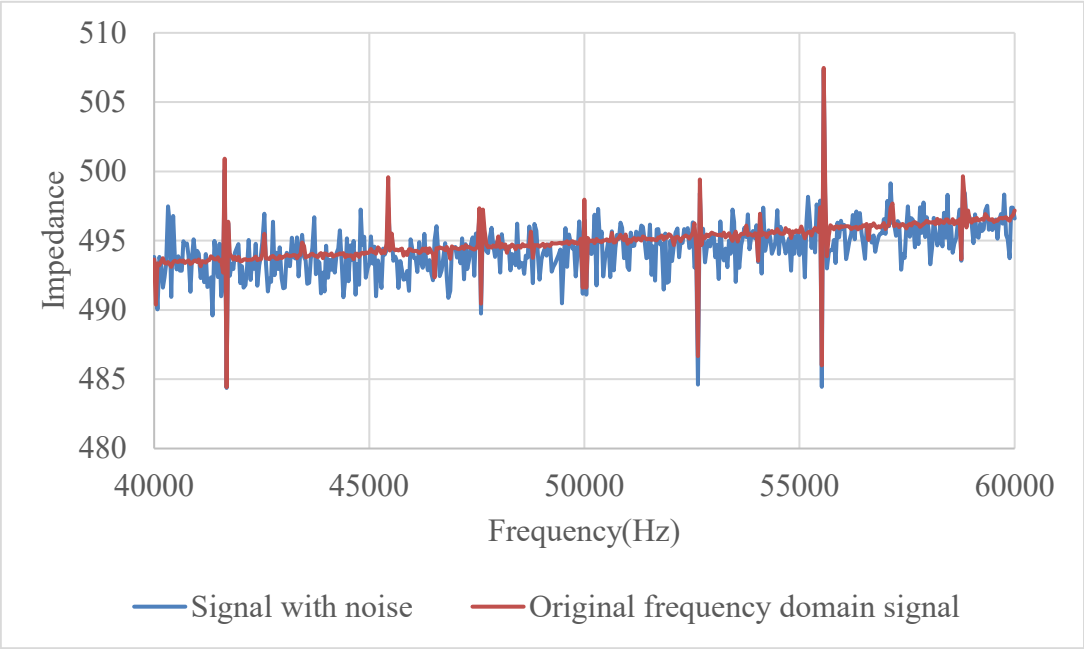

(b)

Figure 3.14 Impedance signals with the noise effect: (a) time domain, (b) frequency domain

The added noise effect could affect the effectiveness of damage detection using the conventional approaches with frequency-domain impedances and the proposed approach with time-domain impedances for TFARMA analysis. The noisy responses are analysed to obtain the RMSD, CC and TFARMA damage indices. Figures 3.15 (a) and (b) show the evolutionary spectra of PZT1 in the healthy and damaged states, respectively. It is observed that when the noise effect is included, the evolutionary spectra become slightly different from the original spectra, as shown in Figures 3.7 (a) and (b). The evolutionary spectra at the other three sensor locations are not given due to the page limit. However, Figure 3.16 shows the calculated RMSD, CC and TFARMA damage indices with noisy impedance responses. It is shown that both the RMSD and CC damage indices may not be able to identify the bolt damage since

their values at the four PZT sensors are very close to the baseline values, indicating that the performance of the RMSD and CC damage indices is biased to the noise effect. However, the TFARMA damage index is still very effective in detecting the existence of the damage, with much higher damage index values compared with the baseline. It is also observed that the damage index from PZT 4 has the highest damage index value and the most sensitive performance in detecting the introduced bolt damage, similar to the observation in Figure 3.13. It is demonstrated that compared with the conventional EMI-based damage detection techniques with frequency-domain impedances, the proposed approach based on the TFARMA model analysis shows a more robust damage detection capacity and a higher sensitivity in identifying the bolt damage in steel truss bridges under the noise effect.

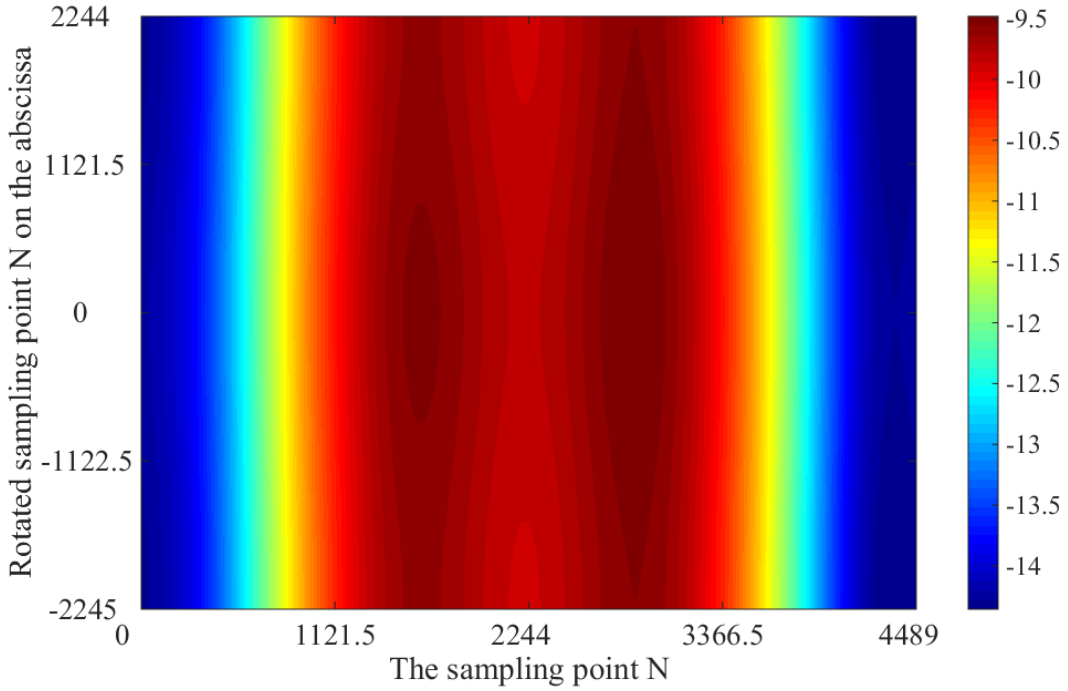

(a)

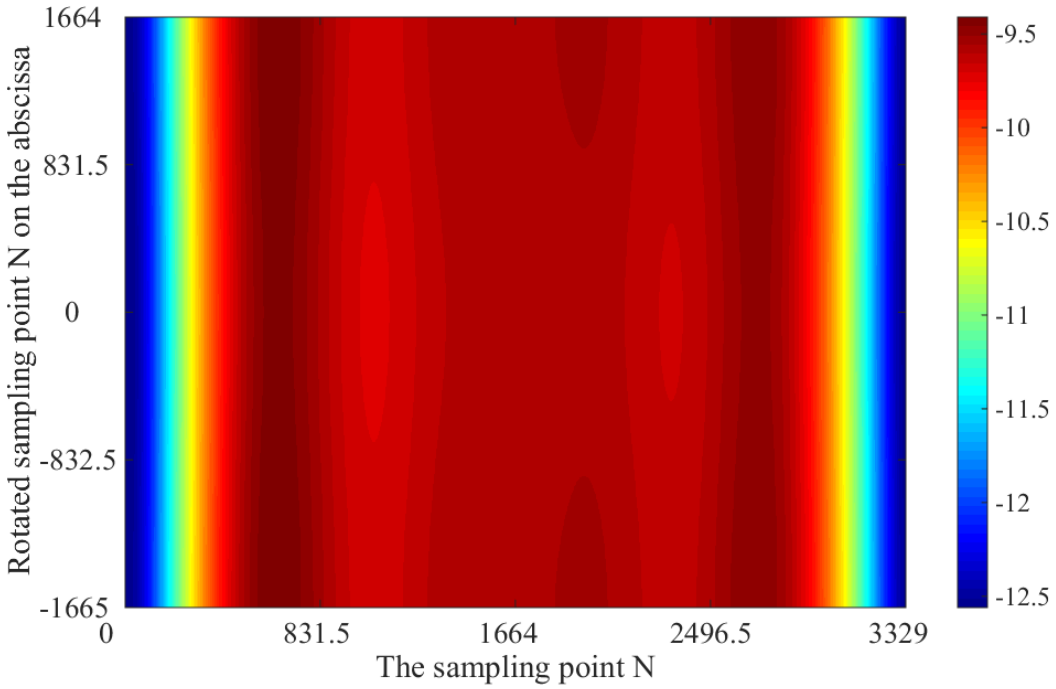

(b)

Figure 3.15 - Evolutionary spectra of the time-domain impedance signal from PZT1 with the noise effect: (a) healthy structure, (b) damaged structure

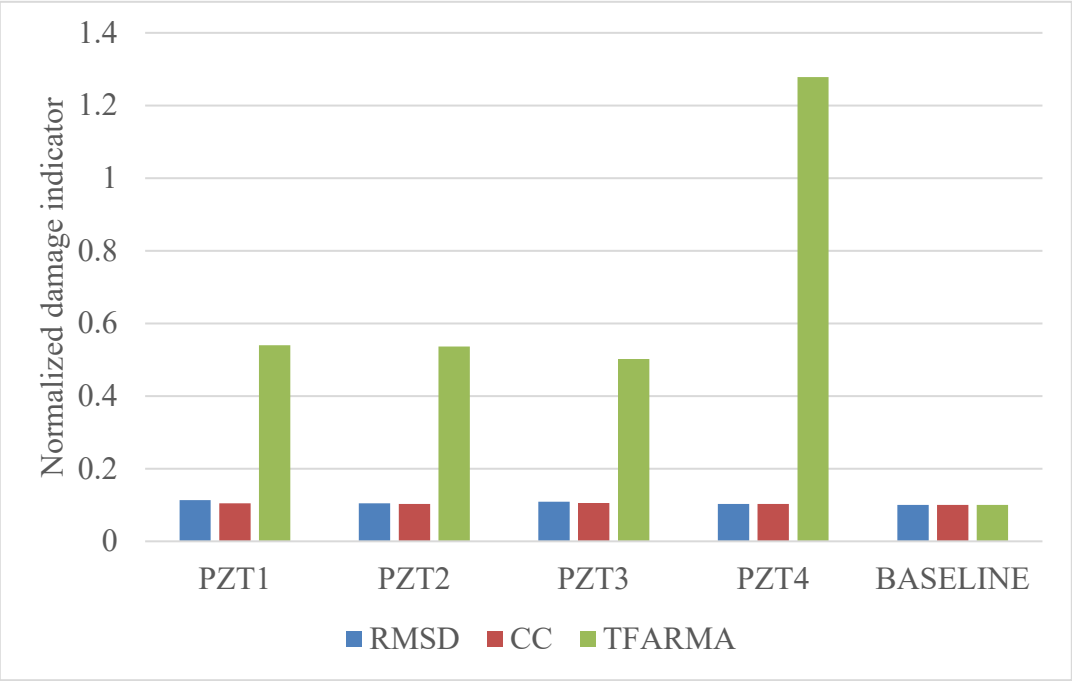

Figure 3.16 - Comparison of RMSD, CC and the proposed TFARMA damage index under the noise effect

3.6 Discussion and Concluding Remarks

This chapter proposes a structural damage detection approach based on analysing the time-domain impedance responses from PZT transducers for SHM of joint connections in steel truss bridges. Evolutionary spectra from TFARMA model analysis in the healthy and damaged states are used to identify the bolt loosening damage in the gusset plate. SVD is performed to analyse the evolutionary spectra and define the TFARMA damage index. The calculated TFARMA damage index is compared with two other conventional frequency-domain impedance-based damage indices, i.e., RMSD and CC. The effectiveness and performance of the proposed approach are validated by experimental studies on a steel truss bridge model in the

laboratory. Compared with the RMSD and CC damage indices, the TFARMA damage index shows a higher sensitivity and an improved performance in detecting bolt damage in the gusset plates of steel truss bridges. The TFARMA damage index also shows a significant improvement in the sensitivity range when using PZT transducers to identify the local damage in the targeted monitoring area by placing the PZT sensor on a different location, such as the chord member connected to the gusset plate. Numerical studies with the inclusion of an extra significant noise effect in the measurements demonstrate that the proposed TFARMA damage index has a more robust and reliable performance in detecting bolt damage in steel truss bridges.

One other interesting question is the effect of different bolts loosening on the performance of the proposed damage index. In a real structure, the preload reduction of bolts will lead to changes in the interface contact characteristics and local stress distributions [73]. Since the PZT transducer is bonded on the structure surface, the impedance response will reflect the changes in dynamic characteristics of the structure. Therefore, different bolts loosening at the same plate will cause different changes in impedance responses. From test results, the damage indicators calculated from different impedance responses of three PZT transducers at different locations on the same gusset plate have slightly distinctions due to the different distances to damage location. [2] However, using one damage indicator is not able to quantify the damage and recognize which bolt is loosened on the gusset plate. This is also the motivation of performing the model-based damage quantification in the next study.

4 Numerical Study on Identification of Minor Structural Damage Based on Electromechanical Impedance Sensitivity and Sparse Regularization

This chapter proposes a structural damage identification approach based on model updating with electromechanical impedance sensitivity and the sparse regularization technique to identify the location and severity of minor damage in structures. The sensitivities of resonance frequency shifts in the impedance responses to the stiffness parameters of the host structure are calculated and used to identify the damage with a small number of resonance frequency shifts. Numerical verifications on a single PZT transducer patch and a PZT patch on a narrow aluminium plate structure are conducted to validate the finite element modelling technique to calculate the impedance. The effectiveness and performance of the proposed structural damage identification approach are demonstrated with numerical simulations on an aluminium plate model to which a PZT transducer patch is attached. The initial finite element model and a limited number of resonance frequency shifts in the impedance responses are used for the identification. Sparse regularization, namely, the l_1 regularization technique, is used for solving the inverse problem. Single and multiple damage scenarios are considered. The effects of noise in the measured impedance signals and the number of available frequency shifts on the performance of the proposed damage identification approach are investigated. The results demonstrate the performance and robustness of the proposed approach.

4.1 Measurement of changes in impedance signatures

In conventional model-based methods using EMI for damage detection, the changes in magnitude of the impedance responses are often used to update the system parameters [21, 74]. However, it is difficult to achieve an accurate identification by making use of the amplitude changes in the impedance curves mainly for the

following two reasons: 1) Structural property changes cause not only variations in the impedance amplitudes but also shifts in the frequencies of the resonances of the impedance curves [2]. The sensitivities of these resonance frequency shifts are expected to be more prominent than the changes in the amplitudes; 2) It is difficult to ensure that the impedance amplitudes match the impedance obtained from real-world measurements in a high frequency range very well because of the effects of noise and modelling errors. The errors in the baseline model cannot be ignored considering the high sensitivity of EMI-based methods in the detection of minor structural damage. Considering these reasons, the resonance frequency shifts in impedance curves are used for model updating and damage identification.

4.2 Inverse problem in EMI-based damage identification

The proposed structural damage identification approach is based on minimizing the difference between the analytical impedance response calculated from the coupled finite element model including the host structure and the PZT patch and the impedance response measured from the damaged structure. As shown in a typical comparison between impedance responses before and after damage [75], there is a significant frequency shift in the impedance responses after the occurrence of structural damage. This indicates that the frequency shifts will be more sensitive in detecting the structural damage. In the inverse problem, the stiffness parameters of the target structure can be identified by adjusting the parameters in the finite element model to minimize the difference between the analytical and measured impedance responses.

There are many types of structural damage in the real world, such as cracks, debonding and corrosion. For most model-based damage identification approaches, damage in the structure is usually assumed to correspond to a stiffness reduction in a specific element [76, 77]. It has been reported that the global modal information, i.e., natural frequencies and mode shapes, may not be very sensitive to minor structural

damage, especially with a certain level of uncertainty in the system and measurement noise in the monitoring data. In contrast, the EMI-based method is more sensitive to minor structural damage, i.e., tiny geometrical changes in the structure, because of the high frequency responses. The high working frequency range of the EMI technique allows the proposed damage detection method to be more sensitive to minor changes in the structure. To emphasize the advantage of using the proposed approach to detect minor structural damage, the damage is simulated as a tiny geometrical change in the cross section of the host structure in this study, which would lead to a minor decrease in the stiffness of the host structure.

When an accurate finite element model for calculating the EMI response is obtained, the model-based method, i.e., sensitivity-based model updating method, can be used to minimize the difference between the impedance response calculated from the numerical model and the impedance response measured from the damaged structure for structural damage identification. Structural system parameters are identified by solving the ill-posed inverse problem with an iterative procedure. The first-order sensitivity-based identification problem can be defined as

$$[S]\{\delta_T\} = \{\delta_f\} \tag{4.1}$$

where $\{\delta_f\}$, $\{\delta_T\}$ and $[S]$ denote the resonance frequency shifts in the measured and analytical impedance curves, the perturbation in the structural stiffness parameters and the sensitivity matrix of the resonance frequency shift with respect to the stiffness parameters of the host structure, respectively. The sensitivity matrix can be obtained by using numerical methods, i.e., the finite difference method. Rewriting Equation (4.1), we have

$$[S]\{\delta_T\} = \begin{Bmatrix} \hat{f}_1 \\ \hat{f}_2 \\ \vdots \\ \hat{f}_n \end{Bmatrix} - \begin{Bmatrix} f_1 \\ f_2 \\ \vdots \\ f_n \end{Bmatrix} \tag{4.2}$$

where n is the number of resonance frequencies in a selected frequency range of the impedance response; $\hat{f}_n$ and f_n represent the n-th resonance frequency of the measured and finite element model impedance responses, respectively.

Equation (4.2) is usually an ill-posed inverse problem. To obtain a stable solution with physical meaning, a widely used regularization method in the engineering field is the so-called damped least-squares method (Tikhonov 1963), which is also called Tikhonov regularization. Recently, the sparse regularization technique has been developed to solve the inverse problem with only a small number of measurements. These two techniques will be described in the following sections.

4.2.1 Tikhonov regularization

One of the key problems in model-based methods for structural damage identification is solving the ill-posed identification equation, i.e., Equation (4.2), accurately, especially with limited measurement information and a significant noise effect. By using the Tikhonov regularization technique, the solution of Equation (4.2) can be expressed as

$$\delta_T = \left(S^T S + \lambda I\right)^{-1} S^T \delta_f \tag{4.3}$$

where λ is the regularization parameter. It is equivalent to minimizing the following objective function

$$f_{Tik} = \left\| S\delta_T - \delta_f \right\|_2 + \lambda \left\| \delta_T \right\|_2 \tag{4.4}$$

where $\| \|_2$ denotes the second norm l_2 . This will provide a balanced solution between the least squares errors and the oscillation of identified system parameters, which leads to a more meaningful solution.

4.2.2 Sparse regularization

In real situations, structural damages usually occur at only a few locations. Therefore, the damage vector will be a sparse vector with most of its items equal to zero or close to zero except for the damaged elements with nonzero items. However, the identified stiffness changes from the Tikhonov regularization technique are usually distributed to most of the elements of the structure. Zhou et al. [52] presented the use of the l_1 norm regularization technique to overcome this limitation of Tikhonov regularization. Another reason to use the sparse regularization technique is based on the fact that usually, only a few shifts in the impedance resonance frequencies are available for the identification in this study; therefore, the identification equation would be an underdetermined problem. To bring a physical understanding and sparse patterns into the solution of the inverse problem, the l_1 norm regularization technique is applied in this study. For this specific problem, the optimization objective function can be written in the following form with the sparsity restriction [6]

$$f_{sparse} = \left\| S\delta_T - \delta_f \right\|_2 + \lambda \left\| \delta_T \right\|_1 \tag{4.5}$$

where $\| \|_1$ denotes the l_1 norm and λ is the regularization parameter. Compared with using conventional Tikhonov regularization, the damage identified using the sparse regularization technique is more often distributed to an individual element with very limited measurement information for an underdetermined problem.

The basis pursuit denoising problem is defined as

$$\text{Minimise } \|\delta_T\|_1 \text{ subject to } \delta_f = S\delta_T \tag{4.6}$$

It can be applied to solve the underdetermined system identification problem with a sparse solution desired. Chen et al. [54] presented a primal-dual logarithmic barrier method to solve this convex optimization problem. In real applications, for example, when measurements with the noise effect are used, it is difficult to have an exact fit to the identification equation. Considering this, Equation (4.7) is used instead,

$$\text{Minimise } \|\delta_T\|_1 \text{ subject to } \left\|S\delta_T - \delta_f\right\|_2 \le \tau \tag{4.7}$$

where the positive parameter τ is an estimated tolerance value. In this study, the abovementioned equation is solved by using the algorithm presented by Van Den Berg and Friedlander [78]. The algorithm was developed to find arbitrary points on the Pareto curve with a root-finding algorithm. To improve the computational efficiency, a duality gap was used to evaluate the quality of approximate solutions. The complete procedure of the spectral projected gradient methods has been given in detail [55]

The flowchart of the proposed structural damage identification approach is shown in Figure 4.1. The impedance responses from the damaged structure are measured, and the analytical impedance responses are calculated with the finite element method using the initial system parameters. The difference between the impedance responses from the damaged and analytical states is then obtained, and the impedance sensitivity matrix is calculated with the analytical finite element. The identification equation is formed to solve the damage parameter vector by using the l_1 norm regularization technique. An iterative scheme, as shown in Figure 4.1, is followed, and the iteration will stop when the following convergence criterion is met.

$$\left\|\frac{\delta_T}{T_i}\right\|_2 \le tolerance \tag{4.8}$$

where T_i is the parameter vector of the segment width of the i^{th} iteration. In this study, the tolerance value is defined as 0.0001.

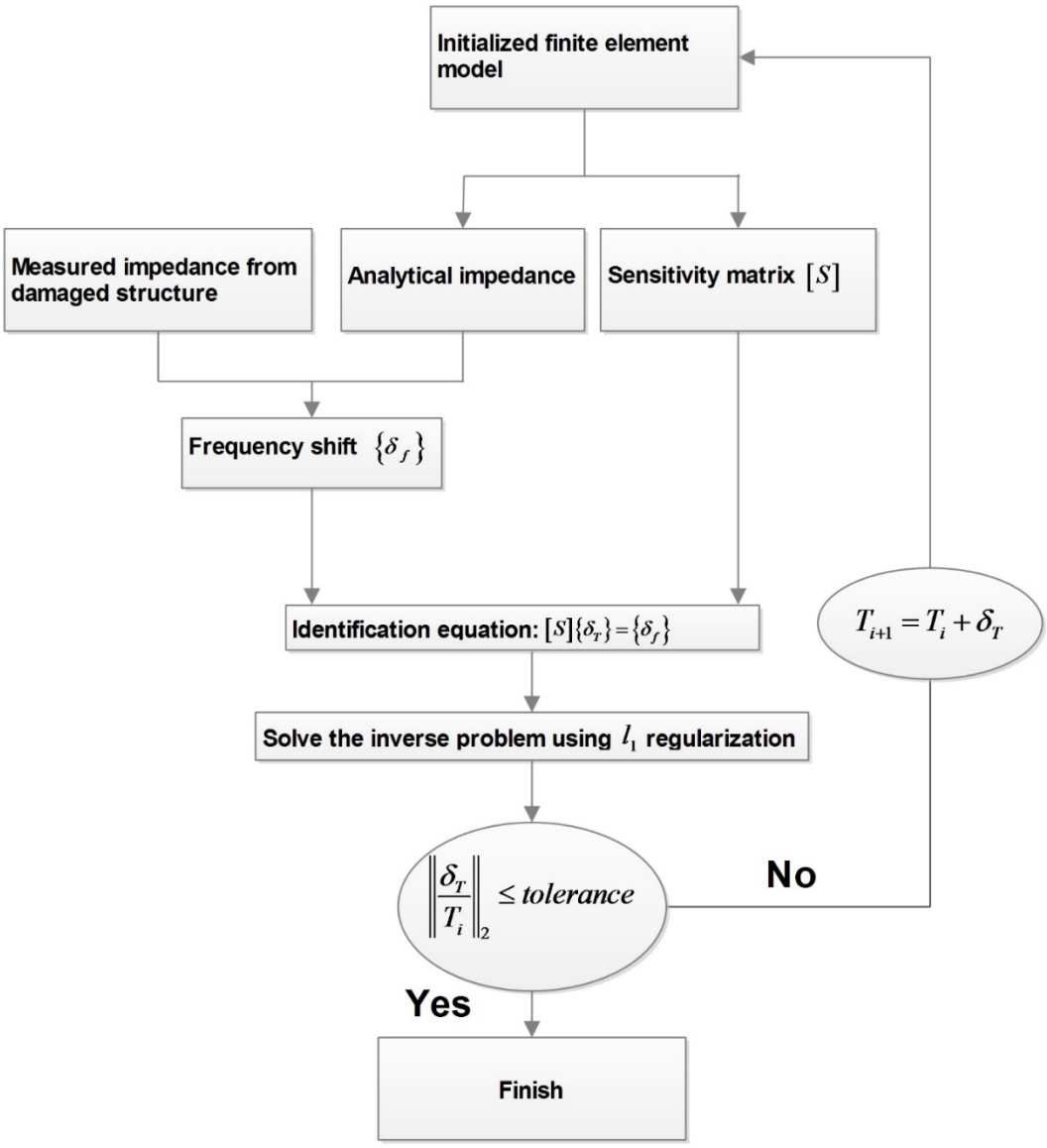

Figure 4.1. Flowchart of the proposed damage identification approach based on impedance sensitivity and sparse regularization

4.3 Finite Element Modelling of the EMI Technique

In this section, EMI calculations of a single PZT patch and PZT-structure coupling are conducted by using the finite element modelling technique. Three-dimensional finite element models of a single freely suspended PZT patch and a PZT patch attached to a beam structure are built for calibrating the impedance responses with previously reported results and validating the finite element modelling technique for impedance calculation.

4.3.1 Damping model

A damping model describes the mechanism of energy dissipation in a structure. The actual relationship between the energy loss and damping force is difficult to model. It can be simplified as a function of velocity or displacement. One of the most commonly used damping models is Rayleigh damping, which can be expressed as a linear combination of the mass and stiffness matrices,

$$C = \alpha M + \beta K \tag{4.9}$$

where M and K are the structural mass and stiffness matrices, respectively; α and β are the damping model coefficients, which can be calculated based on the natural frequencies ω_r and damping ratios ζ_r of the first two modes with the following equation

$$\zeta_r = \frac{\alpha}{2\omega_r} + \frac{\beta\omega_r}{2} \tag{4.10}$$

In most previous studies analysing piezoelectric vibrations, the term relating to the mass matrix in the Rayleigh damping model is ignored, with α equal to zero [43]. In this case, β can be calculated as

$$\beta_r = \frac{2\zeta_r}{\omega_r} \tag{4.11}$$

Lim and Soh [7] reported that a noticeable weakness of using the Rayleigh damping model to study the vibration behaviour of PZT-structural interaction is the limited suitable frequency range. According to Equation (4.11), the monotonically increasing modal damping ratio implies that all modes with a resonance frequency larger than $2/\beta_r$ will be overdamped. However, the modal damping of a real structure is weakly related to frequency. This is the limitation of the Rayleigh model for describing the damping effect in a structure. To overcome the low accuracy caused by this limitation, Lim and Soh [7] developed a finite element model to analyse the impedance responses using the hysteretic damping. Most materials absorb and dissipate energy by themselves as they deform. The energy dissipation is generally associated with the stress-strain hysteresis loop. This kind of structural damping is called hysteretic damping, which is assumed to be weakly related to the mass and mainly dependent on the stiffness of a structure [79].

The hysteretic damping model allows for defining a frequency-independent damping ratio. The damping model coefficient relating to the stiffness β_h can be calculated as

$$\beta_h = \frac{\eta}{\omega} \tag{4.12}$$

where η denotes the mechanical loss factor for the damping, which can be calculated from the frequency-independent damping ratio ξ_h, as used in a previous study (Lim and Soh 2014)

$$\eta = 2\xi_h \tag{4.13}$$

In the hysteretic damping model, $\xi_h = 1/2Q_m$, where Q_m denotes the mechanical quality factor. The structural forced vibration can be expressed as

$$M\ddot{x} + \frac{\eta}{\omega}K\dot{x} + Kx = F(t) \tag{4.14}$$

As defined in Equation (4.9), the damping $C = \beta_h K$. For harmonic vibrations, considering velocity as the derivative of displacement, $x(\mathrm{t}) = x\,\mathrm{e}^{j\omega t}$, Equation (4.11) can be transferred to the complex stiffness matrix characterized model, which is described as

$$M\ddot{x} + (1 + \mathrm{j}\eta)Kx = F(t) \tag{4.15}$$

Compared with the Rayleigh damping model, the hysteretic damping model is normally used to describe the frequency-domain response, as shown in Equation (4.15). By using the frequency-independent damping ratio ξ_h, the hysteretic damping model is able to provide more accurate modal damping and avoid amplitude attenuation in the high frequency range caused by the frequency-dependent damping ratio.

4.3.2 A freely suspended PZT patch

A freely suspended PZT patch with dimensions of 10 mm×10 mm×0.3 mm is simulated by using COMSOL Multiphysics version 5.1, as shown in Figure 4.2(a). Piezoelectric material PIC 151 is used for simulating the PZT patch. The detailed mechanical and piezoelectric property parameters are taken from a previous study [7] and are listed in Table 4.1. To achieve a high accuracy in the simulation results, the hysteretic damping model described in Chapter 2.2 is used.

Table 4.1. Material properties of the used PZT patch

Property	Symbol	Value
Density	ρ	$7760\ kg/m^{-3}$
Compliance	$s_{11}=s_{22}$	$16.8\cdot10^{-12}m^2N^{-1}$
	s_{33}	$19.0\cdot10^{-12}m^2N^{-1}$
	$s_{12}=s_{21}$	$-5.66\cdot10^{-12}m^2N^{-1}$
	$s_{13}=s_{31}$	$-7.11\cdot10^{-12}m^2N^{-1}$
	$s_{23}=s_{32}$	$-7.11\cdot10^{-12}m^2N^{-1}$
	$s_{44}=s_{55}$	$45.0\cdot10^{-12}m^2N^{-1}$
	s_{66}	$45.0\cdot10^{-12}m^2N^{-1}$
Coupling matrix (strain-charge form)	d_{31}	$-2.08\cdot10^{-10}mV^{-1}$
	d_{32}	$-2.08\cdot10^{-10}mV^{-1}$
	d_{33}	$4.23\cdot10^{-10}mV^{-1}$
	d_{15}	$6.1\cdot10^{-10}mV^{-1}$
Relative permittivity	ε_{11}^{S}	1110
	ε_{22}^{S}	1110
	ε_{33}^{S}	852

Considering the symmetric geometry and boundary conditions of a freely suspended PZT patch, only a quarter of it is modelled. In this simulation, a 1V alternating voltage excitation is applied along the perpendicular direction of the plane of the PZT transducer, as shown in Figure 4.2(a). Solid elements are used, and the size of the meshed finite elements is 0.2 mm, which has been demonstrated as being adequately fine to model the electromechanical impedance behaviours at 800 kHz [43]. Usually, each half wavelength should typically consist of three to five nodal points to ensure the accuracy of the finite element simulation to calculate the impedance [80]. The

analytical impedance response obtained from the finite element analysis is compared with the previous experimental result [7] and is shown in Figure 4.2(b). It can be observed that a good agreement is obtained, in terms of both the resonance frequencies and magnitudes. At 600 kHz, the resonance frequencies are very close to those presented in the experimental results. This indicates that the described finite element model accurately simulates the impedance response of a single PZT patch. The simulation results only show a large error in the second resonance peak. The reason for this could be the high sensitivity of electromechanical impedance to the structural boundaries and surface in such a high frequency range. Any minor difference between the experimental and numerical models could cause this error, such as the manufacturing flaws, the variation of boundary condition and the surface roughness, the solder joints on the suspended PZT patch and the interaction between the PZT patch and the wires. The frequency of the second resonance peak is higher than 200 kHz. The impedance behaviour is extremely sensitive in such a high frequency range. A possible reason could be the boundary condition and other details that are hard to simulate in the finite element model, such as the solder joints on the suspended PZT patch and the interaction between the PZT patch and the wires. In this study, the most possible reason could be the bonding of the edges of transducers. The transducers are manually glued on the host structure, it is difficult to control distribution and thickness of the adhesive on edges of PZT patches. This leads to a slight difference between the boundary conditions in test and simulation. A similar observation has been reported in a previous study [30]. This error is due to the edge-roughness-induced secondary vibrations and the uncertainties in the finite element modelling.

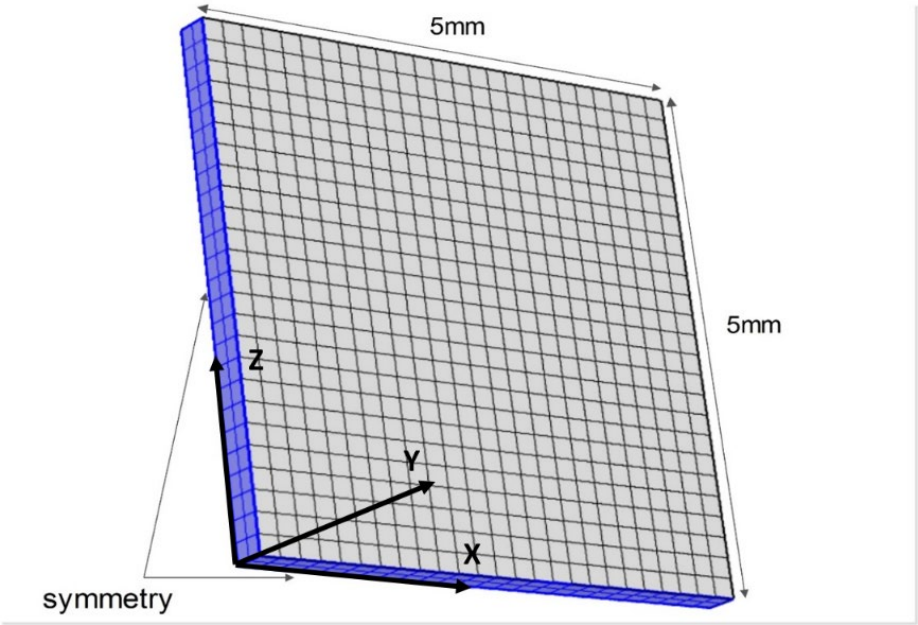

(a)

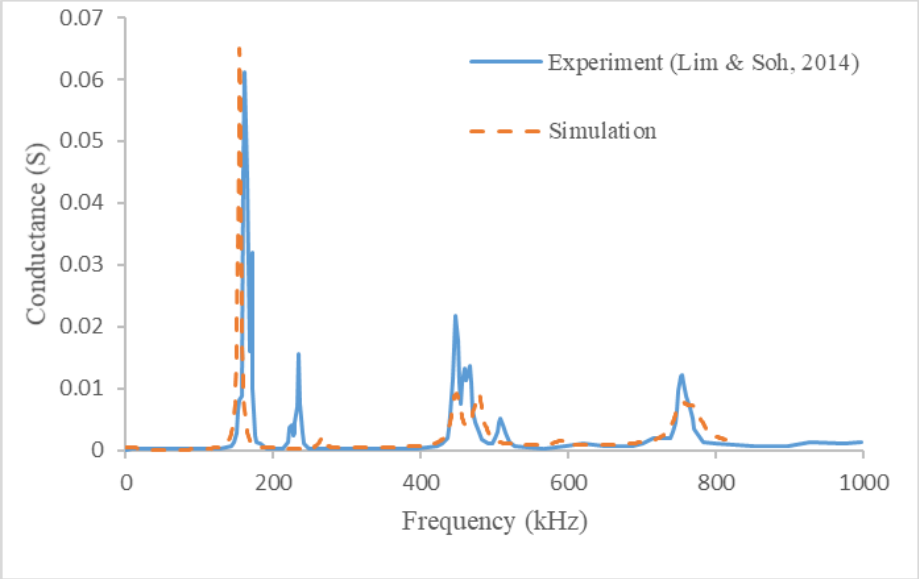

(b)

Figure 4.2 (a) Finite element model of a freely suspended PZT patch; (b) model calibration results for impedance responses

4.3.3 PZT-Structure coupling

When developing the finite element model to consider the PZT-structure coupling, a narrow aluminium plate with the size of 231 mm×26 mm×4 mm is defined as the host structure. A PZT transducer patch with dimensions of 10 mm×10 mm×0.3 mm is bonded onto the centre of the beam. As in the case of the single PZT patch model described above, to improve computational efficiency, a quarter of the PZT-structure coupled finite element model is built considering the symmetry, as shown in Figure 4.3(a). It is assumed that the thickness of the thin bonding layer between the PZT patch and the host structure is 0.05 mm. The material properties of the aluminium beam and the adhesive layer are shown in Table 4.2, obtained from a previous study [7]. The mesh size is set as 0.5 mm for both the structure and the PZT patch, which is sufficiently fine for the selected frequency range of 20-60 kHz.

Table 4.1. Material properties of the aluminium plate and bonding layer

Property	Material	Symbol	Value
Density	Aluminium	ρ	2710 kg/m^{-3}
	Bonding layer		1000 kg/m^{-3}
Young's modulus	Aluminium	Y	70.6 GPa
	Bonding layer		1.4 GPa
Poisson ratio	Aluminium	υ	0.35
	Bonding layer		0.4
Damping ratio	Aluminium	ξ	0.0005
	Bonding layer		0.02

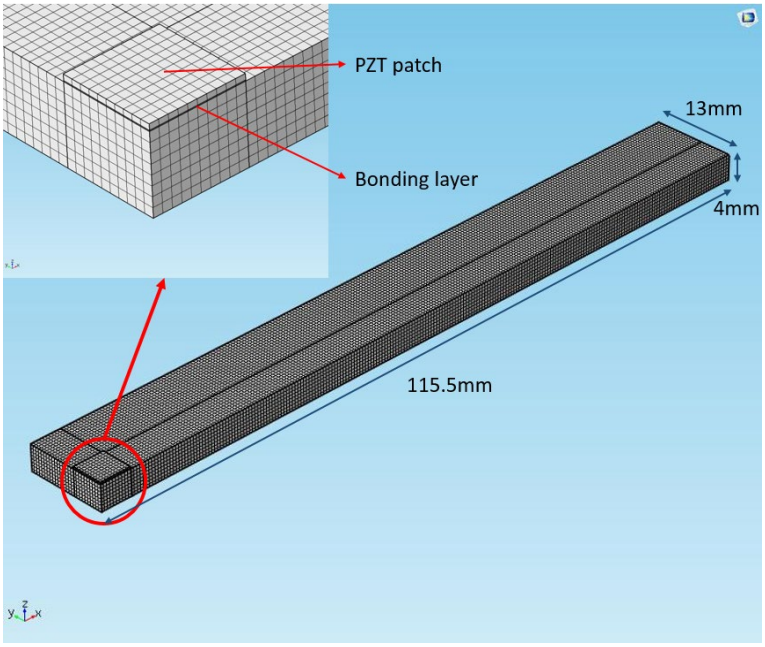
PZT patch
Bonding layer
13mm
4mm
115.5mm

(a)

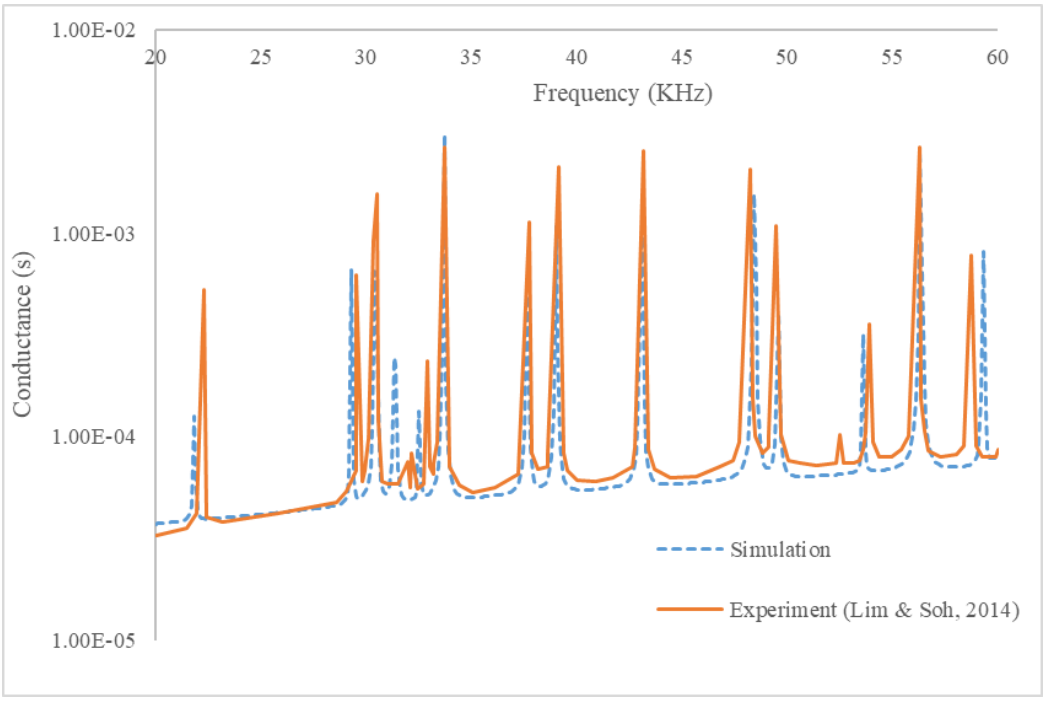
1.00E-02
1.00E-03
1.00E-04
1.00E-05
Conductance (s)
20
25
30
35
40
45
50
55
60
Frequency (KHz)
Simulation
Experiment (Lim & Soh, 2014)

(b)

Figure 4.3 (a) Finite element model of an aluminium beam bonded with a PZT transducer; (b) model calibration of the PZT-structure coupling impedance responses

To validate the accuracy and correctness of the finite element modelling technique, Figure 4.3(b) shows the impedance responses obtained from the finite element analysis compared with the experimental result [7]. Only the impedance responses in the frequency range from 20-60 kHz are shown, and it is observed that most resonance peaks located in this range well match the experimental results. The accuracy in simulating these resonance frequencies is good, and only the magnitudes at some frequencies for the simulated impedance responses cannot exactly match the values obtained in the experimental study. One of the significant reasons for this phenomenon could be the system uncertainties in modelling, such as the manufacturing errors, material inhomogeneity and uncertainties in the thickness and shape of the bonding layer in the experimental study. Another reason is that the resonances in such a high frequency range are very sensitive to the element size and structural geometry [81]. Generally, a good accuracy in simulating the resonance frequencies can be achieved. This also demonstrates that using the shifts in resonance frequencies, especially those with higher energy amplitudes, for structural damage identification would be feasible in subsequent studies on structural damage identification with impedance responses. It should be noted that most resonance frequencies are accurately simulated, especially those with higher energy amplitudes; however, there are some errors observed for a small number of resonance frequencies. When using the shifts in resonance frequencies for model updating, those with high energy amplitudes are preferred to obtain a better identification accuracy.

4.4 NUMERCIAL STUDIES ON DAMAGE IDENTIFICATION

It has been demonstrated that the presented finite element modelling technique is capable of simulating the impedance responses accurately. In this section, only the shifts in the resonance frequencies observed in the selected frequency range of the impedance curve are used for structural damage identification, as the resonance frequencies can be more accurately estimated than the magnitudes. Moreover, the frequency shifts are more directly related to the structural condition changes than the amplitudes, which are affected by many other factors. Considering that only a small number of frequency shifts are obtained in a specific frequency range, the l_1 norm regularization technique is employed to obtain a sparse output in the damage identification. The effectiveness and accuracy will be compared with those of the traditional Tikhonov regularization. The effects of noise in the measured impedance signals and the number of available frequency shifts on the performance of the proposed damage identification approach will be studied.

4.4.1 Damage identification results

With the above accurate numerical modelling technique developed to simulate the PZT-structure interaction and to obtain the impedance, the accuracy and performance of the proposed approach in structural damage identification are investigated. A PZT transducer with dimensions of 10 mm×10 mm×0.3 mm is bonded to the middle of the aluminium beam model with the size of 220 mm×30 mm×4 mm. As shown in Figure 4.4(a), the right side of the host structure is divided into 10 segments. Minor structural damage is simulated by reducing the width of the cross section of a specific individual segment. D1 to D10 represent the reduction in the width of the cross section of the corresponding segment. In this study, since 8-node hexahedral solid elements are used to mesh the model, there should be at least 4 elements per wavelength. The wave velocity travelling in the aluminium plate can be calculated as

$c = \sqrt{E/\rho} = 5104.1(m/s)$, where E and ρ denote the elastic modulus and mass density of the aluminium material, respectively. The element size is selected as 2.5 mm, which is sufficient to cover the frequency range of 20 to 40 kHz used in the following structural damage identification. The coupled PZT-structure model is shown in Figure 4.4(b).

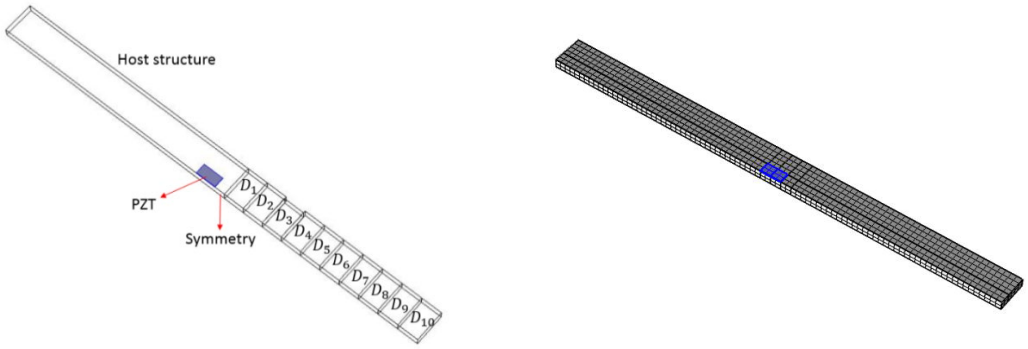

(a) Segments of the host structure

(b) Finite element model of the coupled PZT-structure

Figure 4.4. Coupled PZT-structure model

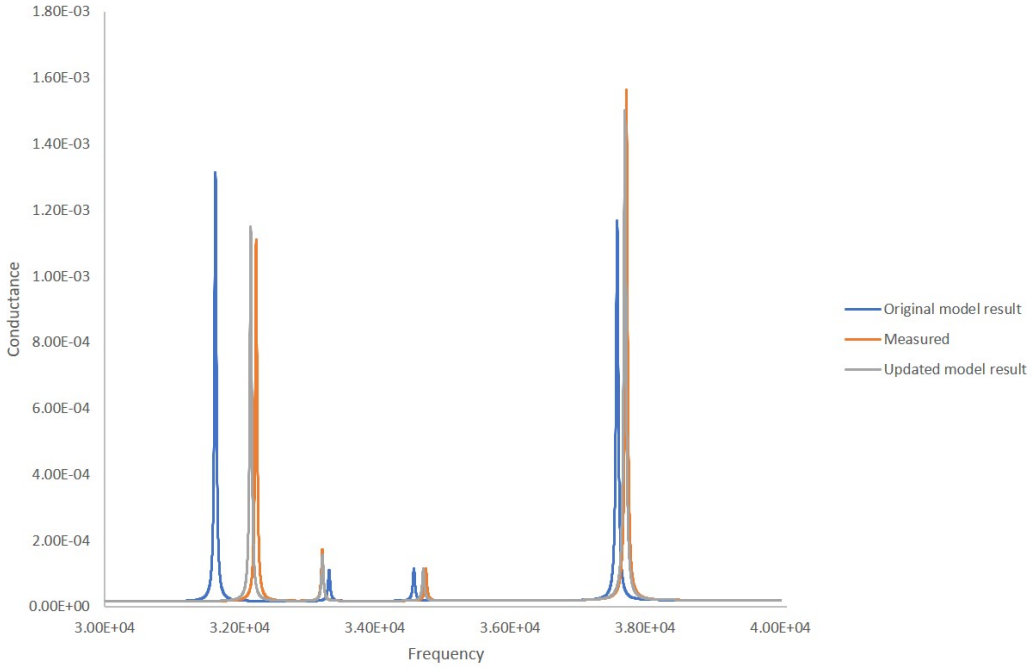

Figure 4.5 Impedance curves between 30 kHz and 40 kHz for the original model, damaged structure and updated model

Single and multiple damage scenarios are considered in this study. For the single damage scenario, a reduction of 0.9 mm in the width of the 3rd segment is simulated. As mentioned in previous sections, the resonance frequency shifts in the impedance responses are expected to be more sensitive and reliable for the identification of the structural damage and will be used for the identification here. Priya et al. [82] presented a study using the EMI technique to identify bolt-loosening damage. Their results showed that the root-mean-square deviation of impedance behaviour between 10 and 50 kHz has a higher sensitivity to the damage. However, the selection of a suitable frequency range depends on the size and type of damage. In this study, considering the mesh size, computational efficiency and number of the resonance frequencies, impedance response in the frequency band of 20 to 40 kHz is selected for

damage identification. Eight resonance frequency shifts are observed in this range. The damage identification procedure as described in Figure 4.1 is followed to update the finite element model and identify the minor structural damage. These 8 frequency shifts and the initial coupled PZT-structure model are used for the damage identification. The l_1 norm regularization technique is used to solve this underdetermined inverse problem by using the 8 available resonance frequency shifts to identify 10 unknown parameters. For the single damage scenario with damage in the 3rd segment, Figure 4.5 shows the impedance curves from the healthy, damaged and updated structure states. Significant frequency shifts are observed due to such minor damage, and the impedance responses between the damaged and updated structural states matched very well. Figure 4.6(a) shows the identification results obtained using both the Tikhonov and l_1 norm regularization techniques for this single damage scenario with 8 frequency shifts. The identification with both the Tikhonov and l_1 norm regularization can successfully identify the location of the introduced damage in the 3rd segment. Minor false predictions in other undamaged segments are observed mainly due to the numerical error associated with solving the optimization problem by employing the sensitivity-based method. The damage severity identified with the l_1 norm regularization technique is 0.88 mm, which is closer to the true damage extent than that obtained from the Tikhonov regularization. As discussed in Chapter 3.2, the solution obtained using the Tikhonov regularization tends to distribute the damage to more elements around the damaged location so that a lower damage severity is identified, which is approximately 0.77 mm in this case. Moreover, several significant false identifications are observed in the solution obtained using Tikhonov regularization, such as 0.17 mm identified in the 4th segment and 0.1 mm in the 7th segment. In contrast, only very small false identifications are observed, e.g., 0.01 mm in the 7th segment and 0.1 mm in the 10th segment, in the identification result obtained with the l_1 norm regularization technique.

A study with even less measurement information is conducted to investigate the robustness of the proposed approach when only a few measured frequency shifts in the impedance responses are available. Figure 4.6(b) shows the identification results with only 2 frequency shifts at approximately 27 kHz and 31 kHz in the damaged structural state. It is observed that the use of Tikhonov regularization fails to identify the simulated damage accurately with only 2 frequency shifts. The predicted reduction in the cross-sectional width of the 3rd segment is only 0.41 mm, and a large false prediction of approximately 0.35 mm is observed in the 7th segment. However, l_1 norm regularization can still successfully identify the location and severity of the introduced damage. The width reduction is identified as 0.93 mm in the 3rd segment, which is very close to the true value of 0.9 mm. No false identification is observed.

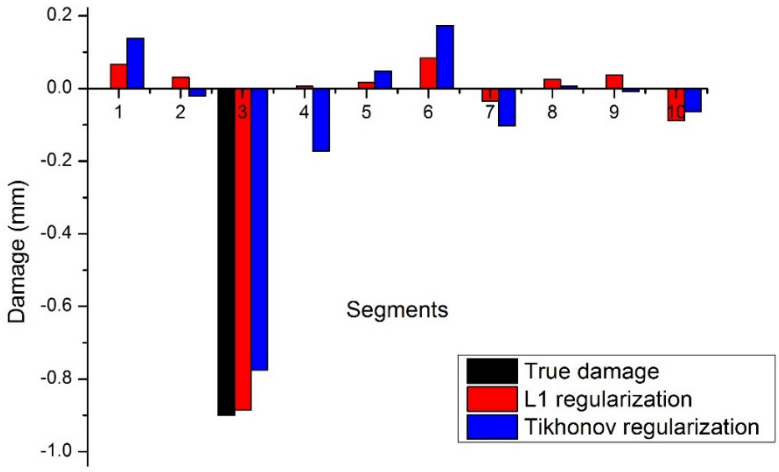

(a)

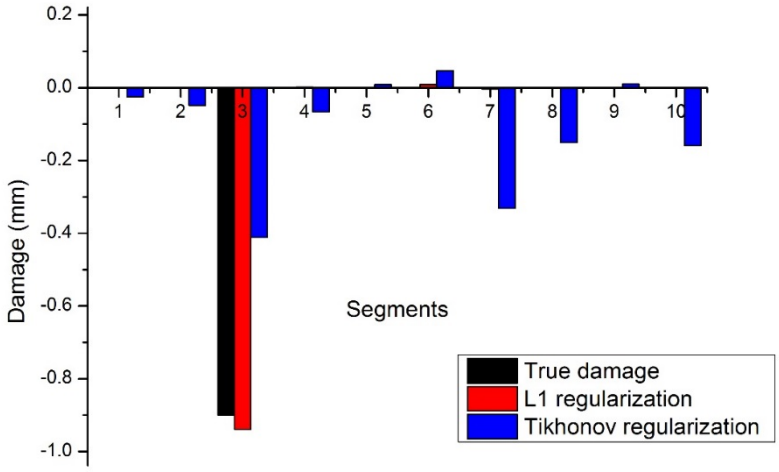

(b)

Figure 4.6 Damage identification results with single damage in the 3rd segment using

(a) 8 frequency shifts; (b) 2 frequency shifts

A multiple damage scenario is further simulated with two locations of damage introduced in the 3rd and 9th segments with 0.5 mm and 0.9 mm width reductions, respectively. It is worth noting that the proposed damage detection identification procedure does not require the number of damages to be defined in advance. The host structure is initially defined as in its undamaged status. For the multiple damage scenario, the same identification procedure is followed to locate and quantify damages based on the measured impedance behavior and the intact model. The identification results using 8 frequency shifts are shown in Figure 4.7(a). Both damage locations can be detected accurately, and the reductions in the cross-sectional width are identified as 0.45 mm and 0.91 in the 3rd and 9th segments, respectively,

when using l_1 norm regularization. These identified damage severities are close to the true values. Several false identifications of approximately 0.01 mm are observed in the 5th, 6th, 8th and 10th segments. The results from Tikhonov regularization underestimate the damage, with larger false identification errors of approximately 0.02 mm in the 1st, 6th, 8th and 10th segments. This again shows the advantage of using l_1 norm regularization for identifying damage with a limited number of frequency shifts in the impedance responses. In this study, for both single and multiple damage scenarios, when 8 frequency shifts are used for identification, the numbers of required iterations until convergence are 3 and 4 when using the Tikhonov regularization and sparse regularization methods, respectively.

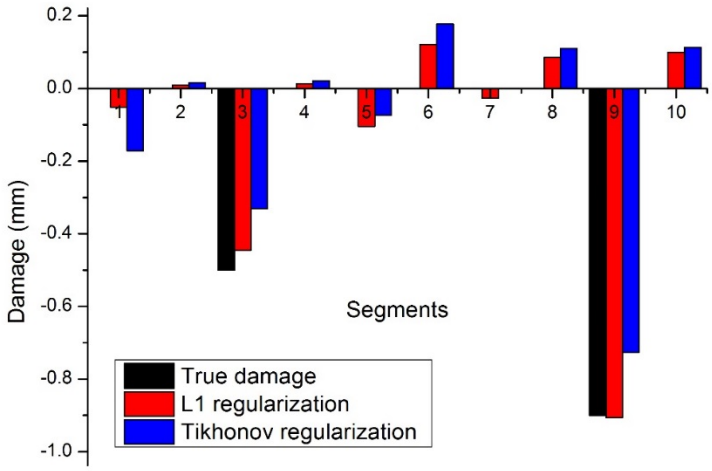

(a)

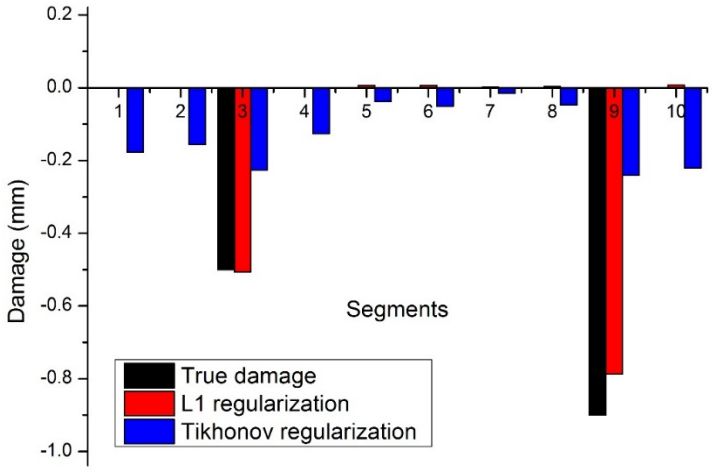

(b)

Figure 4.7 Damage identification results for a multiple damage scenario using

(a) 8 frequency shifts; (b) 2 frequency shifts

When using only 2 frequency shifts in the impedance curves for identification, Figure 4.7(b) shows the results from both the Tikhonov and l_1 norm regularization techniques. It can be observed that the use of Tikhonov regularization fails to identify the damage locations and severities. However, the use of the l_1 norm regularization technique can well identify the two introduced damages. The identified reductions are 0.51 mm and 0.79 mm in the 3rd and 9th segments, respectively. It should be noted that in this study, only one PZT transducer patch is installed, and only a few frequency shifts in the impedance responses are used for identification; however, good identification results can still be obtained by using the proposed approach. These results well demonstrate the advantage of using the sparse regularization

technique over the traditional Tikhonov regularization technique, as well as the effectiveness and accuracy of using only a few frequency shifts in the impedance signals to identify minor structural damage, including single and multiple damage scenarios.

4.4.2 Noise effect in the measurement

Numerical verifications on the use of the proposed approach for structural damage identification considering the noise effect in the impedance measurements are conducted. The impedance responses from PZT transducers in a high frequency range are usually insensitive to the ambient vibrations in the tests. However, an environmental effect, i.e., temperature, on the electromechanical impedance behaviour is significant [83-85]. Gyuhae et al. [84] illustrated that a temperature variation led to a frequency shift in the impedance. Therefore, in this study, the environmental effect is considered as a random shift in the resonance frequencies. In the experimental study conducted by Sepehry et al. [85] and Wandowski et al. [86], temperature variation-caused frequency shifts for selected resonance peaks (between 1 kHz and 20 kHz and between 80 kHz and 90 kHz) were presented. There was a frequency shift of approximately 0.2% in the resonance frequencies in the range from 1 kHz to 20 kHz for a $6\,^{\circ}C$ temperature change. Based on their studies, to simulate the effect of environmental uncertainty, i.e., temperate change, a random shift in the resonance frequencies with a mean value of 0.2% of the resonance frequencies is added to the impedance curve calculated from the damaged finite element model in this study. Only two frequency shifts at 27 kHz and 31 kHz, obtained from the noisy impedance response, are used for identification. For the single damage scenario, the generated frequency shifts are approximately 60 Hz. The damage-induced frequency shift at the resonance frequency of 27 kHz is 365 Hz. This shows that the added frequency shift simulating the noise effect is quite significant.

Figures 4.8(a) and (b) show the damage identification results for both the single and multiple damage scenarios when considering the noise effect in the impedance measurements. It is observed that both the location and severity of the introduced damage are well identified by using the l_1 norm regularization technique. The effect due to the noise in the measured impedance on the identification results obtained using the l_1 norm regularization techniques is not significant. The identified width reduction in the 3rd segment in the single damage scenario is 0.995 mm with the noisy impedance response. A few minor false identifications are observed. For the multiple damage scenario, it can be observed that the proposed approach gives good accuracy in detecting the location and severity of minor structural damages. However, the use of Tikhonov regularization is not able to produce acceptable damage identification results. The identified damage severities are far less than the true values, and a number of false identifications are obtained. This approach even fails to identify the damages in the multiple damage scenario. The results considering the noise effect well demonstrate the effectiveness and robustness of the proposed approach for structural damage identification using impedance frequency shifts and the sparse regularization technique.

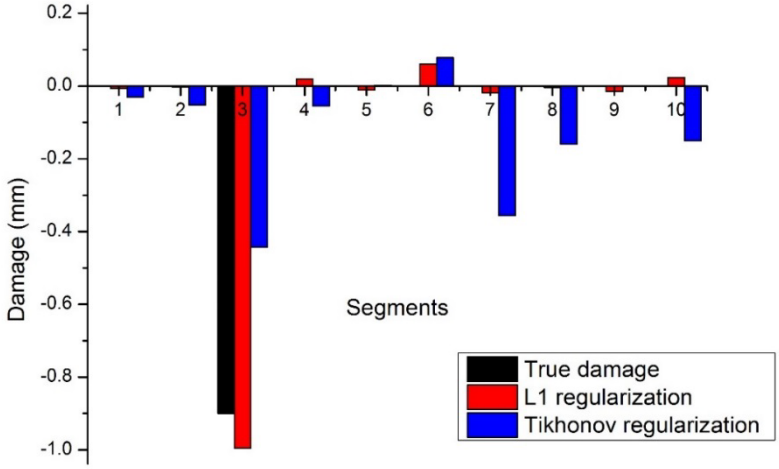

(a)

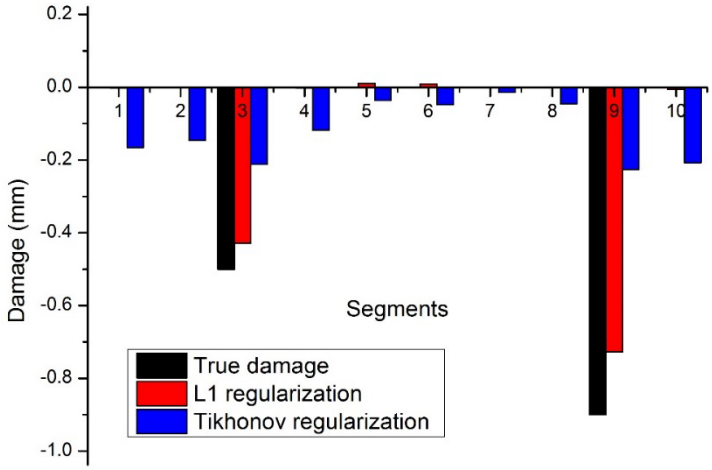

(b)

Figure 4.8 Damage identification results using 2 frequency shifts with the noise effect: (a) single damage scenario; (b) multiple damage scenario

4.5 Discussion and Concluding Remarks

This chapter proposes a minor structural damage identification approach based on model updating with impedance sensitivity and sparse regularization. The sensitivities of impedance resonance frequency shifts to the cross section parameters of the host structure are calculated and used to identify the damage with only a few frequency shifts in the impedance responses before and after damage. The damage location and severity are identified. The effectiveness and performance of the proposed approach are demonstrated with numerical simulations on a narrow aluminium plate, where a PZT transducer patch is bonded. The finite element modelling technique used to calculate the impedance response is verified by calibrating the models of a single PZT patch and the PZT-structural interaction. Numerical studies on damage identification for a PZT transducer bonded to an aluminium plate are conducted. Only a small number of frequency shifts in a specific frequency range are used for the identification with the sparse regularization, namely, the l_1 norm regularization technique. The effectiveness and accuracy are compared with those of the traditional Tikhonov regularization. The performance of the proposed method with noisy impedance signals and a lower number of available frequency shifts for damage identification is also investigated. The results demonstrate that the proposed approach can well identify both the location and severity of the simulated structural damage, even if the measured signal is noisy and the number of frequency shifts in the measured data is limited.

5 Experimental study on structural damage identification using sparse regularization and impedance sensitivity for a beam structure

The objective of the experimental study is: 1) To obtain the impedance behaviour from an undamaged structure and update the FE model; and 2) To identify the simulated damage based on the experimental results acquired from the damaged structure using the proposed method. The detailed procedures are illustrated in the following sections.

5.1 Test of the EMI technique with a surface-bonded PZT transducer

To investigate the performance of using the proposed approach in structural damage localization and quantification, experimental tests are conducted on a narrow aluminium beam to which two PIC 255 PZT transducers are bonded, as shown in Figure 5.1. The piezoelectrical properties of the PZT transducers provided by the manufacturer are listed in Table 5.1. The dimensions of the aluminium beam and the PZT transducer are 300mm×45mm×4mm andϕ8×0.25mm, respectively, as shown in Figure 5.2. Epoxy glue is used to bond the transducer onto the beam, and the thickness of the bonding layer is maintained at approximately 0.15 mm. The PZT transducers are placed 70 mm from the ends of the aluminium beam. Table 5.1 shows the material properties of the host structure and bonding layer. The free boundary condition is produced by placing the aluminium beam on a soft foam. To acquire the electromechanical impedance response, the PZT transducer is driven by an EVAL-AD5933EB impedance analyser, which is connected to a computer. As mentioned in previous sections, the resonance frequency shifts in the impedance responses are expected to be more sensitive and reliable to identify the structural damage and will

be used for the identification. Priya et al. [82] presented the study using EMI technique to identify the bolt loosen damage, and showed the RMSD of impedance behaviour in 10-50 kHz has a higher sensitivity to the damage. However, the selection of the suitable frequency range depends on the structural mesh size and type of damage. In this study, considering the mesh size, computational efficiency and the number of the resonance frequencies, the impedance response in a frequency band from 20-30 kHz is selected for damage identification. The sweeping frequency range is defined from 20 kHz to 30 kHz, with a sweeping voltage of 1 V. Two undamaged specimens are shown in Figure 5.3. To ensure that the measured impedance responses from undamaged specimens are stable and repeatable, three PZT transducers each are bonded onto two undamaged aluminium beams for measuring the baseline impedance. It is noted that two PZT transducers are placed at symmetric locations on a specimen. The impedance responses measured from these three transducers are used for the model update in the subsequent section to calibrate the initial PZT-structure coupled finite element model.

Table 5.1 Mechanical properties of the host structure and bonding layer

Parameters	Host structure	Bonding layer
Density	2710 kg/m^{-3}	1000 kg/m^{-3}
Young's modulus	70.6 GPa	1.4 GPa
Poisson ratio	0.35	0.4
Hysteretic damping ratio	0.0005	0.02

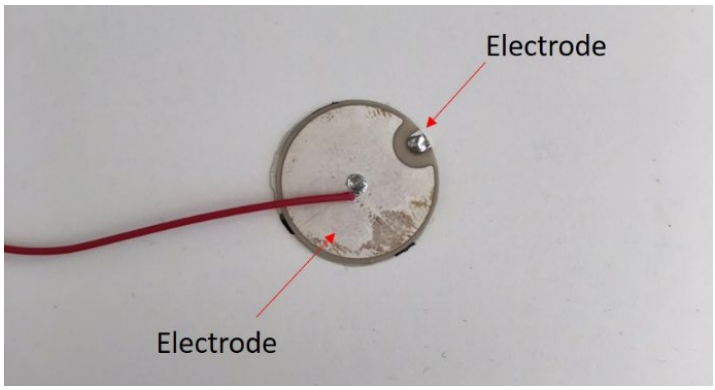

Figure 5.1 PIC 255 cylindrical piezoelectric transducer

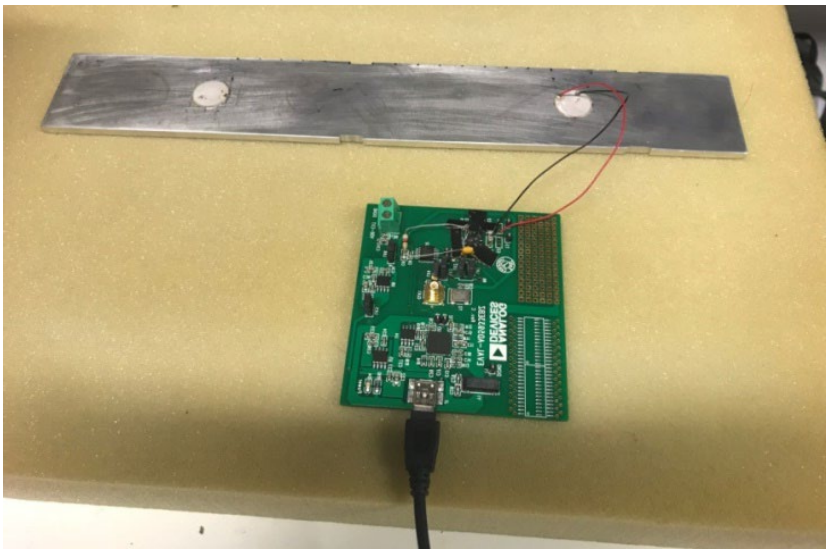

Figure 5.2. PZT-structure interaction test setup

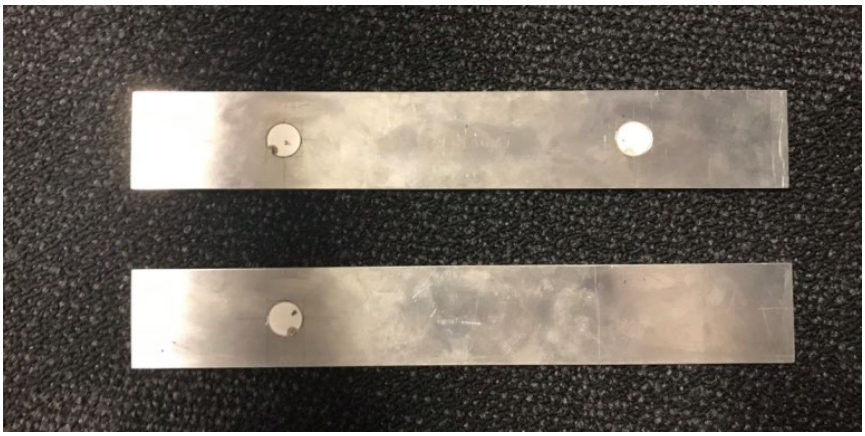

Figure 5.3. Configuration of pristine specimens

5.2 Finite element model calibration for PZT-structure interaction

Figure 5.4 shows the finite element model of a PZT transducer bonded onto an aluminium beam to simulate the PZT-structure coupling in the experimental tests. Considering the symmetry, only half of the structure and PZT transducer are simulated to increase the computational efficiency. In the finite element model, a 4-node tetrahedral element is used to mesh the PZT transducer, bonding layer and host structure around the transducer. An 8-node hexahedral solid element is employed to mesh the rest of the aluminium beam. COMSOL Multiphysics permits the application of a constant voltage input to the PZT transducer in harmonic analysis. This input represents a sinusoidal frequency sweeping. A 1 V voltage is applied to the top surface of the PZT transducer as a boundary condition in the software. Following the recommendation of Makkonen et al. [80], there should be at least 4 nodes for each wavelength. The impedance behaviour between 20 kHz and 30 kHz is selected for damage identification. Since the 8-node hexahedral solid element is applied to the numerical study and the wave velocity travelling in aluminium can be estimated by $c = \sqrt{E/\rho} = 5104.1(m/s)$, the element size is fixed at 2 mm to balance the computational efficiency and simulation accuracy.

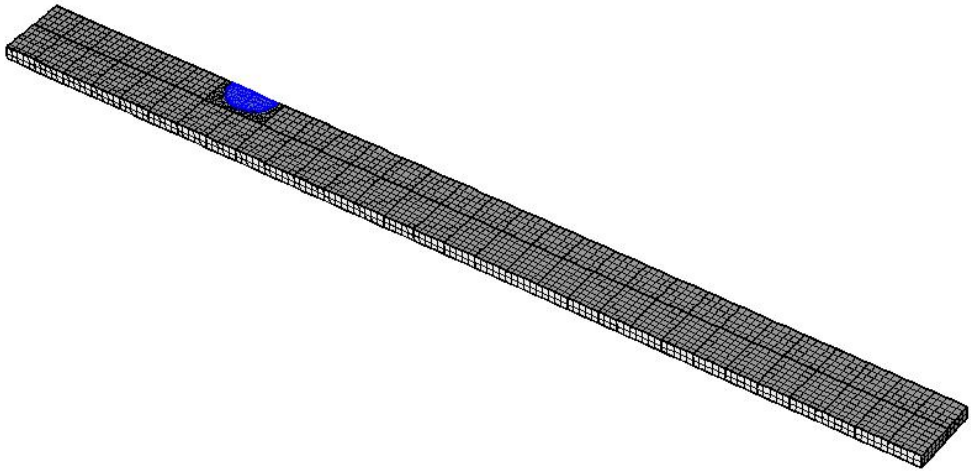

Figure 5.4 Isotropic view of half of the coupled finite element model with a PZT attached on aluminum beam

Table 5.2 Piezoelectric properties of PIC 255 PZT transducer

Parameters		Value provided by manufacturer	Updated value
Density (kg/m^3)	ρ	7760	7760
Compliance (m^2N^{-1})	S_{11}, S_{22}	1.590×10^{-11}	1.568×10^{-11}
	$S_{12}=S_{21}$	-6.599×10^{-11}	-6.599×10^{-11}
	$S_{13}=S_{31}$	-7.376×10^{-12}	-7.376×10^{-12}
	S_{33}	2.097×10^{-11}	2.170×10^{-11}
	S_{44}, S_{55}	4.492×10^{-11}	4.135×10^{-11}
	S_{66}	4.319×10^{-11}	4.319×10^{-11}
Piezoelectric coupling coefficient (mV^{-1})	$h_{31}=h_{32}$	1.740×10^{-10}	1.820×10^{-10}
	h_{33}	3.940×10^{-10}	3.904×10^{-10}
	d_{24}	5.35×10^{-10}	5.35×10^{-10}
	d_{15}	5.35×10^{-10}	5.35×10^{-10}
Electric permittivity	ε_{11}	1649	1649
	ε_{22}	1649	1649
	ε_{33}	1750	1750
Hysteretic damping ratio	ξ_{PZT}	0.00625	0.0126

The material properties listed in Tables 5.1 and 5.2 are adopted as initial values. A basic sensitivity analysis is carried out to estimate the sensitivity of the impedance signatures to the material parameters of the PZT transducer. Each parameter in Table 1 is altered with a change of 5%, and several of the most sensitive parameters to the

resonance peaks, including the compliance parameters S_{11}, S_{22}, S_{33}, S_{44}, and S_{55}, the piezoelectric coupling coefficients h_{31} and h_{33}, and the damping ratio ξ_{PZT}, are selected for model updating. The resonance peak frequency shifts in the impedance response between 20 kHz and 30 kHz are used for the model calibration. After updating, a good match between the analytical and testing impedance is achieved. The final updated parameters are also listed in Table 5.2. Comparisons of the impedance signature and resonance frequencies between the analytical results after model calibration and the experimentally measured results are shown in Figure 5.4 and Table 5.3, respectively. The impedance signatures of these three different transducers on the intact structures agree well with each other, indicating consistency in the measurements and their repeatability. As shown in Figure 5.5, the analytical impedance calculated from the finite element model has good agreement with that measured by the three PZT transducers. The resonance peak frequencies listed in Table 5.3 show that the finite element model after updating provides a good accuracy in model calibration, representing the experimental testing structure. Most analytical resonance peak frequencies well match the test results, except for a minor difference in the 3rd peak. Consequently, the shifts in the other 6 resonance frequencies are used for damage detection in the subsequent studies.

It should be noticed that even though a good accuracy in simulating the resonance frequencies is achieved, there are some notable errors in the magnitudes of impedance responses. One of the primary reasons could be the system uncertainties in the coupled system material properties and contact surface. Even minor uncertainties could cause a large difference in the high frequency range of the impedance calculation. On the other hand, the exactly matched magnitudes of impedance are not necessary in this study, since the resonance frequency shifts are used to identify structural damage. This also demonstrates the necessity to develop the proposed approach since only a few numbers of reliable measurements, i.e. those six resonance frequency shifts in this case, need be used for identification by using the sparse

regularization to enhance the accuracy and efficiency of model updating and structural damage identification.

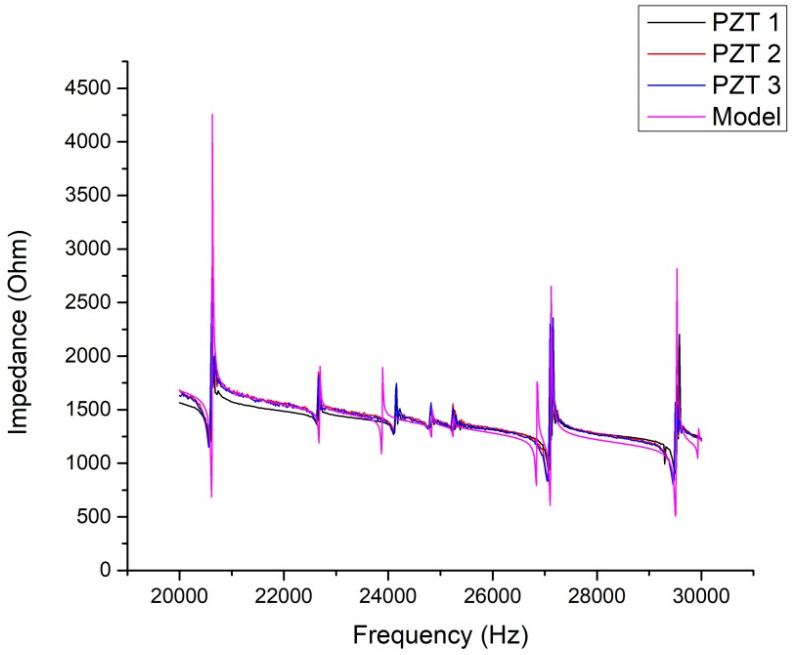

Figure 5.5 Comparison of impedance behaviours acquired from the surface-bonded PZT transducer between the FE model and experiments

Table 5.3 Resonance peak frequencies extracted from tests and simulation.

Peak No.	Test result (Hz)			Simulation (Hz)
	PZT1	PZT2	PZT3	
1st	20620	20620	20620	20621
2nd	22660	22660	22660	22666
3rd	24160	24160	24160	23895
4th	24830	24820	24820	24820
5th	25240	25240	25240	25240
6th	27140	27160	27160	27154
7th	29550	29540	28540	29529

5.3 Damage simulation and finite element model for damage identification

The calibrated finite element model serves as the baseline model to investigate the accuracy and performance of the proposed approach in damage identification with experimental testing measurements. The aluminium beam is divided into 30 segments, each with a length of 10 mm. Minor structural damage is simulated by slightly reducing the widths of both sides of a specific segment. The damage factor can be calculated by $p_i = \frac{a - a'}{a}$, where a and a' are the widths of the undamaged and damaged segments, respectively. The values of p_1, p_2 … p_{30} of the segments are the stiffness factors to be identified. For damage identification iteration, the mesh size at both edges with saw cuts of the aluminium beam depends on the size of the damages, as the cut depth could be smaller than 2 mm, the fixed mesh size of the whole structure. For example, to simulate a 0.5 mm depth cut, the cut edges of the aluminium beam are meshed with a size of 0.5 mm, as shown in Figure 5.6.

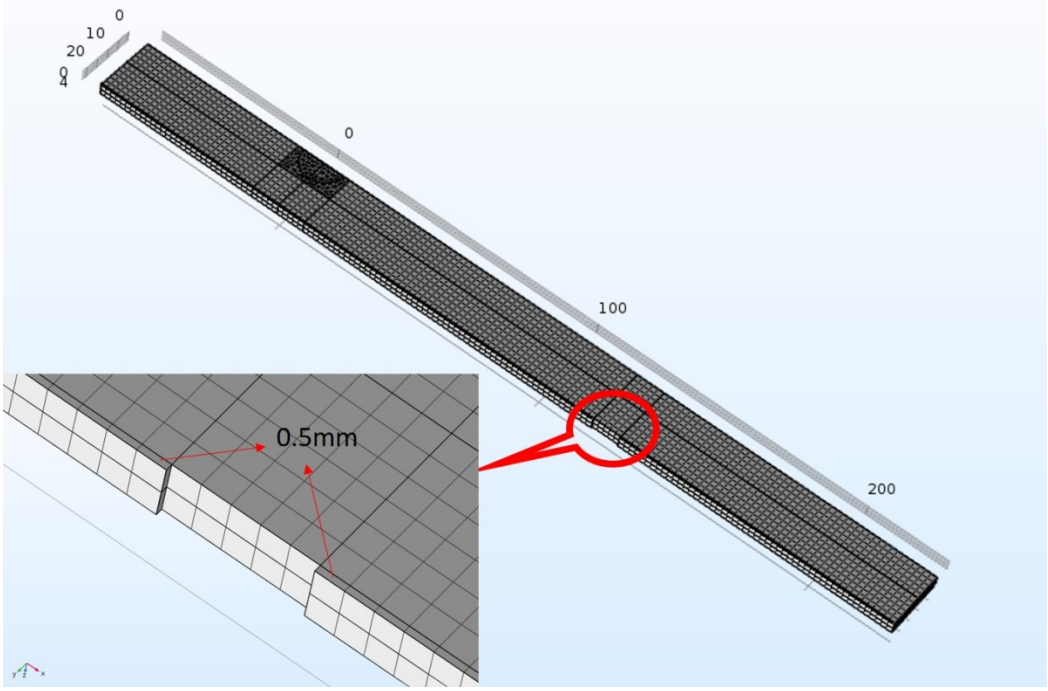

Figure 5.6. Mesh of the edge of the damaged aluminium beam

Figure 5.7 shows the flowchart of the proposed damage identification approach. The initial finite element model calibration is conducted to develop a baseline model. The damage identification procedures in this study are described as follows

Step 1: Build the PZT-structure coupled finite element model with the initial system parameters, and calibrate the initial finite element model with impedance measurements from intact structures;

Step 2: Measure the impedance responses from damaged structures, and calculate the analytical impedance from the finite element analysis with the initial system parameters;

Step 3: Obtain the impedance resonance frequency shifts $\{\delta_f\}$ between the measured and analytical impedance resonance frequencies;

Step 4: Calculate the sensitivity matrix of the resonance frequency shifts with respect to the system parameters to be identified;

Step 5: Identify the structural damage vector $\{\Delta p\}$ by solving the optimization problem as shown in Eq. (4), and update the structural system parameter vector;

Step 6: If the following convergence criterion is met, the iteration process is completed. Otherwise repeat Steps 2-5.

$$\left\| \frac{\Delta p}{p_i} \right\|_2 \leq tolerance \tag{6}$$

where p_i is the structure system parameter vector of the i^{th} iteration, Δp is the perturbation in the structure system parameter vector. In this study, the *tolerance* is defined as 0.0001.

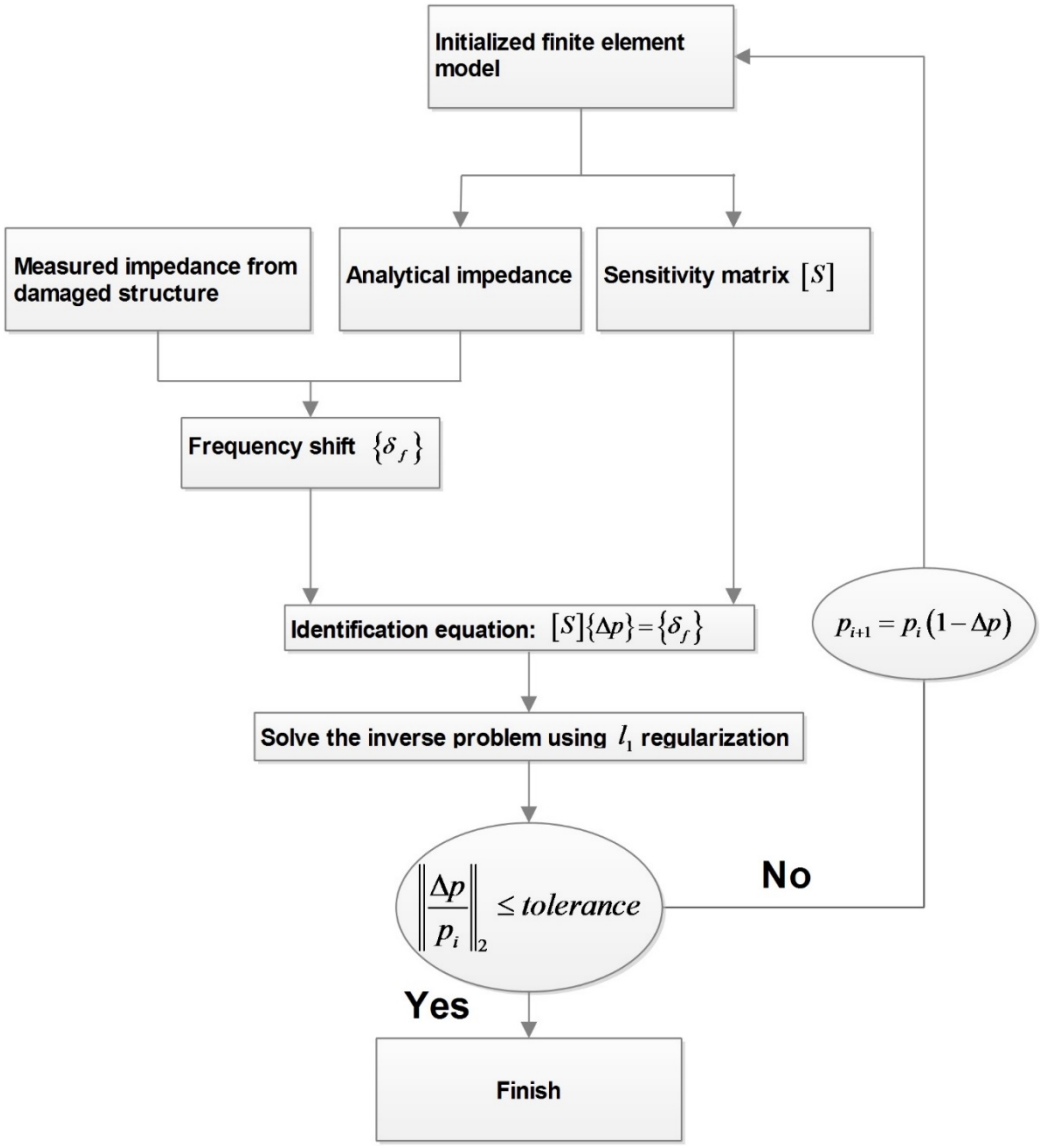

Figure 5.7. The flowchart of the proposed approach

Four damage scenarios are designed in the experimental studies, including two single damage scenarios, namely S1 and S2, and two multiple damages scenarios, i.e. M1 and M2. The detailed settings in these damage scenarios are listed in Table 5.4. For each scenario, the above described procedure is followed to identify the structural damage with the corresponding extracted resonance frequency shifts.

Table 5.4 Details of damage scenarios in experimental studies

Damage scenario	Damage location	Damage severity
S1	21st Segment	p_{21}=4.4%
S2	5th Segment	p_5=4.4%
M1	17th Segment	p_{14}=6.6%
	5th Segment	p_{26}=4.4%
M2	10th Segment	p_{10}=4.4%
	19th Segment	p_{19}=2.2%

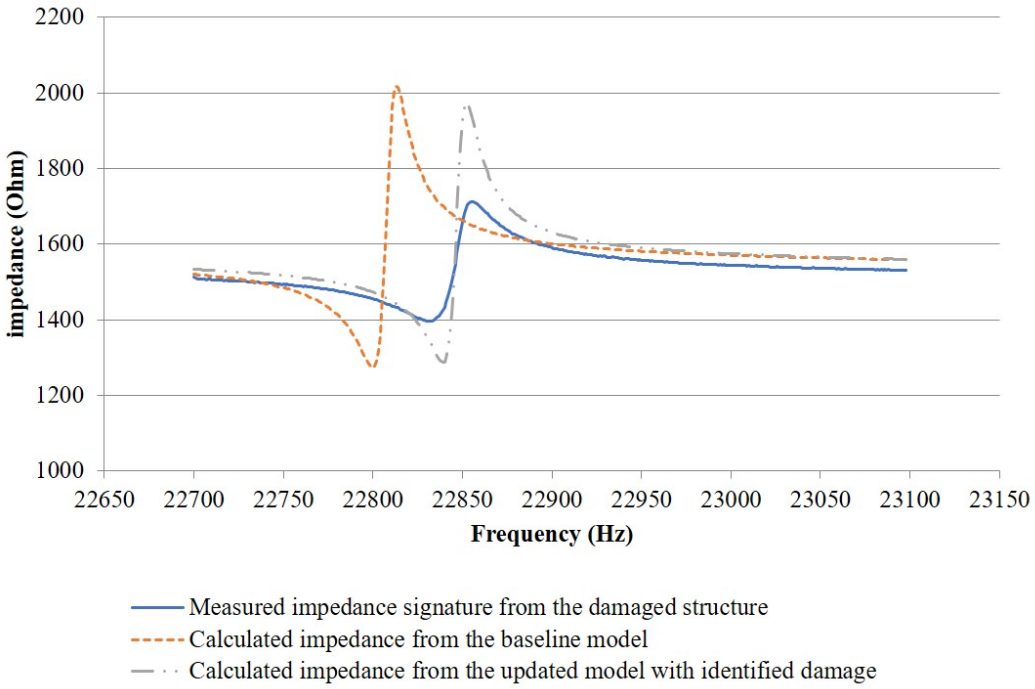

Figure 5.8. Impedance signature between 22700 Hz and 23200 Hz

5.4 Identification results obtained using Tikhonov regularization and sparse regularization method

With the calibrated finite element model, the accuracy and performance of the proposed approach are investigated in this section, and the results will be compared with those obtained from Tikhonov regularization. The identification using the Tikhonov regularization and l_1 norm regularization methods for the single damage scenarios listed in Table 5.4 is conducted. The impedance curves measured from the damaged beam are used for comparison with those from the baseline model to obtain the resonance frequency shifts. A total of six frequency shifts, as mentioned in Section 5.3, are used to identify the damage in 30 segments. For example, the impedance curves of the first resonance frequency obtained by experimental test from the damaged structure with damage scenario M1, the baseline model and the updated model with identified damage are shown in Figure 5.8. It can be observed that there is a significant resonance frequency shift between the impedance responses under the undamaged and damaged states. After updating the model parameters and damage, the calculated impedance from the updated model matches well with the measured one from the damaged structure. To ensure that the identification results are repeatable and reliable, the impedance responses of two PZT transducers at symmetric locations are used for the identification for each scenario.

As mentioned before, it is unnecessary to completely match the impedance amplitudes, since the frequency shifts of the resonance peaks have been selected as the measurements of changes in impedance responses. The identification results for the two single damage scenarios are shown in Figure 5.9 and Figure 5.10. It is observed that the use of the Tikhonov regularization method correctly identifies the damage locations in the 21st and 5th segments in these two scenarios, respectively, with the largest predicted damage severity located in the actual damaged segment. However, the identified severities in the damaged segments obtained using the Tikhonov regularization method are less than half of the actual damage values. In

contrast, the proposed approach based on the l_1 regularization method identifies the damage accurately with sparse solutions. The identified damage severities are $p_{21} = 4.55\%$ and 4.61%, with relative errors of only 2.4% and 3.8%, respectively, for single damage scenario S1 using the impedance responses of the two symmetric PZT transducers. For single damage scenario S2, the prediction of the damage severities using the impedance responses of the two PZT transducers are $p_5 = 4.71\%$ and 4.65%. The relative errors are 7% and 5.6%. The damage severities predicted through the impedance responses of the two PZT transducers on the same beam are very close. This means that the identifications are reliable. In terms of the false identification of undamaged segments, there are numerous non-zero elements in the non-sparse solution output using the Tikhonov regularization method. The values of the 18th and 24th segments in the first scenario predicted using the impedance response from PZT 1 and PZT 2 are significant. For scenario S2, the values of the 4th and 27th segments identified with PZT 2 are significant and up to 1%. The value of the 24th segment identified by PZT 1 even exceeded 1.5%. On the other hand, the proposed approach based on the l_1 regularization method provides a few non-zero elements, as stated previously. The values of these false identifications are much smaller than the true damages in the 5th and 21st segments. As shown in Figures 5.10(a) and (b), the largest value of these false identifications is only approximately 0.465% at the 20th segment identified by PZT 2, and the largest falsely identified damage index value is approximately -0.47%.

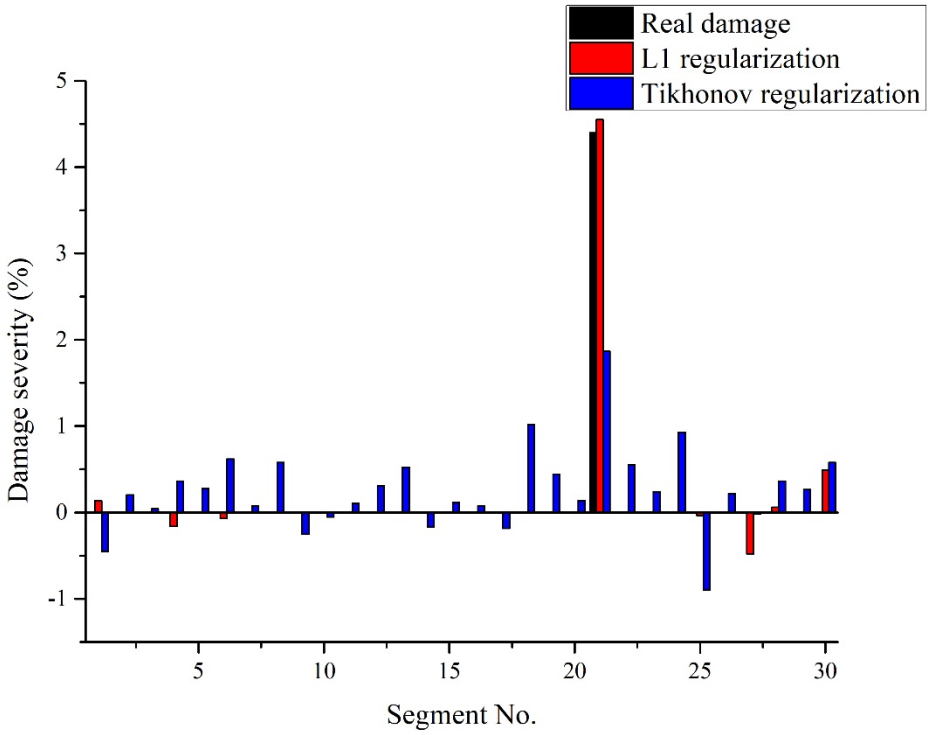
Real damage
L1 regularization
Tikhonov regularization
Damage severity (%)
5
4
3
2
1
0
-1
5
10
15
20
25
30
Segment No.

(a)

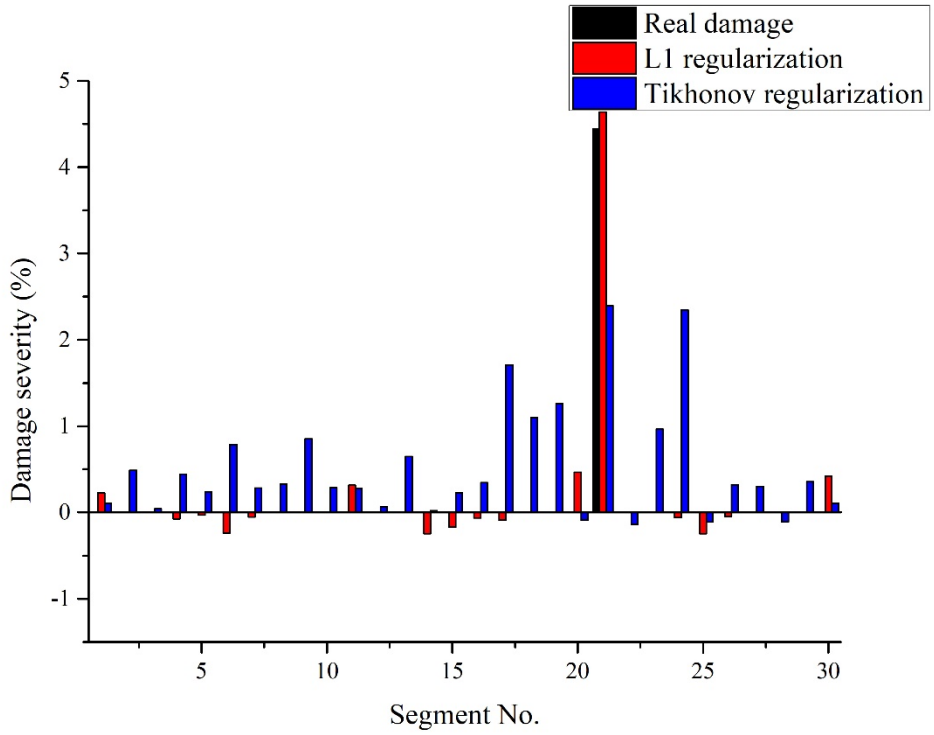

(b)

Figure 5.9 Comparison of the identification results for the single damage scenario S1 obtained by the l_1 regularization method and Tikhonov regularization method: (a) PZT 1, (b) PZT2

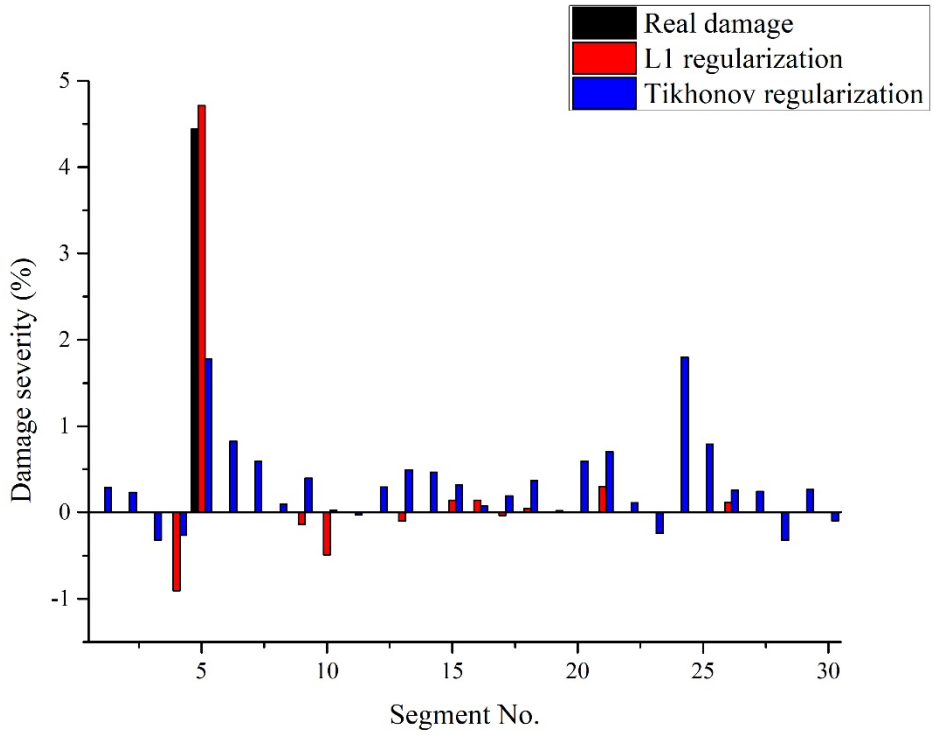
Real damage
L1 regularization
Tikhonov regularization
Damage severity (%)
5
4
3
2
1
0
-1
5
10
15
20
25
30
Segment No.

(a)

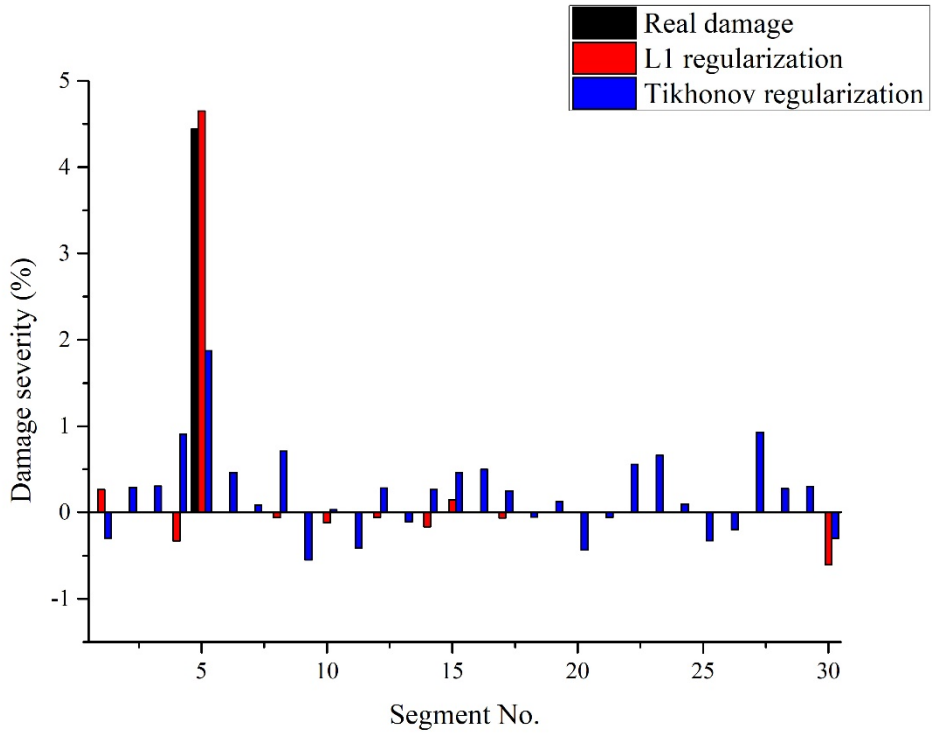

(b)

Figure 5.10 Comparison of the identification results obtained for the single damage scenario S2 by the l_1 regularization method and Tikhonov regularization method: (a) PZT 1; (b) PZT 2

The identification of the two multiple damage scenarios listed in Table 5.4 will be performed. Comparisons between the identification results obtained using the Tikhonov regularization and l_1 regularization methods are shown in Figure 5.11 and Figure 5.12. For each scenario, the identifications of two PZT transducers at symmetric locations are also compared in these figures. For the first multiple damage

scenario M1, using the impedance responses of PZT1, the Tikhonov regularization method identifies similar severities in the 5th, 17th and 25th segments. The severity values of the 5th, 14th and 17th segments identified by PZT2 are similar. The falsely predicted damage severity identified with PZT1 in the undamaged 25th segment and the damage severity identified with PZT2 in the undamaged 14th segment are even greater than that in the 5th segment. It is difficult to determine the number of damage segments without any prior information. In Figures 5.12(a) and (b), there are several large non-zero damage indices observed at the locations near the damaged segment, i.e., the 9th, 12th and 13th segments. The damaged segments are located correctly, but the severities are significantly underestimated, especially in the 5th segment. On the contrary, the use of the proposed approach with l_1 regularization identifies the damage locations and severities with a high accuracy and few minor false identifications. The non-zero values on undamaged segments obtained with the proposed approach are much smaller than those in the damaged segments. Again, the identifications of the two PZT transducers on the same beam provide similar results in the multiple damage scenarios as well. The reliability of the proposed method is validated.

To investigate the robustness of the proposed approach, numerical studies on the single damage scenarios are conducted. A comparison between the frequency shifts extracted from the measured impedance signatures and numerical simulations of both single damage scenarios is shown in Table 5.5. It is observed that uncertainties, i.e., manufacture defects, surface roughness and the noise effect, would lead to significant discrepancies between the model predictions and test results, with relative errors from 2% to 35%. Nevertheless, the proposed approach can still provide a good accuracy in identifying damage locations and severities. Good robustness and effectiveness are demonstrated by the identification results.

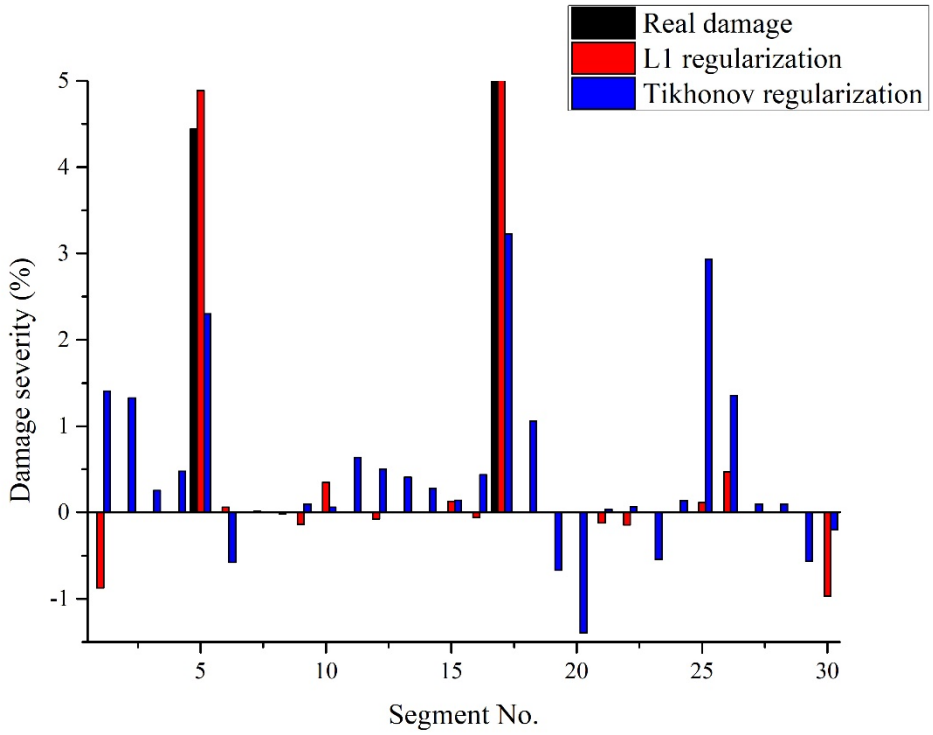
Real damage
L1 regularization
Tikhonov regularization
Damage severity (%)
5
4
3
2
1
0
-1
5
10
15
20
25
30
Segment No.

(a)

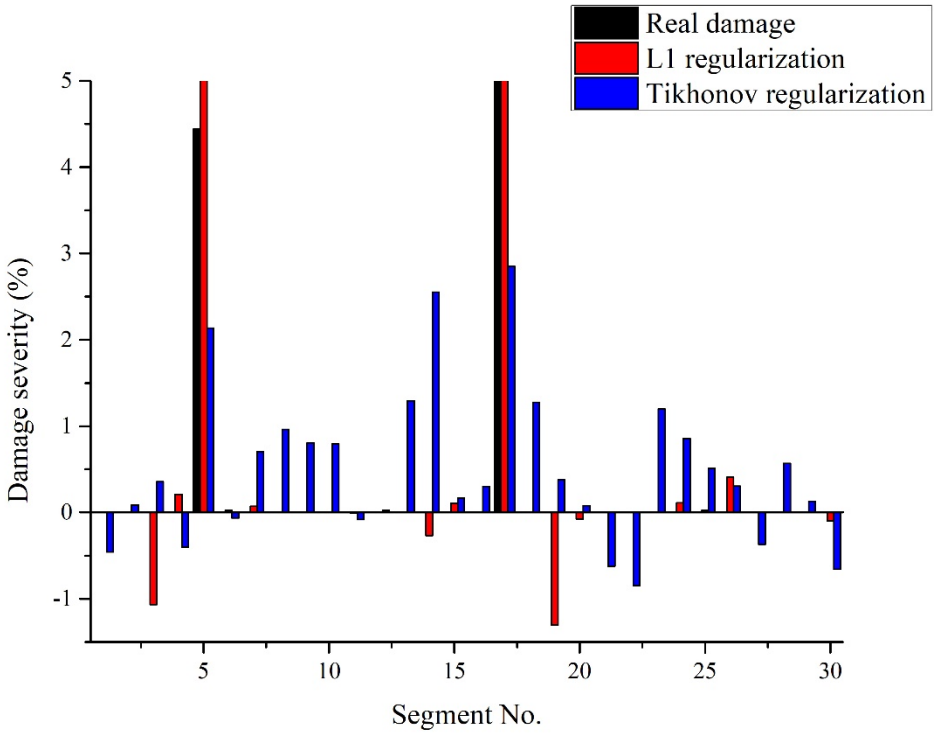

(b)

Figure 5.11. Comparison of the identification results for the multiple damage scenario M1 obtained by the l_1 regularization method and Tikhonov regularization method: (a) PZT1, (b) PZT2

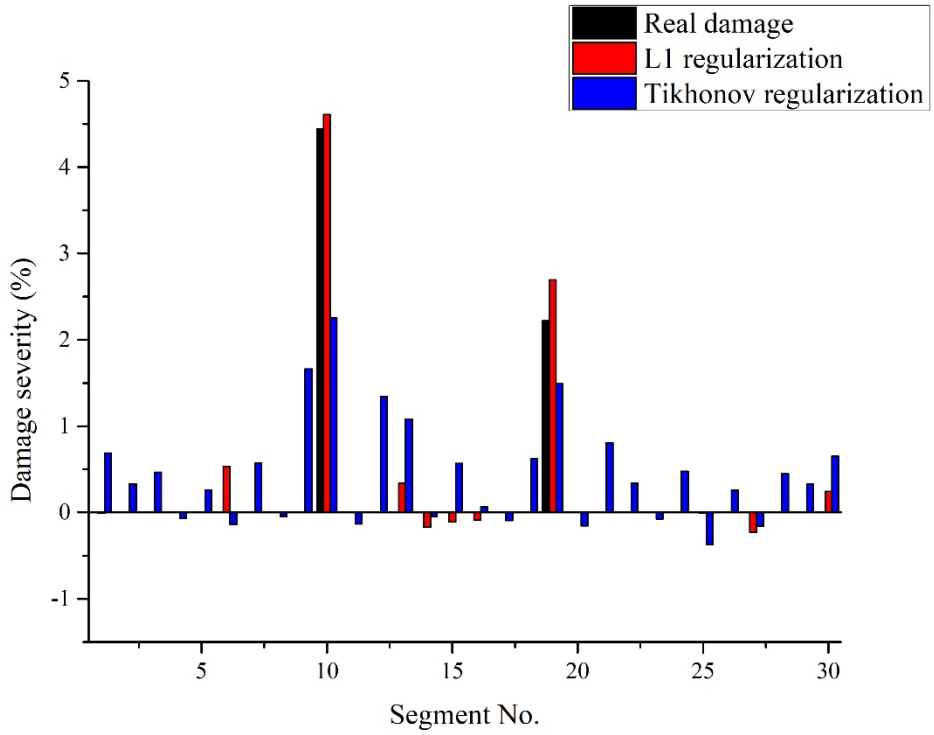
Real damage
L1 regularization
Tikhonov regularization
Damage severity (%)
5
4
3
2
1
0
-1
5
10
15
20
25
30
Segment No.

(a)

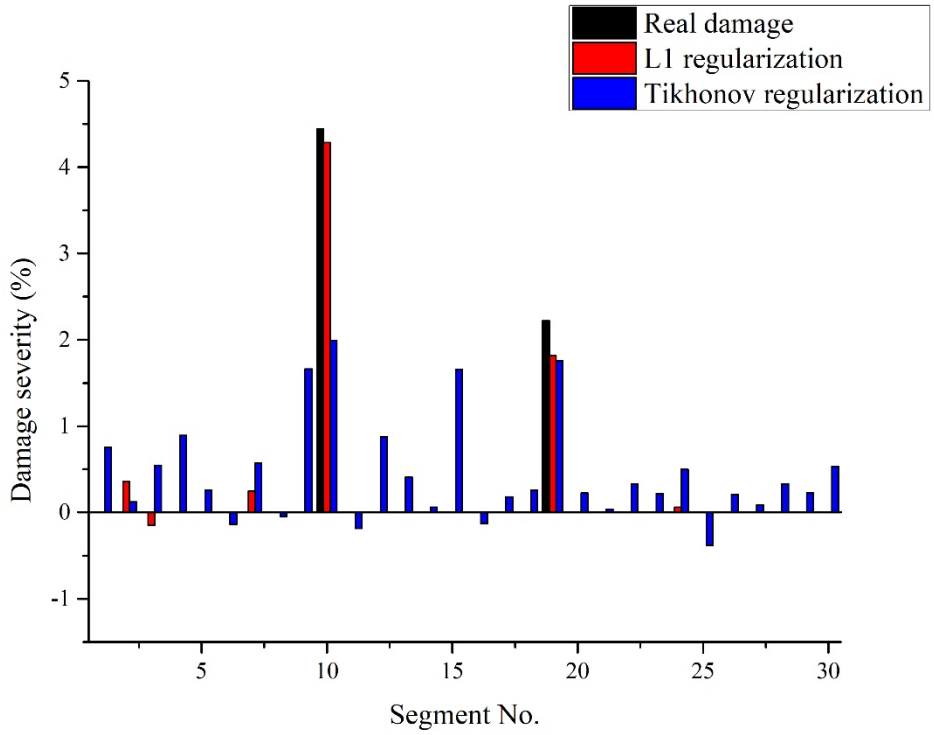

(b)

Figure 5.12. Comparison of the identification results for the multiple damage scenarios obtained by the l_1 regularization method and Tikhonov regularization method: (a) scenario M1, (b) scenario M2

Table 5.5. Comparison of frequency shifts obtained from test results and simulations

Frequency shift	Scenario S1		Scenario S2	
	Test result	Numerical study	Test result	Numerical study
δ_{f_1}	40 Hz	55 Hz	-47 Hz	-48 Hz
δ_{f_2}	-53 Hz	-50 Hz	-44 Hz	-56 Hz
δ_{f_3}	-31 Hz	-48 Hz	41 Hz	32 Hz
δ_{f_4}	-22 Hz	-15 Hz	-39 Hz	-51 Hz
δ_{f_5}	67 Hz	51 Hz	-71 Hz	-90 Hz
δ_{f_6}	-11 Hz	-8 Hz	-91 Hz	-84 Hz

5.5 Numerical study on the sensitivity range of the proposed damage detection method

The above studies have demonstrated the accuracy and effectiveness of using the proposed approach for structural damage identification with experimental testing data. In this section, the sensitivity range of the proposed approach is investigated using numerical analysis. The sensitive range is usually determined by many factors, i.e. the number of unknowns in the inverse identification problem, the change in the resonance frequency shifts in the impedance response and the number of available resonance frequencies in the selected frequency range. The relationship between the number of measurement data and damage severity has been discussed by Zhou et al. [52]. They observed that identifying a severer damage may need a less number of measurement data. However, when using impedance based techniques, the dimension, i.e. the length of the structure is significant, since this may significantly increase the number of elements and the computational demand. In this section, numerical studies are conducted on the aluminium beams with difference lengths. The lengths of

specimens are defined as 400mm, 500mm and 600mm respectively. The widths and thicknesses of all these three specimens are kept the same as 45mm and 4mm, respectively. The PZT-structure coupled finite element models are built and used to calculate the impedance. The proposed approach is used to identify the structural damage. In all the scenarios, PZT transducers are located at 70 mm away from the left end of the aluminium beam. The host structures are further divided into a number of segments with each of 10 mm length. Structural damages in all these specimens are defined as $p = 2.22\%$ in the segment which is at the right end of the structure and is farthest from the PZT transducer.

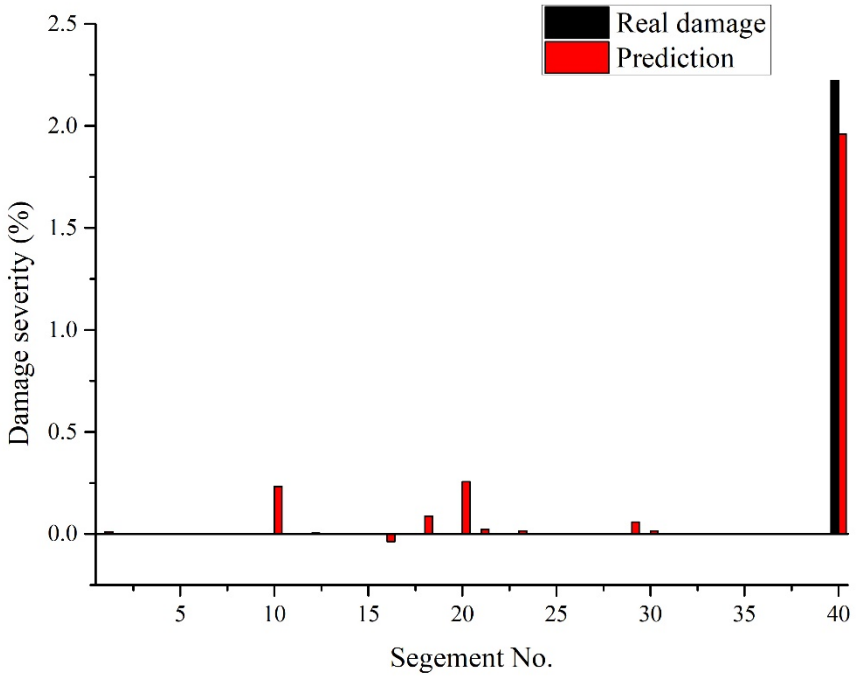

(a)

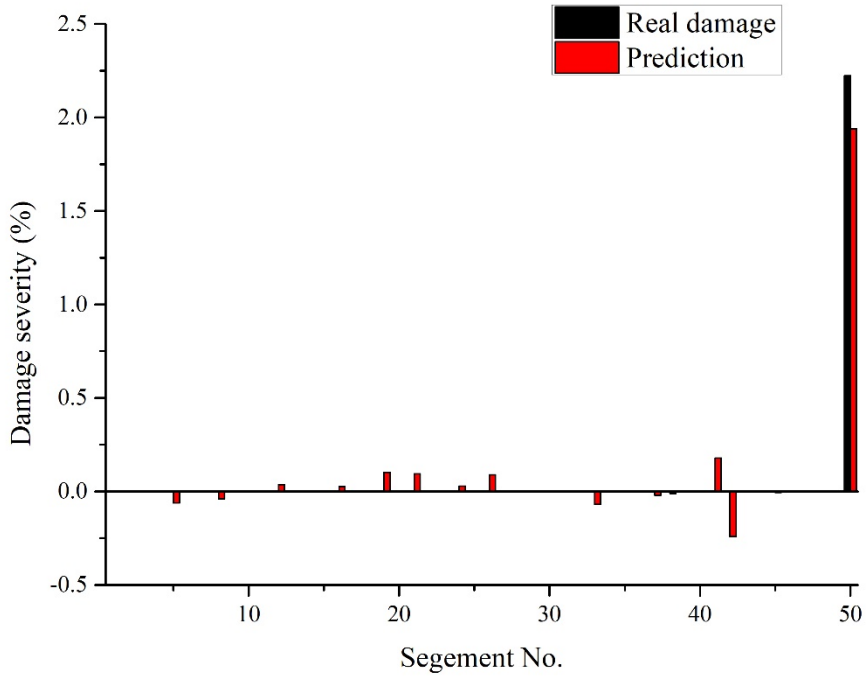
Real damage
Prediction
Damage severity (%)
2.5
2.0
1.5
1.0
0.5
0.0
-0.5
10
20
30
40
50
Segement No.

(b)

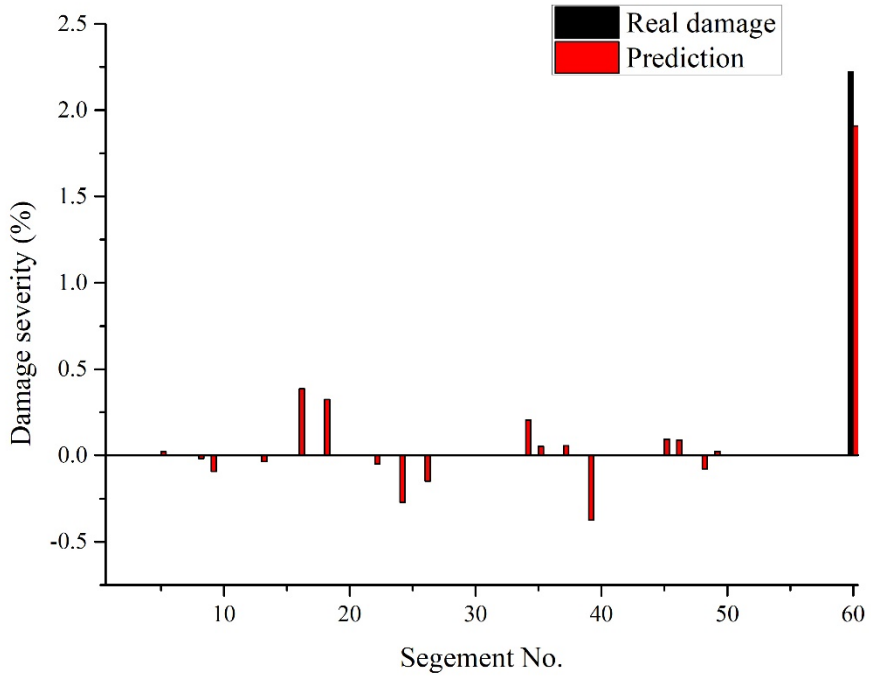

(c)

Figure 5.13 Identification results for specimens of different lengths obtained using the l_1 regularization method: (a) 400 mm, (b) 500 mm, (c) 600 mm

Impedance responses for undamaged and damaged specimens are calculated, and the resonance frequency shifts are obtained. The numbers and values of resonance frequency shifts for each damage scenario are listed in Table 6. Figure 5.13 shows the damage identification results by using the proposed approach for the above three specimens. It can be observed that the damaged locations defined in all these three scenarios can be correctly identified. For the specimen with 400mm length, 8 frequency shifts are used to identify the damage in 40 segments. The identified

damage in the 40th segment is 1.95%, which is close to the true value. A few false identifications are observed, such as 0.233% in the 10th segment and 0.265% in the 20th segment. The identification results for the 500mm specimen are shown in Figure 5.13(b). For this scenario, 11 resonance frequency shifts are available to identify the structural damage in 50 segments. It is observed that the damage severity in the real damaged segment is predicted accurately. The maximum false identification is lower than 0.2%, which is much smaller than the damage extent in the damaged segment. Then the length of the host structure is increased to 600mm with 60 segments. The number of resonance peaks is 13 for this scenario. With a longer beam structure with more segments, a higher computational demand is required. The identification results as shown in Figure 5.13(c) indicate that the location and damage severity can still be correctly predicted, although the accuracy is lower than two previous scenarios. The identified damage index for the damaged element is 1.9%. The false predictions in the 16th and 18th segments are 0.38% and 0.32%, respectively. The damage index values are still much smaller comparing with those in the damaged segment. The above studies indicate that the detection by using the proposed approach with a sensitivity range of 600mm is reliable.

Due to the high computational demand, numerical studies are only conducted for the damage identification of the above three specimens. However, the sensitivity range of the proposed approach can be estimated from the comparison of the values in the resonance frequency shifts between undamaged and damaged specimens. As can be seen from Table 5.6, the resonance frequency shifts caused by the damage in the farthest element on the right end are decreasing when the length of the specimen is increasing to 1000mm. Considering the discrepancies between testing and simulation results listed in Table 5.6, the error would be larger than the frequency shifts caused by the real structural damage when the specimen length reaches to 1000mm. This demonstrates that the proposed method could fail to identify the damage effectively when the beam is longer than 1000mm, even with a sufficient number of resonance frequency shifts, since the changes in the resonance frequencies are too minor.

Table 5.6. Frequency shifts of specimens with different lengths

Specimen (length)	300 mm	400 mm	500 mm	600 mm	800 mm	1000 mm
Frequency shift of resonance peaks (Hz)	-53	-25	-38	-14	-11	-3
	-29	-36	-36	-36	-9	-7
	-47	-20	4	-15	-10	-6
	-55	15	-17	-18	-8	-7
	-31	-44	-26	2	-10	-6
	-41	-28	-19	-28	-11	-8
		-41	-32	-17	-8	-8
			-17	15	-6	1
			-27	-24	-16	-8
				-32	-8	-5
				-16	-9	-8
				-11	-9	-4
				-14	-9	-3
					-12	-7
					-8	-1
					-11	-6
					-9	-1
					-10	-6
					-8	-7
						-3
						-7
						-1
						-6
						-1
						-6
						-7

5.6 Conclusion

This paper presents experimental validations on using the sparse regularization technique and electromechanical impedance sensitivity for structural damage localisation and quantification. Model updating is performed to quantify the damage with only a limited number of available resonance frequency shifts and to overcome the limitations of conventional non-model based EMI methods for SHM. It is noted that only a few resonance frequency shifts are employed to identify the damage via a number of unknown parameters of the entire host structure. The l_1 regularization method is utilized to solve the underdetermined inverse problem, as the number of measured frequency shifts in the impedance is considerably smaller than the number of structural parameters. Compared with using the amplitudes of impedance changes, the advantage of using resonance frequency shifts is that a higher sensitivity to the damage can be obtained and a better accuracy in simulating the resonance frequencies can be achieved. The performance of the proposed approach is verified by experimental studies. The identification results demonstrated that the proposed approach can accurately identify the structural damage with testing data. It must be noted that uncertainties and a certain level of noise exist in the tests. Parametric studies are further carried out to discuss the sensitivity range of the proposed approach based on numerical analysis. Damage can be identified correctly when the length of the aluminium increases up to 600 mm, with 60 unknown segments to be identified but only 13 available resonance frequency shifts. Numerical studies also show that the measured frequency shifts will decrease with increasing length of the testing specimen. A minor damage in a specimen longer than 800 mm cannot be reliably detected in this study.

In the following section, the sparse regularization based sensitivity approach is applied to detect damage on a beam structure. The number of unknowns reaches 100. An accurate finite element model for the aluminium beam with a surface-bonded PZT

patch is developed. Experimental studies are also carried out to validate the performance of the proposed method.

6 Experimental study of damage identification based on sparse regularization and impedance sensitivity for plate structures

This chapter investigates the application of the proposed damage identification method based on sparse regularization and impedance sensitivity to relatively complex structures, i.e. plate structures. The three-dimensional finite element model for the aluminium plate with a surface-bonded PZT patch is developed and calibrated by experimental testing results. The accuracy and performance of the proposed method are validated by experimental studies on plate structures.

6.1 Background

As mentioned in Chapter 2, it is difficult to localize structural damage only based on the estimation of the statistical damage indicator by using the non-model based EMI technique. For the damages of the same severity, the value of the statistical damage indicator only depends on the distance between the locations of the damage and the PZT patch. To distinguish the damages at different locations that have the same distance from the measuring point, artificial intelligence approaches based on EMI techniques is carried out. The relevant applications have been reviewed in Chapter 2.2. The main drawback of the aforementioned methods is that the impedance responses of multiple PZT transducers are necessary. Moreover, training of the neural network is still based on the evaluation of phenomenological characteristics of the impedance signature, which is not explicitly related to the properties of the host structure. Therefore, the selected frequency range and networks are not suitable for different structures or damages. For the model-based EMI technique, it is difficult to achieve accurate prediction using an analytical model. Even though the SEM model shows a higher computational efficiency than the finite element model, it is mainly applied for the damage detection of beam structures, which only need a one-

dimensional simulation. Sepehry et al. [87] presented the two-dimensional SEM model for a plate structure. The predicted impedance response between 10 kHz and 14 kHz basically matched the experimental results. However, it was still inapplicable to model-based damage detection due to non-negligible errors.

Although the performance of finite element modelling in the prediction of the high-frequency impedance response has been provided by other researchers [7, 43], a large number of unknowns of segments or even elements have to be identified. On the other hand, the changes in structural parameters normally manifest themselves around the resonance peaks in the impedance signature in very limited numbers of measurements. Under such a situation, the identification problem becomes a highly underdetermined problem.

The significance of the studies in this chapter is using the proposed approach based on the sparse regularization to solve the underdetermined inverse problem and correctly identify the changes in structural properties of plate structures.

6.2 Experimental setup

To experimentally validate the accuracy of the built finite element model for the PZT-plate structure interaction and the performance of the proposed damage identification method, a $300mm \times 300mm \times 4mm$ square aluminium beam with a surface-bonded PZT patch is used as the test specimen in this study. The experimental test uses a PZT transducer similar to that introduced in detail in the last chapter. The location of the surface-bonded PZT transducer is shown in Figure 6.1. To ensure that the test results are repeatable and reliable, two same specimens under the intact condition are adopted for the baseline test. Commercial epoxy glue is used to mount the transducers.

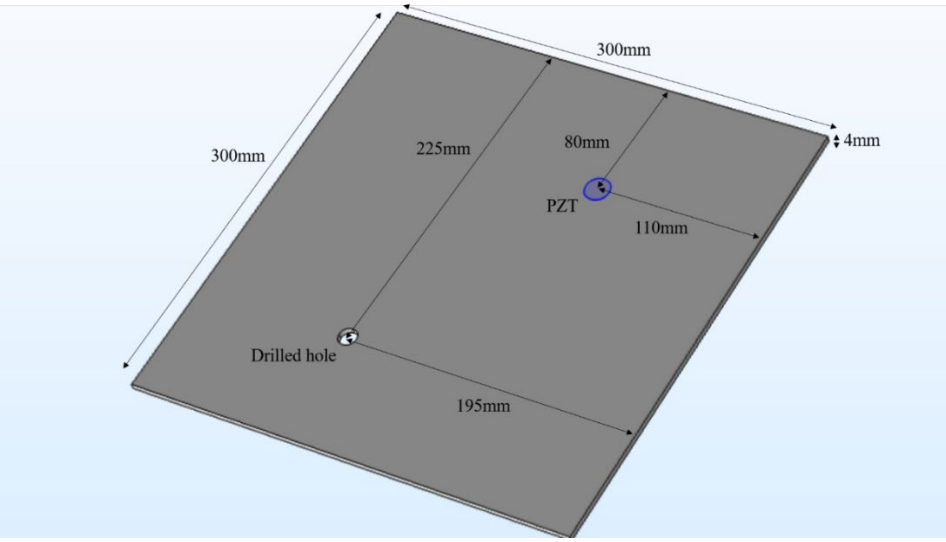

Figure 6.1 Damaged aluminium plate with a surface-bonded PZT transducer

Damage is simulated as a hole created by a hand drill with a diameter of 6 mm. To localize the damage via the sensitivity-based model updating method, the aluminium plate is further divided into 100 square segments. Each square area has a size of $10mm \times 10mm$. In other words, there are 100 unknown parameters of the host structure in the inverse identification. The experimental configuration is shown in Figure 6.2. In the study, the impedance analyser EVAL-AD5933 is used for sensing and actuation of the PZT patch. The driving voltage of the PZT transducer is configured at 1 volt. The specimens are placed on a soft foam to simulate the free boundary condition.

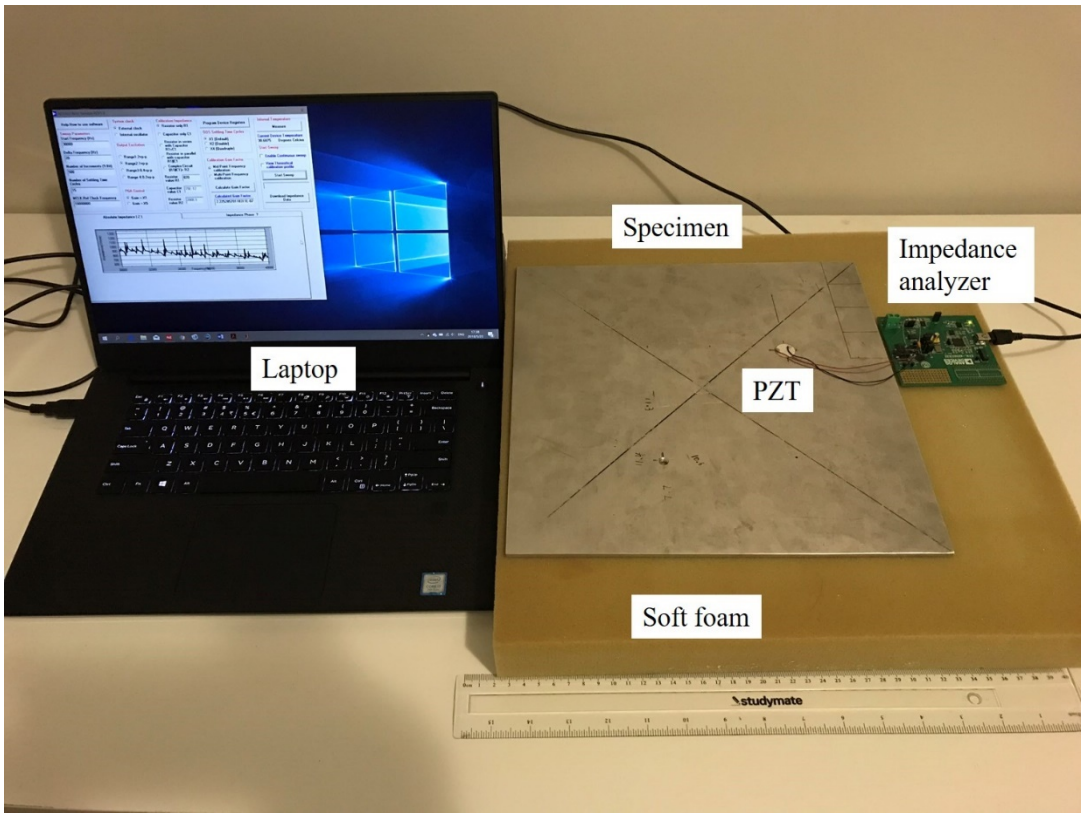

Figure 6.2 Configuration of the experimental test

6.3 Finite element model of the PZT-plate structure interaction

To quantify the damage with the sensitivity based method using model updating, finite element modelling of the aluminium structure under the intact condition with a surface-bonded PZT transducer is performed. With the successfully calibrated finite element models of the PZT-beam structure interaction in previous chapters, the finite element modelling technique is extended to predict the PZT-plate structure interaction. In this study, a three-dimensional finite element model is developed in COMSOL Multiphysics 5.2, with an eight-node solid element adopted for meshing. The cylinder PZT transducer is first modelled in COMSOL Multiphysics 5.2 using

the property parameters in accordance with PIC 255, which are provided by the manufacturer as given in Table 6.1. The properties of the aluminium plate and bonding layer from the manufacturer are listed in Table 6.2. The hysteretic damping model is adopted to define the damping of the PZT transducer, bonding layer and host structure. In addition to the baseline calibration procedure presented in Chapter 5, these parameters from manufacturers are initially used for the simulation and then updated based on the experimental testing results.

Following the comments of Makkonen et al. [80], three to five nodal points for each half wavelength are necessary to ensure sufficient accuracy for the prediction. In this case, the wave velocity travelling in the aluminium plate can be calculated as $c = \sqrt{E_{Al} / \rho_{Al}} = 5104.1(m/s)$, where E and ρ denote the elastic modulus and mass density of the aluminium material, respectively. The element size is selected as 2.5 mm, which is sufficient to cover the frequency range of 20 to 30 kHz used in the following structural damage identification. In Figure 6.3, it can be observed that convergence is reached at the eight-node hexahedron element size of 2.5 mm in the high frequency range from 40200 Hz to 41000 Hz. Thus, it could be concluded that the 2.5 mesh size of the eight-node hexahedron element would be sufficiently fine for the finite element modelling of the plate structure with a surface-bonded PZT patch. The developed coupled PZT-plate structure model is shown in Figure 6.4.

Table 6.1 Piezoelectric properties of PIC 255 from the manufacturer

Parameters	Symbols	Values	Unit
Density	ρ	7760	kg/m^3
Hysteretic damping ratio		0.00625	
Compliance	s_{11}	1.590E-11	m^2/N
	$s_{12} = s_{21}$	-5.699E-12	m^2/N
	$s_{13} = s_{31}$	-7.376E-12	m^2/N
	$s_{22} = s_{33}$	2.097E-11	m^2/N
	$s_{23} = s_{32}$	-7.376E-12	m^2/N
	$s_{44} = s_{55}$	4.492E-11	m^2/N
	s_{66}	4.319E-11	m^2/N
Piezoelectric strain coefficients	d_{31}	-1.74E-10	m/V
	d_{32}	-1.74E-10	m/V
	d_{33}	3.94E-10	m/V
	d_{24}	5.35E-10	m/V
	d_{15}	5.35E-10	m/V
Electric permittivity	ε_{11}	1649	
	ε_{22}	1649	
	ε_{33}	1750	

Table 6.2 Property parameters of the aluminium plate and bonding layer from the manufacturer

Property	Symbol	Value	Unit
Density (aluminium)	ρ	2710	kg/m^{-3}
Young's modulus (aluminium)	Y	70.6	GPa
Poisson ration (aluminium)	ν	1.4	
Damping ratio (aluminium)	ξ	0.35	
Density (adhesive)	ρ	1000	kg/m^{-3}
Young's modulus (adhesive)	Y	1.4	GPa
Poisson ratio (adhesive)	ν	0.4	
Damping ratio (adhesive)	ξ	0.02	

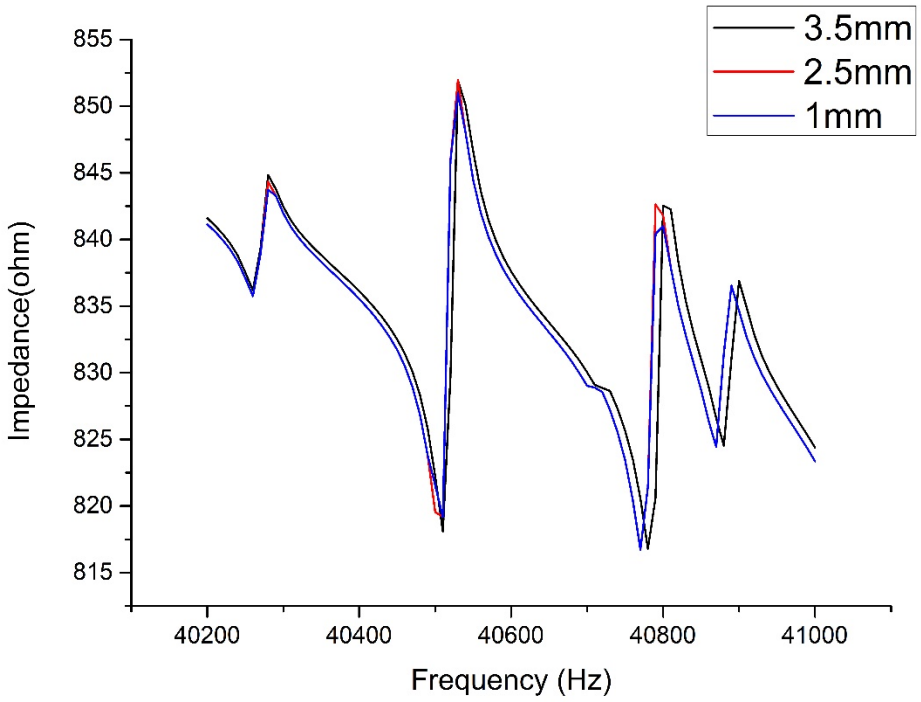

Figure 6.3 Impedance signatures for the numerically simulated PZT-structure interaction with different mesh sizes between 40000 Hz and 40400 Hz

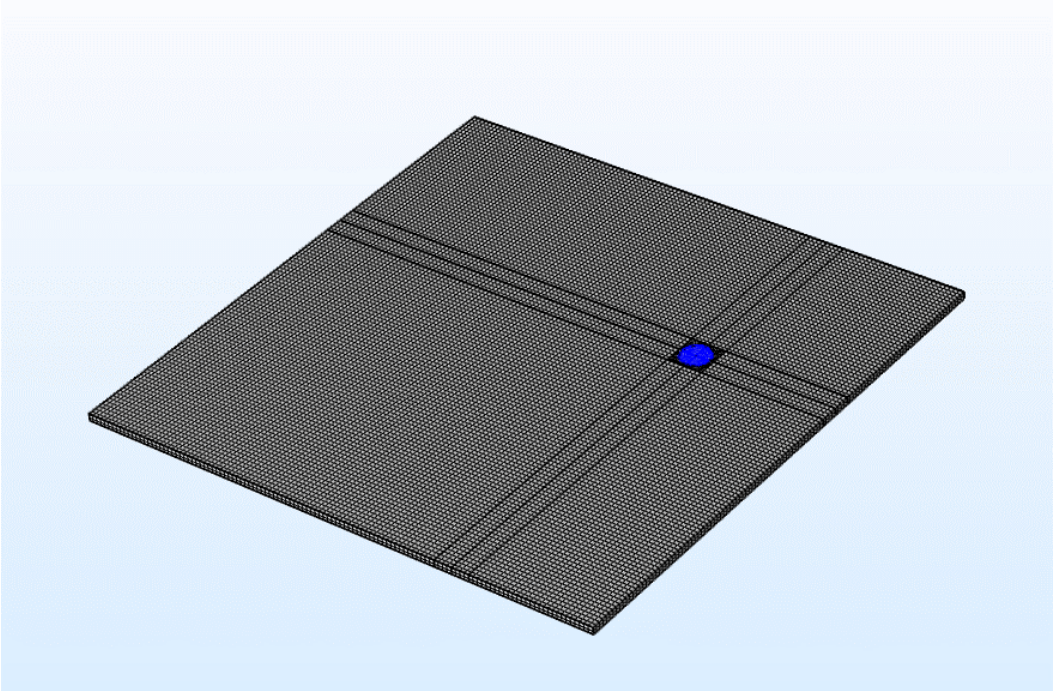

Figure 6.4 Finite element model of an aluminium plate with a surface-bonded PZT transducer

Based on the sensitivity analysis of the parameters to the resonance peaks, the most sensitive parameters are selected to be updated. The modified parameters are shown in Table 6.3. Figure 6.5 suggests that the finite element model provided a reasonable simulation that well matched the test results of the impedance signatures of the coupled PZT transducer and plate structure. It should be noted that the prediction of frequencies of the resonance peaks completely match with the test results. In other words, the outcome has sufficient accuracy for damage identification using the impedance sensitivity based model updating method. The remaining difference between the magnitudes of the numerical results and the test results could be caused by manufacturer errors and other inevitable uncertainties. However, the imperfection would not influence the proposed identification method, as only frequency shifts of

resonance peaks are defined as the measurement of impedance changes, which will be used for the subsequent damage identification.

Table 6.3 Modified parameters of piezoelectric material in FE modelling

Parameters (PZT)	Unit	Value (Manufacturer)	Value (Updated)
Density	kg/m^3	7800	7760
Mechanical loss factor		80	65
Compliance	$10^{-12}m^2N^{-1}$		
S11		15.9	13.8
S33		20.97	21.70
S66		45.9	43.19
Piezoelectric strain coefficient	$10^{-10}mV^{-1}$		
h31		-1.853	-1.74
Damping ratio (bonding layer)		0.016	0.022
Young's modulus (aluminium)	N/m^2	72e9	70.8e9

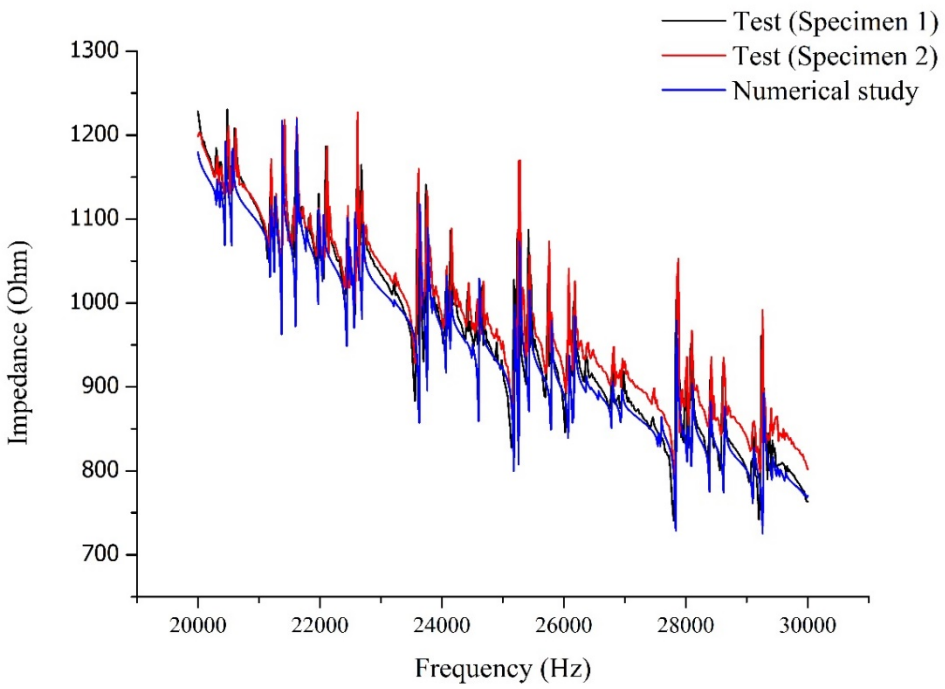

Figure 6.5 Comparison of the impedance signatures from test specimens and the developed finite element model

6.4 Damage identification in a plate structure

For finite element modelling, many possible failure modes and damage phenomena could be simulated as changes in the bending stiffness of the elements [77]. In this study, damage to the aluminium plate is simulated as a reduction in the Young's modulus of the segments. In this case, the formulation of the inverse identification problem can be represented as

$$[S]\{\Delta E\} = \{\Delta f\} \tag{6.1}$$

where $\{\Delta E\}$ denotes the Young's modulus changes in each segment of the host structure, $\{\Delta f\}$ represents the resonance frequency changes in the impedance signature corresponding to changes in the structural bending stiffness, and $[S]$ is the sensitivity matrix of the resonance frequencies with respect to the Young's modulus. Then, the Young's modulus of the host structure can be presented as

$$\overline{E}_i = E_{initial}\left(1+\eta_i\right) \tag{6.2}$$

where η_i ($0 \le \eta \le -1$) is the damage factor of the i^{th} segment. In this case, $\eta = 0$ denotes that the segment is in the intact condition, while $\eta = -1$ denotes that the segment is completely damaged. In Chapters 4 and 5, the sparse regularization techniques has been used with a promisingly high accuracy in the solutions of the highly underdetermined problem. For this case, the sparse regularization method is used for damage identification. The identification result is compared with that of the l_2-regularization based method.

In this study, the frequency shifts of 28 resonance peaks in the impedance signatures between 20 kHz and 30 kHz are selected for damage identification. In the first step, the host structure is divided into 100 square segments of equal size, and the Young's modulus change in these segments is estimated. The damaged segments will then be further divided into 9 square segments. The stiffness changes of these sub-segments will be calculated in order to acquire the precise location and severity of the structural damage.

It should be noted that the structural damage is simulated in a different form: the Young's modulus of each segment is used for model updating in the proposed damage identification method, but the actual structural damage is simulated as a drilled hole. It is necessary to estimate the equivalent Young's modulus change

corresponding to the drilled hole in the damaged segment. According to Li et al. [88], the damage effect on the structure is equivalent to a bending stiffness reduction of the whole segment. Thus, the Young's modulus changes of the drilled plate segment can be approximately estimated by the displacement method in the finite element analysis. The equivalent stiffness changes can be calculated based on displacements along the axis of the thickness direction produced by a unit force. The finite element models for the calculation of the equivalent Young's modulus change are shown in Figures 6.6 and 6.7. In this numerical study, the segments are fixed on one side, and a unit force is applied on the free side of the segment. The analytical stiffness reductions of the damaged 30 mm×30 mm segment and the 10 mm×10 mm segment are 5.32% and 48.9%, respectively. These theoretical values are considered as the approximate stiffness reduction caused by the drilled hole damage in this study.

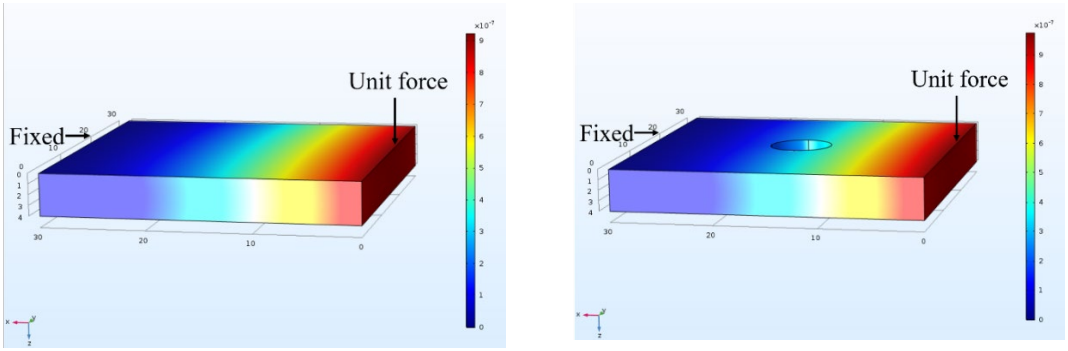

(a) undamaged (b) damaged

Figure 6.6 Finite element model for the equivalent Young's modulus change (30 mm×30 mm segment)

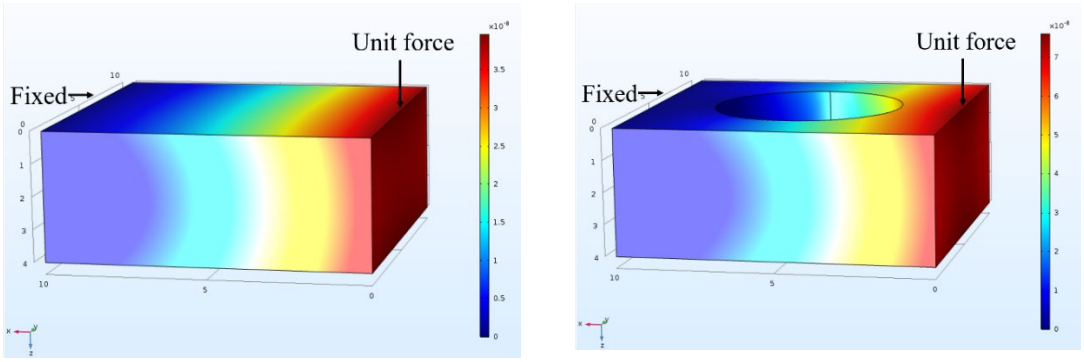

(a) undamaged (b) damaged

Figure 6.7 Finite element model for the equivalent Young's modulus change (10 mm×10 mm segment)

6.5 Identification results and discussions

In this section, experimental tests on the undamaged and damaged plates are conducted and the identification results are obtained to validate the accuracy and effectiveness of the proposed approach. The experimental studies are conducted to localize and quantify the severity of the structural damage on the aluminium plate. The configuration of the host structure and surface-bonded PZT transducer is introduced in Section 6.2. The frequency shifts are used as the measurements of the change in the impedance signature. On the other hand, there are more than 30 resonance peaks in the impedance signature from 20 kHz to 30 kHz. Considering the errors between the prediction of the finite element model analysis and the experimental testing results, 28 of these resonance peaks are selected for the identification. The peak frequencies of the undamaged structure, damaged structures and finite element model under the intact state are compared in Table 6.4. The

predictions of the finite element model are sufficiently accurate for damage identification.

As introduced in Section 6.2, a single damage scenario is considered here. There are 100 potential damaged locations on the thin aluminium plate. The actual location and severity of the damage are presented in Figure 6.8. The subscripts i and j denote segment D_{ji}. Thus, the actual damage is contained in segment D_{78}. The damage indicator $\eta = \left(E_d - E\right)/E$, where E and E_d denote the Young's modulus of the segment under the intact state and the damaged state, respectively. The severity of the drilled hole is equivalent to the Young's modulus decrease, which is estimated by the displacement method in the finite element analysis. It is noted that the damage effect of the drilled hole is simplified to the Young's modulus decrease with an approximate value under the condition that only bending stiffness is considered.

Table 6.4 Comparison of frequency shifts obtained from test results and simulations

Experimental result		Finite element model (Hz)
Undamaged (Hz)	Damaged (Hz)	
20317.4	20280.4	20317.1
20383.8	20349.7	20386.3
20497.2	20475.2	20512.6
21207.2	21202.4	20127.2
21269.8	21233.6	21274.4
21395.2	21360.1	21384.7
21613.9	21589.6	21617.4
21820.3	21786.2	21811.6
21980.1	21955.5	21981.4
22107.9	22076.4	22098.3
22444.7	22419.0	22449.8
22601.7	22558.7	22594.5
23221.4	23206.3	23220.0
23640.5	23610.1	23640.2
24076.8	24051.9	24079.9
24143.9	24132.2	24144.6
25191.1	25188.4	25192.7
25276.9	25262.0	25274.3
25444.6	25411.5	25444.6
26177.0	26158.4	26180.1
26371.2	26366.2	26371.7
26800.5	26778.7	26800.0
26971.9	26950.4	26968.2
27850.1	27824.3	27850.0
28110.3	28084.9	28114.1
28402.2	28390.2	28406.4
29118.3	29111.5	29118.7
29180.1	29137.6	29180.4

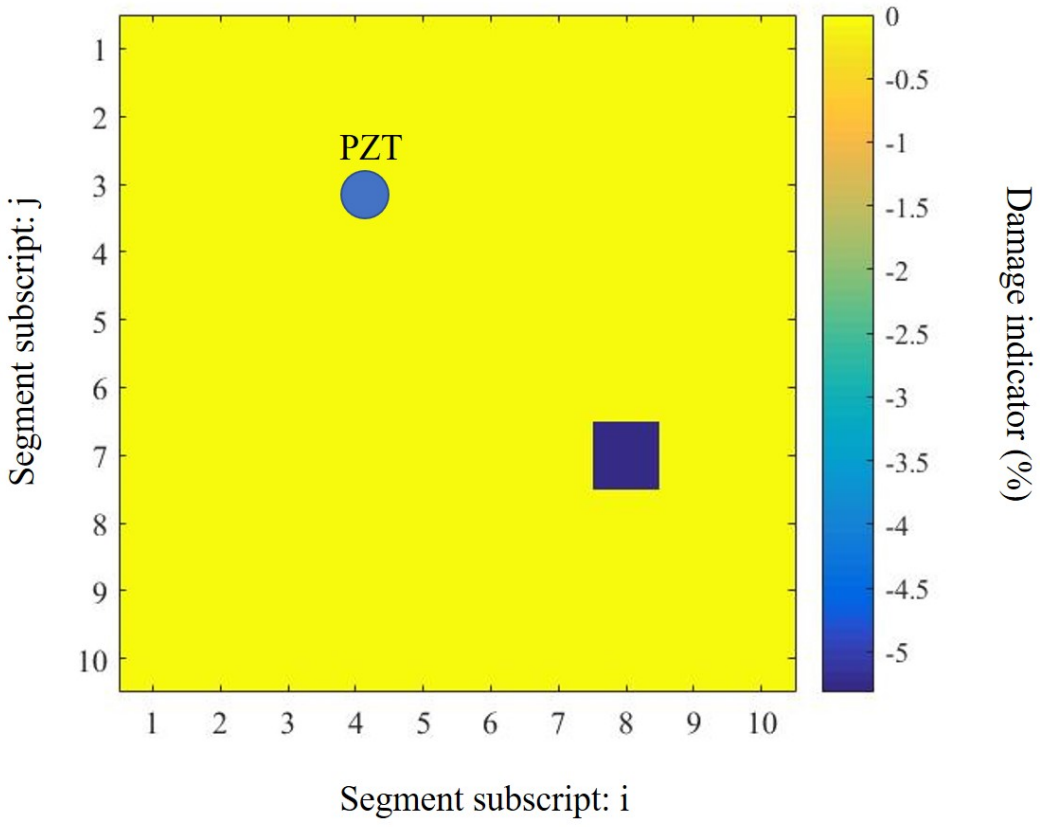

Figure 6.8 Location and severity of the actual damage

Figure 6.9 shows the identification results estimated by the sensitivity approach using the frequency shifts of the resonance peaks listed in Table 6.3 based on the l_2 regularization method. As mentioned in Chapter 2.10, the solution of the l_2 regularization method tends to distribute the damage on numerous elements, introducing a large error and a number of false predictions in the undamaged

segments. In the actual damaged segment D_{78}, the identified damage severity is -2.067%, which is less than half of the estimated Young's modulus decrease in the damaged segment. The false predictions in D_{46} and D_{67} are approximately -1.7%. It is hardly possible to exclude them from the damaged segments without any prior knowledge. The prediction results as shown in Figure 6.9 fail to well identify or indicate the correct location of the structural damage.

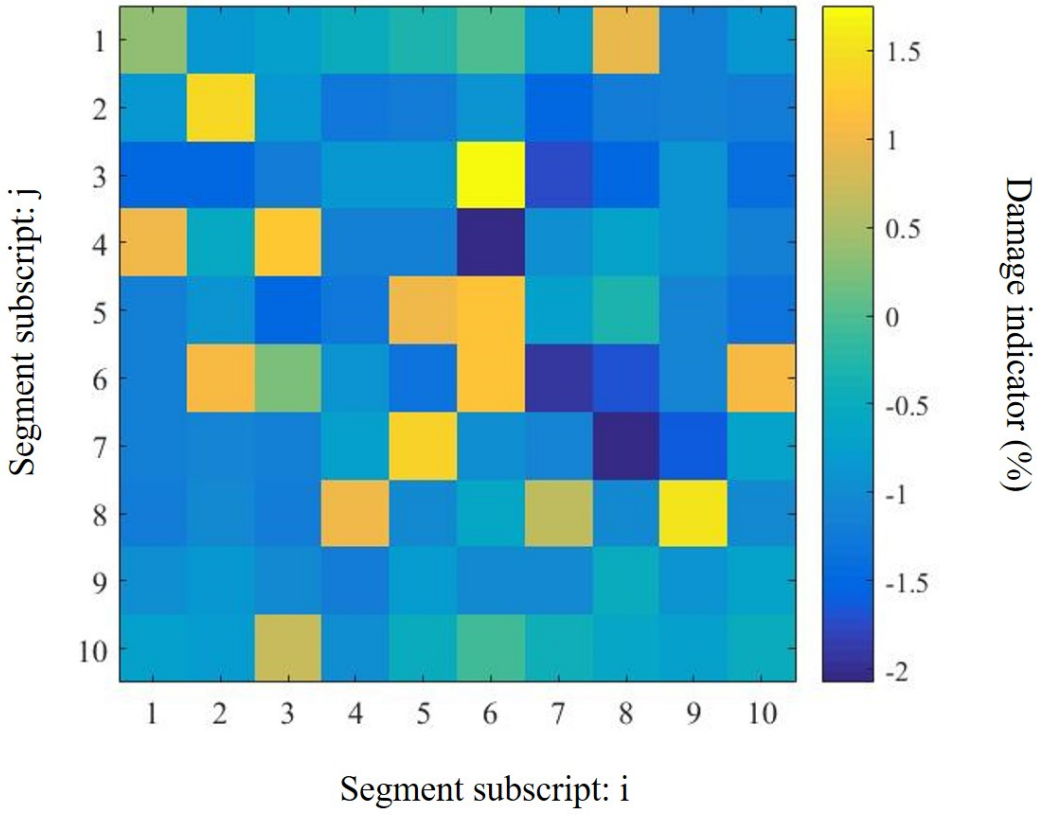

Figure 6.9 Damage identification results obtained using l_2 regularization

In contrast, the identification results by using the l_1 regularization method as shown in Figure 6.10 clearly indicate the correct damage location and severity. The predicted damage severity in the segment D_{78} is -4.28%, which is close to the actual damage value of 5.32%. It is noted that the Young's modulus change corresponding to the actual damage is estimated. Thus, the prediction of the l_1 regularization method can be regarded as a relatively accurate identification result. In addition, the false predictions in the undamaged segments are much lower than the prediction in the damaged segment. The maximum value is only -0.5% at only a couples of locations. The location of the introduced damage can be identified accurately.

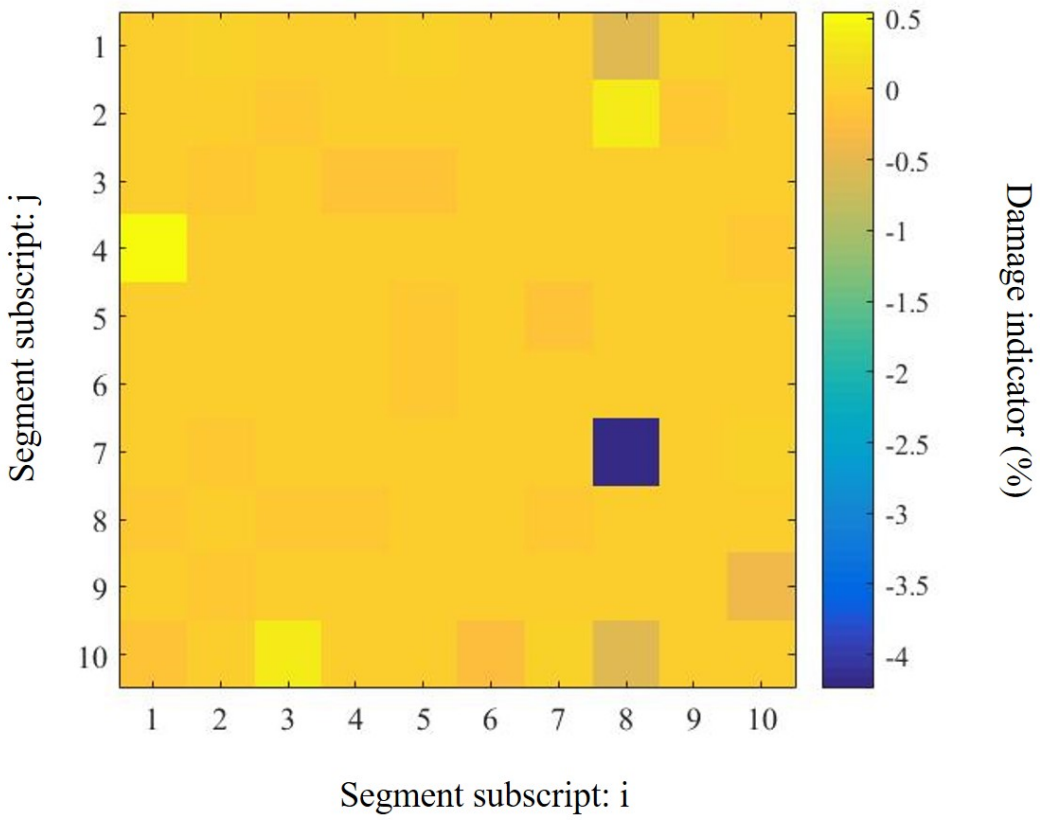

Figure 6.10 Damage identification results of the plate structure obtained using the

proposed method

To further identify a more accurate location of the damage, segment D_{78} is divided into 9 square segments, each measuring 10 mm×10 mm. The identification result for segment D_{78} is shown in Figure 6.11. The location of the actual damage is the centre of segment D_{78}. Using the l_1 regularization method, the largest value of the prediction is on the center element of the segment D_{78}, with a stiffness reduction of -46.8%. There is only a -2.1% error between the predicted and real damage indicator.

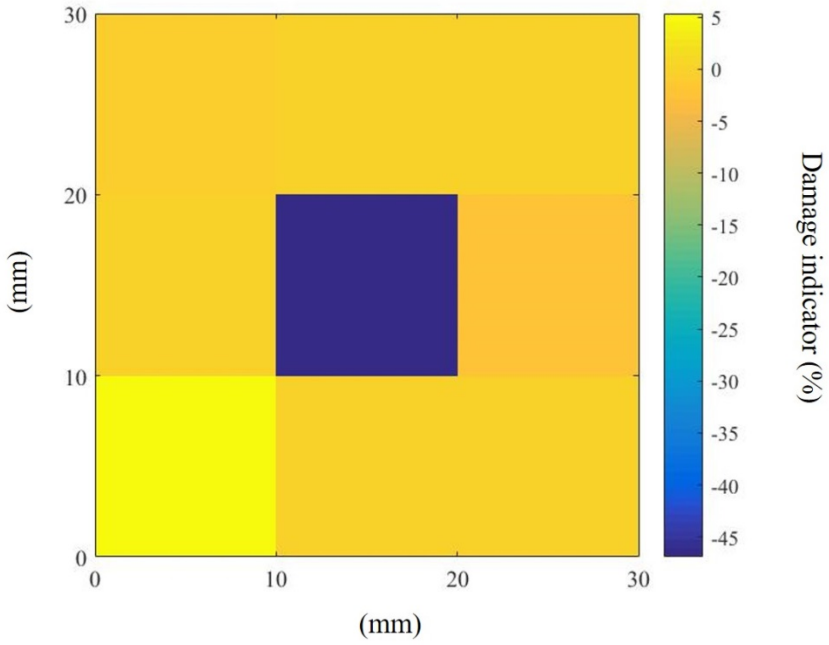

Figure 6.11 Identification results for the damaged segment

6.6 The effect of environmental uncertainty on the proposed approach

In this section, experimental studies are conducted to evaluate the performance of the proposed method under the effect of environmental uncertainty, i.e. the temperature conditions of the conducted tests. The investigation focuses on the influence of temperature variation on the impedance signature. Experimental tests are carried out in a normal range of outdoor temperature. Extreme temperature is not considered in this study.

6.6.1 Previous studies

Due to the nature of piezoelectric materials, the electrical property of a piezoelectric transducer is sensitive to variation in the environmental conditions, such as temperature and humidity. For a system monitoring of an actual outdoor structure, the temperature difference between day and night could lead to non-negligible changes in the electromechanical impedance signature. A brief review of the research on the effects of temperature variation on the EMI technique has been presented in Chapter 4.6. Since Sun et al. [89] investigated the significant changes in the electrical impedance of piezoelectric transducers due to varying temperature, efforts have been made to resolve the errors in the EMI-based SHM method. Temperature variation causes both vertical and horizontal shifts in the electrical impedance signature. Sun et al. [89] proposed a function correlation analysis for compensation. However, based on experimental studies on bolted pipe, reinforced aluminium composites and precision parts, Gyuhae et al. [84] noted that the proposed correlation method would not work for the impedance signature with a small distortion. It is also found that the real part of the impedance signature changes insignificantly with temperature.

Thus far, most of the studies about compensation methods to counteract the effects of temperature on the impedance signature are based on the non-model based EMI

technique using statistical damage indicators, such as RMSD. For the model-based EMI technique, the impact of temperature variations on the performance of damage detection is rarely studied. However, the changes caused by the environmental uncertainty could lead to significant errors and false predictions.

6.6.2 Temperature effects on the impedance responses of a plate structure

In this study, the changes in the impedance signature caused by varying temperature are investigated. Tests are carried out based on the experimental configuration introduced in Chapters 5 and 6. In the experimental study of damage detection for an aluminium plate, the undamaged and damaged specimens are placed in the laboratory at 23.5 ℃, and the temperature is measured both with a thermometer and a temperature sensor on the impedance analyser board, EVAL-AD5933. This state is considered the reference state of measurement. Then, the specimens are placed in an outdoor condition at a 15 ℃ temperature. To test the tolerance of the proposed damage identification approach, the finite element model is still calibrated using the experimental results obtained from the laboratory condition at 23.5 ℃. Then, the damaged specimen is placed in the outdoor environment. The identification results are based on the impedance signature acquired from the damaged specimens at a temperature of 15 ℃. The identification results will indicate the performance of the proposed damage detection method under different temperature conditions.

Figure 6.12 illustrates the temperature effect on the impedance signatures of the PZT transducer bonded onto an undamaged plate specimen. In this case, decreasing temperature leads to a significant vertical shift in the impedance signature. It is worth noting that the horizontal shift is slight compared with that in the vertical direction. Meanwhile, the distortion in the impedance curves is negligible. For this reason, the selection of the resonance peaks for the proposed method will not change due to the temperature variation. Figure 6.13 shows the typical effect of temperature on the

resonance peaks in the impedance signature of the damaged structure. Since the proposed approach only considers the horizontal frequency shifts of the resonance peaks, the effect of decreasing the temperature to 15 ℃ can be viewed as an increase in the overall stiffness of the structure.

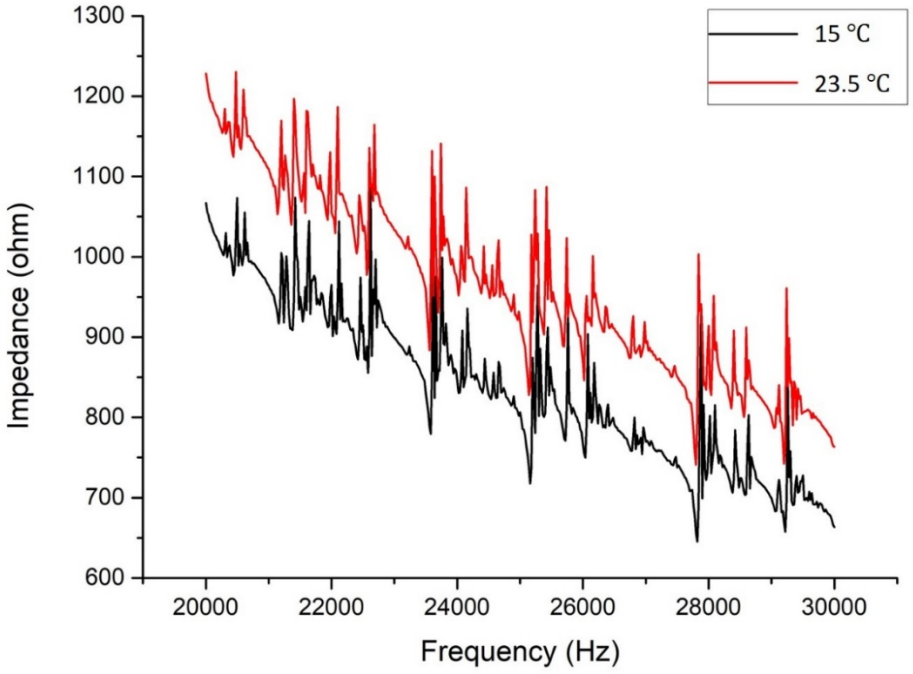

Figure 6.12 Impedance responses of an undamaged aluminium plate under different temperatures

Table 6.4 lists the frequencies of the first three resonance peaks selected for the proposed damage detection method. The change in resonance frequencies due to varying temperature is approximately 4 to 10 Hz, which is approximately 15% of the frequency shifts caused by the structural damage.

Table 6.4 Frequency of the first three resonance peaks with temperature variation

Test result (damaged) (Hz)		Finite element model (undamaged) (Hz)
23 ℃	15 ℃	
20280.4	20288.3	20317.1
20349.7	20357.5	20386.3
20475.2	20483.1	20512.6

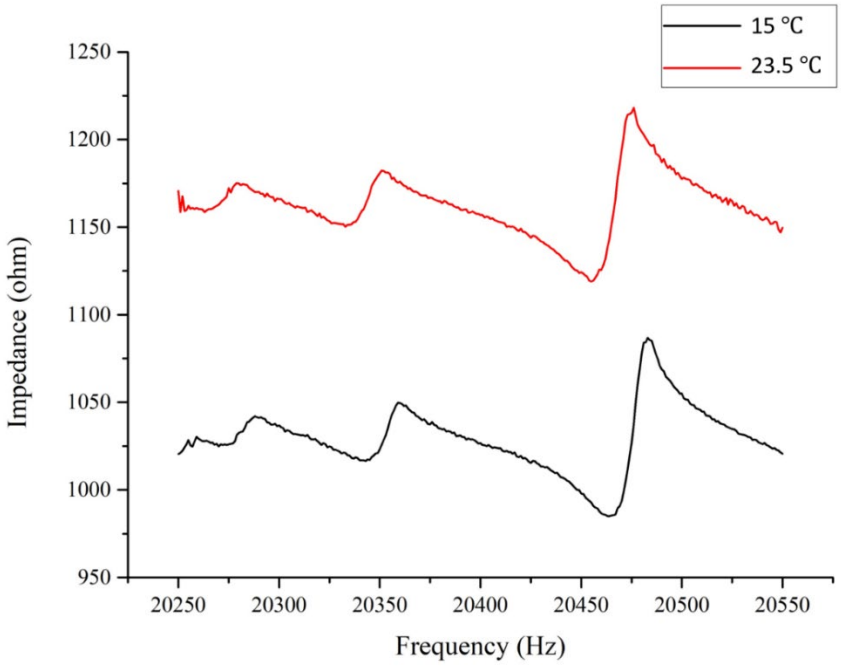

Figure 6.13 Impedance responses of a damaged aluminium plate under different temperatures

With a 8.5 ℃ difference in temperature, the damage identification result obtained using the proposed method is shown in Figure 6.14. Without any prior information, the prediction correctly indicates the location of the drilled damage hole on the aluminium plate based on the impedance signature with a temperature variation. Even though the identified damage severity is lower than the prediction obtained using the impedance signature acquired from the reference temperature, with a decrease of 4.23% in the Young's modulus, the value is still much larger than the predictions in the undamaged segments and close to the approximate actual damage severity. Compared with the result without temperature variations, a little more false predictions in the undamaged segments are observed. Once again, the values of these false predictions are much smaller than the identified damage in the segment D_{78}.

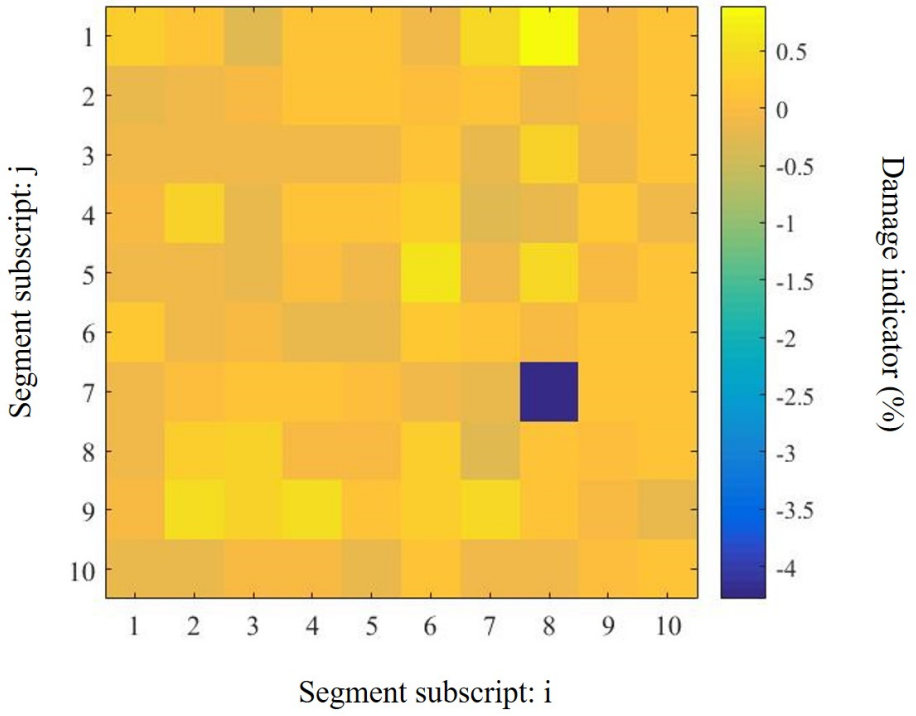

Figure 6.14 Damage identification results of the plate structure considering the temperature variation

6.7 Discussions and concluding remarks

In this chapter, the proposed method is used for damage identification in an aluminium plate with a surface-bonded PZT transducer. An accurate finite element model is developed based on the studies on finite element modelling of EMI simulations in previous chapters. The accuracy of the developed finite element model is verified by the testing results of the aluminium plate under the intact condition. Considering the number of potential locations of damage, only a small number of frequency shifts in the impedance response from a single PZT transducer are used for

damage identification. The predictions obtained using the l_2 norm regularization show that the solutions are distributed on more elements than when using the proposed method based on sparse regularization. Consequently, non-negligible false predictions for undamaged locations are obtained when using the l_2 norm regularization. However, the identification using the l_1 norm regularization method provides accurate location and severity of the damage with only a low level of false identifications. The effect of environmental uncertainty is also investigated in this chapter. The experimental testing under different temperature conditions are conducted and the measured impedance responses are used for identification. The results demonstrate that the proposed approach is not significantly affected by the temperature variations in the testing conditions. The tolerance performance of the propose method with a larger temperature variation will be further studied.

7 Conclusions and Discussions

7.1 Conclusions

Non model and model based EMI techniques are investigated in this PhD thesis. An innovative structural damage identification approach based on impedance sensitivity and sparse regularization techniques is proposed, and the effectiveness and performance are comprehensively investigated in this research. Through numerical modelling and experimental tests, this study maximized the benefits of the EMI-based SHM method. To improve the sensitivity of the non-model based conventional EMI-based SHM methods, the TFARMA model is used to analyse the acquired time-domain electromechanical impedance response. The SVD-based damage indicator is calculated using the time-frequency evaluation spectra. As shown in Chapter 3, experimental studies on a laboratory-scale steel truss bridge model are carried out to validate the performance of the proposed time-frequency analysis method based on TFARAM to identify the structural damage in a relatively complex structure by using the impedance measurement. Bolt loosening damage is applied to the gusset plate in the steel truss bridge model for identification. Compared with the conventional frequency-domain impedance based damage indicators, i.e., RMSD and CC, the TFARMA based damage index shows a significant improvement in sensitivity for detecting bolt loosening damage in the gusset plate of steel truss bridges. The noise effect on the proposed method is also investigated through numerical studies. A significant amount of extra noise is added to the original time-domain impedance response. The identification results demonstrate that the proposed TFARMA based damage index has a more robust and reliable performance in identifying the bolt loosening damage in the gusset plate of steel truss bridges.

The damage indices calculated using the impedance responses from the PZT transducers at different locations are also discussed in Chapter 3. According to the comparison between the evaluation spectra of 4 PZT transducers, the TFARMA based damage index estimated with the PZT transducer placed on the chord member

connected to the gusset plate shows a significant higher sensitivity to bolt loosening damage. It is worth noting that this phenomenon is not demonstrated through the conventional frequency-domain based statistical damage indicators. The sensitivity of these statistical indicators, i.e., RMSD and CC, are only related to the distance between the PZT transducer and the damage location. The reason is that the time-frequency analysis spectra based indicator shows the changes in both frequency-domain and time-domain patterns.

To overcome the limitation of non-model based EMI methods in damage quantification, a new model-based damage detection method using the sensitivity of the electromechanical impedance is proposed in Chapter 4. An accurate finite element model is developed to simulate the impedance response of the surface-bonded PZT transducer. The frequency shifts of the resonance peaks in the impedance responses are used as the measurements of the variations in the impedance response. The sensitivity of the resonance frequency shifts in the impedance responses with respect to structural stiffness parameters are calculated for model updating. To identify a large number of system parameters using only a small number of frequency shifts in a specific frequency range, the sparse regularization, or so-called l_1 regularization technique, is applied to solve the inverse identification problem. Numerical studies of single and multiple damage scenarios are conducted to validate the effectiveness and accuracy of the proposed method. The identification results are compared with those calculated from the traditional Tikhonov regularization. The results demonstrate that the sparse regularization technique could correctly predict the location and severity of the structural damage, however, the results from the conventional Tikhonov regularization method show large errors and false predictions.

The robustness of the proposed approach is also investigated in Chapter 4. According to studies on the effects of temperature on the impedance response, a random frequency shift is added to the measured impedance responses. The damage identification results show that the proposed approach can still correctly predict the

location and severity of minor damage with negligible false predictions, while the Tikhonov regularization method fail to identify the damage.

Experimental studies on the application of the model-based EMI technique using the sparse regularization method to an aluminium beam structure have been presented in Section 5. Minor structural damage is simulated as a reduction in the width of the cross section of the specific individual segment. The finite element model of the impedance response of a single PZT transducer on a beam structure is developed and calibrated using the experimental testing results of the structure in its pristine condition. Frequency shifts of the resonance peaks in the impedance response between 20 kHz and 30 kHz are selected to identify the damages. The performance of the proposed method is validated with two single damage scenarios and two different multiple damage scenarios. The results show that the proposed l_1 -regularization based damage identification method identifies the damage location and severity accurately. Compared with the results from the Tikhonov regularization method, the use of the sparse regularization technique significantly reduces the number and magnitude of false predictions. In addition, the sensitivity range of the proposed approach is discussed based on parametric studies. Numerical analyses of identification accuracy for specimens with different sizes are carried out. The results show that the proposed approach can successfully identify the damage when the length of the beam structure increases up to 600 mm. Since the measured frequency shifts decrease to single digits when the specimen is longer than 800 mm, the damage could not be reliably detected by the proposed approach in this case.

The proposed sparse regularization based EMI method is applied to identify the damage on a plate structure in Chapter 6. Experimental studies are conducted on an aluminium plate in the laboratory. A three-dimensional finite element model is developed to simulate the impedance response of a single PZT transducer bonded to the aluminium plate. The simulated impedance responses of the undamaged structure are calibrated by experimental testing results. The frequencies of resonance peaks in

the simulated impedance response well match with the experimental results. Structural damage is simulated by a hole drilled in specimens. For damage identification, the plate is further divided into 100 segments, and the Young's modulus variations of the segments are defined as the severity of the damage in the simulations. The results show that the proposed method can accurately locate and quantify the damage. Furthermore, the temperature effect on the robustness and performance of the proposed approach is investigated with experimental studies. Specimens are placed in the laboratory and outdoor environments at different temperatures. The proposed approach has been proven effective under a change in temperature conditions between day and night.

Overall, this thesis first improves the sensitivity of the EMI based SHM technique on a structure with complex geometry and connections using a new time-frequency analysis method, TFARMA model. Then, physical insights into the impedance response of a surface-bonded PZT transducer and the effects of structural damage on the host structure are investigated through finite element analysis. The simulation results well match with the test results. Therefore, the calibrated model is applied to the model-based damage identification using the impedance sensitivity. The sparse regularization technique is applied, in place of the conventional Tikhonov regularization, to identify a large number of unknown system parameters with only a few measurements. Experimental studies on beam and plate structures demonstrate the performance and robustness of the proposed approach.

7.2 Suggestions for further work

This thesis comprehensively discusses the application of non-model based and model-based EMI-based SHM methods. Based on the experiences and results obtained in this research, the following suggestions can be made for further work.

The current studies only investigate the performance of the TFARMA model-based damage indicator on a structure with bolt loosening damage in the laboratory. Future studies may focus on investigating the possibility of identifying different types of damage and the exact sensitivity radius of PZT transducers for identification of the gusset plate conditions in truss bridges. The effect of temperature variation is reported to be one major problem in the application of the EMI technique. A temperature change could cause a frequency shift in the impedance response signal. Because of this, the effect of temperature on the performance of the proposed approach should also be further investigated.

In this thesis, no external loading is applied to the host structure; therefore, no significant deformation or bending occurs for the tested structure. The temperature variation has been considered as the only uncertainty. In practice, the stress status could also have an influence on the impedance response. More researches on the effect of stress status on the impedance measurement will be conducted in future work.

More different damage types could be considered in the finite element modelling for future work. The proposed model-based EMI method can be applied to debonding detection of FRP/concrete interfaces or composite materials.

The effect of temperature on the impedance response and the performance of the proposed damage identification method is investigated. However, the temperature variation could cause the damage identification to fail with temperature variations larger than 5 ℃. For these cases, compensation methods could be developed and the further studies are recommended.

References

[1] Board N T S (2008). Collapse of I-35W highway bridge, Minneapolis, Minnesota, August 1, 2007, Author Washington, DC.

[2] Peairs D M, Park G and Inman D J 2004 Improving accessibility of the impedance-based structural health monitoring method *Journal of Intelligent Material Systems and Structures* **15** 129-139.

[3] Annamdas V G M 2012 Facts of piezo impedance technique in crack propagation studies for an engineering structure *International Journal of Aerospace Sciences* **1** 8-15.

[4] Souza P R and Nóbrega E G O 2017 An effective structural health monitoring methodology for damage isolation based on multisensor arrangements *Journal of the Brazilian Society of Mechanical Sciences and Engineering* **39** 1351-1363.

[5] Fan X, Li J and Hao H 2016 Piezoelectric impedance based damage detection in truss bridges based on time frequency ARMA model *Smart Struct. Syst* **18** 501-523.

[6] Hernandez E M 2014 Identification of isolated structural damage from incomplete spectrum information using l 1-norm minimization *Mechanical Systems and Signal Processing* **46** 59-69.

[7] Lim Y Y and Soh C K 2014 Towards more accurate numerical modeling of impedance based high frequency harmonic vibration *Smart Materials and Structures* **23** 035017.

[8] Farrar C R and Worden K 2007 An introduction to structural health monitoring *Philosophical Transactions of the Royal Society of London A: Mathematical, Physical and Engineering Sciences* **365** 303-315.

[9] Meitzler A, Tiersten H, Warner A, Berlincourt D, Couqin G and Welsh III F (1988). IEEE standard on piezoelectricity, Society.

[10] Kumar S 1991 Smart Materials for Acoustic or Vibration Control Pennsylvania State University

[11] Giurgiutiu V and Zagrai A N 2000 Characterization of piezoelectric wafer active sensors *Journal of Intelligent Material Systems and Structures* **11** 959-976.

[12] Kessler S S, Spearing S M and Atalla M J 2002 In-situ damage detection of composites structures using Lamb wave methods *Proceedings of the first European workshop on structural health monitoring* Paris, France 374–381.

[13] Rogers C 1996 An impedance-based system modeling approach for induced strain actuator-driven structures *Journal of Vibration and Acoustics* **118** 323.

[14] Annamdas V G M and Soh C K 2010 Application of electromechanical impedance technique for engineering structures: review and future issues *Journal of Intelligent Material Systems and Structures* **21** 41-59.

[15] Park G, Sohn H, Farrar C R and Inman D J 2003 Overview of piezoelectric impedance-based health monitoring and path forward *Shock and Vibration Digest* **35** 451-463.

[16] Sun F P, Chaudhry Z, Liang C and Rogers C 1995 Truss structure integrity identification using PZT sensor-actuator *Journal of Intelligent Material Systems and Structures* **6** 134-139.

[17] Zagrai A N and Giurgiutiu V 2001 Electro-mechanical impedance method for crack detection in thin plates *Journal of Intelligent Material Systems and Structures* **12** 709-718.

[18] Tseng K K and Naidu A 2002 Non-parametric damage detection and characterization using smart piezoceramic material *Smart Materials and Structures* **11** 317.

[19] Sun R, Sevillano E and Perera R 2015 Debonding detection of FRP strengthened concrete beams by using impedance measurements and an ensemble PSO adaptive spectral model *Composite Structures* **125** 374-387.

[20] Vieira Filho J, Baptista F G and Inman D J 2011 Time-domain analysis of piezoelectric impedance-based structural health monitoring using multilevel wavelet decomposition *Mechanical Systems and Signal Processing* **25** 1550-1558.

[21] Wang X and Tang J 2009 Damage identification using piezoelectric impedance approach and spectral element method *Journal of Intelligent Material Systems and Structures* **20** 907-921.

[22] Lopes V, Park G, Cudney H H and Inman D J 2000 Impedance-based structural health monitoring with artificial neural networks *Journal of Intelligent Material Systems and Structures* **11** 206-214.

[23] Min J, Park S, Yun C-B, Lee C-G and Lee C 2012 Impedance-based structural health monitoring incorporating neural network technique for identification of damage type and severity *Engineering Structures* **39** 210-220.

[24] Giurgiutiu V and Zagrai A 2005 Damage detection in thin plates and aerospace structures with the electro-mechanical impedance method *Structural Health Monitoring* **4** 99-118.

[25] Na S and Lee H 2013 Neural network approach for damaged area location prediction of a composite plate using electromechanical impedance technique *Composites Science and Technology* **88** 62-68.

[26] Selva P, Cherrier O, Budinger V, Lachaud F and Morlier J 2013 Smart monitoring of aeronautical composites plates based on electromechanical impedance measurements and artificial neural networks *Engineering Structures* **56** 794-804.

[27] Kim J and Wang K 2014 An enhanced impedance-based damage identification method using adaptive piezoelectric circuitry *Smart Materials and Structures* **23** 095041.

[28] Liang C, Sun F and Rogers C 1994 Coupled Electro-Mechanical Analysis of Adaptive Material Systems—Determination of the Actuator Power Consumption and System Energy Transfer *Journal of Intelligent Material Systems and Structures* **5** 12-20.

[29] Zhou S, Liang C and Rogers C 1995 Integration and design of piezoceramic elements in intelligent structures *Journal of Intelligent Material Systems and Structures* **6** 733-743.

[30] Bhalla S and Soh C K 2004 Structural health monitoring by piezo-impedance transducers. I: Modeling *Journal of Aerospace Engineering* **17** 154-165.

[31] Bhalla S and Soh C K 2004 Structural health monitoring by piezo–impedance transducers. II: applications *Journal of Aerospace Engineering* **17** 166-175.

[32] Yang Y, Xu J and Soh C K 2005 Generic impedance-based model for structure-piezoceramic interacting system *Journal of Aerospace Engineering* **18** 93-101.

[33] Annamdas V G M and Soh C K 2008 Three-dimensional electromechanical impedance model for multiple piezoceramic transducers—structure interaction *Journal of Aerospace Engineering* **21** 35-44.

[34] Park G, Cudney H H and Inman D J 2000 An integrated health monitoring technique using structural impedance sensors *Journal of Intelligent Material Systems and Structures* **11** 448-455.

[35] Kuang Y-D, Li G-Q and Chen C-Y 2006 Dynamic analysis of actuator-driven circular arch or ring using impedance elements *Smart Materials and Structures* **15** 869.

[36] Xu J, Yang Y and Soh C K 2004 Electromechanical impedance-based structural health monitoring with evolutionary programming *Journal of Aerospace Engineering* **17** 182-193.

[37] Yang Y and Hu Y 2007 Electromechanical impedance modeling of PZT transducers for health monitoring of cylindrical shell structures *Smart Materials and Structures* **17** 015005.

[38] Park H W 2014 Understanding the electromechanical admittance of piezoelectric transducers collocated on a finite beam from the perspective of wave propagation *Journal of Intelligent Material Systems and Structures* **25** 2122-2140.

[39] Sepehry N, Bakhtiari-Nejad F and Shamshirsaz M 2014 Thermo-electro-mechanical impedance based structural health monitoring of plates *Composite Structures* **116** 147-164.

[40] Lerch R 1990 Simulation of piezoelectric devices by two-and three-dimensional finite elements *IEEE transactions on ultrasonics, ferroelectrics, and frequency control* **37** 233-247.

[41] Fairweather J A and Craig K C 1998 Incorporating finite element techniques to simplify the impedance modeling of active structures *5th Annual International Symposium on Smart Structures and Materials* International Society for Optics and Photonics 602-613.

[42] Annamdas V G M and Soh C K 2007 Three-dimensional electromechanical impedance model. I: Formulation of directional sum impedance *Journal of Aerospace Engineering* **20** 53-62.

[43] Yang Y, Lim Y Y and Soh C K 2008 Practical issues related to the application of the electromechanical impedance technique in the structural health monitoring of civil structures: I. Experiment *Smart Materials and Structures* **17** 035008.

[44] Zhang Y, Xu F, Chen J, Wu C and Wen D 2011 Electromechanical impedance response of a cracked Timoshenko beam *Sensors* **11** 7285-7301.

[45] Hamzeloo S R, Shamshirsaz M and Rezaei S M 2012 Damage detection on hollow cylinders by electro-mechanical impedance method: Experiments and finite element modeling *Comptes Rendus Mecanique* **340** 668-677.

[46] Doyle J F 1997 *Wave Propagation in Structures: Spectral Analysis Using Fast Discrete Fourier Transforms* (Springer)

[47] Esteban J 1996 Modeling of the sensing region of a piezoelectric actuator/sensor *Doctoral dissertation* VA: Virginia Polytechnic Institute and State University

[48] Ritdumrongkul S, Abe M, Fujino Y and Miyashita T 2003 Quantitative health monitoring of bolted joints using a piezoceramic actuator–sensor *Smart Materials and Structures* **13** 20-29.

[49] Lee U and Kim J 2001 Spectral element modeling for the beams treated with active constrained layer damping *International Journal of Solids and Structures* **38** 5679-5702.

[50] Peairs D M, Inman D J and Park G 2007 Circuit analysis of impedance-based health monitoring of beams using spectral elements *Structural Health Monitoring* **6** 81-94.

[51] Wang Y and Hao H 2010 An introduction to compressive sensing and its potential applications in structural engineering *The 11th international symposium on structural engineering* 1089-1094.

[52] Zhou X-Q, Xia Y and Weng S 2015 L1 regularization approach to structural damage detection using frequency data *Structural Health Monitoring* **14** 571-582.

[53] Tropp J A 2004 Greed is good: Algorithmic results for sparse approximation *IEEE Transactions on Information theory* **50** 2231-2242.

[54] Chen S S, Donoho D L and Saunders M A 2001 Atomic decomposition by basis pursuit *SIAM review* **43** 129-159.

[55] Van den Berg E and Friedlander M P 2011 Sparse optimization with least-squares constraints *SIAM Journal on Optimization* **21** 1201-1229.

[56] Yang J N, Lei Y, Pan S and Huang N 2003 System identification of linear structures based on Hilbert–Huang spectral analysis. Part 1: normal modes *Earthquake engineering & structural dynamics* **32** 1443-1467.

[57] Yang J N, Lei Y, Lin S and Huang N 2004 Hilbert-Huang based approach for structural damage detection *Journal of engineering mechanics* **130** 85-95.

[58] Rucka M and Wilde K 2006 Application of continuous wavelet transform in vibration based damage detection method for beams and plates *Journal of Sound and Vibration* **297** 536-550.

[59] Yi T-H, Li H-N and Gu M 2013 Wavelet based multi-step filtering method for bridge health monitoring using GPS and accelerometer *Smart Structures and Systems* **11** 331-348.

[60] Li J and Hao H 2014 Substructure damage identification based on wavelet-domain response reconstruction *Structural Health Monitoring* **13** 389-405.

[61] Li J, Hao H and Zhu H-P 2014 Dynamic assessment of shear connectors in composite bridges with ambient vibration measurements *Advances in Structural Engineering* **17** 617-637.

[62] Li J and Hao H 2015 Damage detection of shear connectors under moving loads with relative displacement measurements *Mechanical Systems and Signal Processing* **60** 124-150.

[63] Da Silva S, Dias Junior M and Lopes Junior V 2008 Structural health monitoring in smart structures through time series analysis *Structural Health Monitoring* **7** 231-244.

[64] Zahedi F and Huang H 2017 Time–frequency analysis of electro-mechanical impedance (EMI) signature for physics-based damage detections using piezoelectric wafer active sensor (PWAS) *Smart Materials and Structures* **26** 055010.

[65] Jachan M, Matz G and Hlawatsch F 2007 Time-frequency ARMA models and parameter estimators for underspread nonstationary random processes *IEEE Transactions on Signal processing* **55** 4366-4381.

[66] Feng Z, Liang M and Chu F 2013 Recent advances in time–frequency analysis methods for machinery fault diagnosis: A review with application examples *Mechanical Systems and Signal Processing* **38** 165-205.

[67] Stoica P 1997 *Introduction to spectral analysis* (Prentice hall)

[68] Wax M and Kailath T 1983 Efficient inversion of Toeplitz-block Toeplitz matrix *IEEE Transactions on Acoustics, Speech, and Signal Processing* **31** 1218-1221.

[69] Jachan M, Hlawatsch F and Matz G 2005 Linear methods for TFARNA parameter estimation and system approximation *Statistical Signal Processing, 2005 IEEE/SP 13th Workshop on* IEEE 909-914.

[70] Song H, Lim H and Sohn H 2013 Electromechanical impedance measurement from large structures using a dual piezoelectric transducer *Journal of Sound and Vibration* **332** 6580-6595.

[71] Baptista F G and Vieira Filho J 2009 A new impedance measurement system for PZT-based structural health monitoring *IEEE Transactions on Instrumentation and Measurement* **58** 3602-3608.

[72] Park G, Cudney H H and Inman D J 2000 Impedance-based health monitoring of civil structural components *Journal of infrastructure systems* **6** 153-160.

[73] Shao J, Wang T, Yin H, Yang D and Li Y 2016 Bolt looseness detection based on piezoelectric impedance frequency shift *Applied Sciences* **6** 298.

[74] Shuai Q, Zhou K, Zhou S and Tang J 2017 Fault Identification Using Piezoelectric Impedance Measurement and Model-based Intelligent Inference with Pre-screening *Smart Materials and Structures* **26** 045007.

[75] Albakri M I and Tarazaga P A 2017 Electromechanical impedance–based damage characterization using spectral element method *Journal of Intelligent Material Systems and Structures* **28** 63-77.

[76] Lu Z and Law S 2007 Features of dynamic response sensitivity and its application in damage detection *Journal of Sound and Vibration* **303** 305-329.

[77] Xia Y and Hao H 2003 Statistical damage identification of structures with frequency changes *Journal of Sound and Vibration* **263** 853-870.

[78] Van Den Berg E and Friedlander M P 2008 Probing the Pareto frontier for basis pursuit solutions *SIAM Journal on Scientific Computing* **31** 890-912.

[79] Lesieutre G 2001 *Damping in finite element models* (Encyclopedia of Vibration (New York: Academic))

[80] Makkonen T, Holappa A, Ella J and Salomea M 2001 Finite element simulations of thin-film composite BAW resonators *IEEE transactions on ultrasonics, ferroelectrics, and frequency control* **48** 1241-1258.

[81] Chaudhry Z A, Joseph T, Sun F P and Rogers C A 1995 Local-area health monitoring of aircraft via piezoelectric actuator/sensor patches *Smart Structures & Materials' 95* International Society for Optics and Photonics 268-276.

[82] Priya C B, Reddy A L, Rao G R, Gopalakrishnan N and Rao A R M 2014 Low frequency and boundary condition effects on impedance based damage identification *Case Studies in Nondestructive Testing and Evaluation* **2** 9-13.

[83] Koo K-Y, Park S, Lee J-J and Yun C-B 2009 Automated impedance-based structural health monitoring incorporating effective frequency shift for compensating temperature effects *Journal of Intelligent Material Systems and Structures* **20** 367-377.

[84] Gyuhae P, Kabeya K, Cudney H H and Inman D J 1999 Impedance-based structural health monitoring for temperature varying applications *JSME International Journal Series A Solid Mechanics and Material Engineering* **42** 249-258.

[85] Sepehry N, Shamshirsaz M and Abdollahi F 2011 Temperature variation effect compensation in impedance-based structural health monitoring using neural networks *Journal of Intelligent Material Systems and Structures* **22** 1975-1982.

[86] Wandowski T, Malinowski P and Ostachowicz W 2016 Delamination detection in CFRP panels using EMI method with temperature compensation *Composite Structures* **151** 99-107.

[87] Sepehry N, Bakhtiari-Nejad F and Shamshirsaz M 2017 Discrete singular convolution and spectral finite element method for predicting electromechanical impedance applied on rectangular plates *Journal of Intelligent Material Systems and Structures* 1045389X17689931.

[88] Li J, Law S and Ding Y 2012 Substructure damage identification based on response reconstruction in frequency domain and model updating *Engineering Structures* **41** 270-284.

[89] Sun F P, Chaudhry Z A, Rogers C A, Majmundar M and Liang C 1995 Automated real-time structure health monitoring via signature pattern recognition *Smart Structures and Materials 1995: Smart Structures and Integrated Systems* International Society for Optics and Photonics 236-248.